Development of an imaging system dedicated to the acquisition analysis and multispectral characterisation of skin lesion

Romuald Jolivot

UNIVERSITÉ DE BOURGOGNE
U.F.R. SCIENCES ET TECHNIQUES
LABORATOIRE LE2I

THESE

Présentée et soutenue publiquement pour l'obtention du grade de

Docteur de l'Université de Bourgogne
Spécialité : Instrumentation et Informatique de l'Image
par

Romuald Jolivot
Le 07-12-2011

Développement d'un outil d'imagerie dédié à l'acquisition, à l'analyse et à la caractérisation multispectrale des lésions dermatologiques

Development of an imaging system dedicated to the acquisition, analysis and multispectral characterisation of skin lesions

Jury

Klaus BÖHM	Professeur - i3mainz, Allemagne	Examinateur
Michel JOURLIN	Professeur - Laboratoire Hubert Curien, France	Rapporteur
Yves LUCAS	MCF-HDR - Institut Prisme, France	Examinateur
Franck MARZANI	Professeur - Laboratoire Le2i, France	Directeur de thèse
Fabrice MÉRIAUDEAU	Professeur - Laboratoire Le2i,France	Président du Jury
Jean SEQUEIRA	Professeur - Laboratoire LSIS, France	Rapporteur
Pierre VABRES	PUPH - CHU de Dijon, France	Co-directeur de thèse

Résumé

L'évaluation visuelle de lésions cutanées est l'analyse la plus couramment réalisée par les dermatologues. Ce diagnostic s'effectue principalement à l'oeil nu et se base sur des critères tels que la taille, la forme, la symétrie mais principalement la couleur. Cependant, cette analyse est subjective car dépendante de l'expérience du praticien et des conditions d'utilisation. Nous proposons dans ce manuscrit (1) le développement d'une caméra multispectrale spécialement conçue pour un usage en dermatologie. Cette caméra multispectrale se base sur la technologie de roue porte-filtres composée de filtres interférentiels et d'un algorithme basé sur les réseaux de neurones générant un cube hyperspectral de données cutanées. Cet ensemble combine l'avantage d'un spectrophotomètre (information spectrale), et celui d'une caméra (information spatiale). Son intérêt est également de délivrer une information reproductible et indépendante des conditions d'acquisition. La mise en place d'un protocole d'acquisition de données de peaux saines issues de cinq des six phototypes existants a permis la validation de notre système en comparant les spectres générés par notre système avec des spectres théoriques acquis par un spectrophotomètre professionnel. (2) La réflectance spectrale de données de peau fournit une information précieuse, car directement liée à sa composition en chromophores. La mesure quantitative des propriétés optiques du tissu cutané peut être basée sur la modélisation de la propagation de la lumière dans la peau. Pour cela, nous nous sommes appuyés sur le modèle de Kubelka-Munk, auquel nous avons associé une méthode d'optimisation basée sur les algorithmes évolutionnaires. Cette dernière apporte une réponse à l'inversion de ce modèle. À partir de cette approche, la quantification de divers paramètres de la peau peut être obtenue, tels que la mélanine et l'hémoglobine. (3) La validation de cette méthodologie est effectuée sur des données pathologiques (vitiligo et melasma) et permet de quantifier une différence de composition entre zone saine et zone affectée sur une même image.
MOTS CLÉS : Dermatologie; Imagerie multispectrale; Reconstruction spectrale; Modèle de propagation de la lumière dans la peau; Algorithmes évolutionnaires.

Abstract

Visual evaluation of cutaneous lesions is the analysis the most commonly performed by dermatologists. This diagnostic is mainly done by naked eye and is based on criterion such as the size, shape, symmetry but principally on colour of the lesions. However, this analysis is subjective because it depends on the practician experience and the acquisition conditions. We propose in this dissertation (1) the development of a multispectral camera specifically dedicated for dermatological use. This device is based on a filter wheel composed of interferential filters and a neural network-based algorithm, generating a hyperspectral cube of cutaneous data. This setting combines advantage of both spectrophotometer (spectral information) and digital camera (spatial information). Its main interest is also to provide reproducible information which is independent of the acquisition conditions. The setting-up of an acquisition protocol of healthy skin data from five of the six exisiting skin phototypes allows the validation of our system by comparing spectra generated by our system and theoretical spectra acquired by professional spectrophotometer. (2) Skin spectral reflectance provides precious information because it is directly linked to the skin chromophore composition. Quantitative measure of cutaneous tissue optical properties can be based on the modelisation of light propagation in skin. For this purpose, we based our method on Kubelka-Munk model with which we associated an optimization method based on evolutionary algorithm. This method helps for the model inversion. Using this approach, quantification of diverse parameters of skin can be obtained such as melanin and haemoglobin. (3) The validation of this model is performed on disease skin data (vitiligo and melasma) and allows to quantify difference between healthy and affected skin area within a single image.
KEY-WORDS: Dermatology; Multispectral imaging; Spectral reconstruction; Light propagation model in skin; Evolutionnary algorithms.

Acknowledgments

I would like to begin expressing my gratitude to Pr. Franck Marzani. I am very grateful for his availability, his precious advices, help, patience and mostly his confidence and believe in my work. Our numerous scientific and friendly exchanges have greatly helped me to complete this PhD work. He has always been available to answer my numerous questions and his constant supports at time needed. More than a supervisor he became of friend to me.

I would like to express my gratitude to Dr. Pierre Vabres, which despite his busy schedule, found the time to give me advice and information about the dermatological side of the project.

My best thanks go to the reviewers of my thesis Professor Michel Jourlin and Professor Jean Sequeira. I would like to thanks them for taking the time to review my thesis and their interesting and accurate feedbacks that help me improve the overall quality of my work.

I am grateful to Professor Klaus Böhm who accepted to be part of my PhD defence. Similarly, I want to thank Yves Lucas who joined the PhD defence. His corrections improved the readability of my thesis and our previous discussions were always interesting.

Finally I would like to thank Professor Fabrice Mériaudeau for accepting to be the president of my thesis jury. I have known him for more than 6 years and his support and friendliness have been a great source of inspiration. I am grateful for his international

contacts that help me to work around the world.

My gratefulness to Professor Fadzil for welcoming me in his lab at UTP. It allowed performing data collection with the great help of Hermawan. I also want to thanks Dr. Roshida Baba, Dr. Norashikin, Hospital Kuala Lumpur and Serdang Hospital for welcoming me in their services.

I would like to thanks Yannick for reading and correcting my thesis, it has been very helpful and it was a pleasure working with you, even only for few months.

I got the chance to spend these three years among many colleagues in the lab. I wish to thank them because we always got the chance to work in a friendly environment. I had fun working, chatting, drinking coffee and so many other things with them. So thank you Alain, Bastien B., Bastien C.(super stagiaire), Bertrand, Gerald, July, Jean Baptiste, Pierre, Pierre-Jean and all the other lab members that I got the chance to meet. A special thank to Camille for being herself, it was great to be able to discuss with you about work but also about many other things.

Finally, I would like to express my greatest recognition to my family. They continuously supported me during all my studies throughout my up and down. They always have been here for me even when I was far away. To my friend Anthony, despite mostly being on the other side of the world, you always cheer me up, you are a true buddy. I would also like to thanks Lertrusdachakul family (Pom, Pupae, Khun maa, Khun Paw and Indy) for their continuous encouragement and kindness.

I would like to thank the financial support provided by Conseil Régional de Bourgogne, France and laboratoire Bioderma, France which made the thesis possible.

Romuald Jolivot

Dijon

January 5, 2012

Contents

List of Figures

List of Tables

Glossary

ANN =Artificial Neural Networks

AOTF =Acousto-Optic Tunable filter

CSLM =Confocal Scanning Laser Microscopy

DRS =Diffuse Reflectance Spectroscopy

FWHM =Full Width at Half Maximum

GA =Genetic Algorithm

GFC =Goodness of Fit Coefficient

HSI =HyperSpectral Imaging

IR =InfraRed

KM =Kubelka-Munk

LCTF =Liquid Crystal Tunable Filter

MC =Monte Carlo

MRI =Magnetic Resonance Imaging

MSAS =Modified Spectral Angle Similarity

MSI =MultiSpectral Imaging

NIR =Near-Infrared spectrum

NPCD =Non-Polarized light Contact Dermoscopy

OCT =Optical Coherence Tomography

PCD =Polarized Contact Dermoscopy

PD =Polarized light Dermoscopy

PNCD =Polarized Non-Contact Dermoscopy

RC =Reflectance Cube

RecP =Reconstruction Percentage

RMSE =Root Mean Squared Error

RTE =Radiative Transfert Equation

SPT =Skin PhotoType

SSV =Spectral Similarity Value

US =UltraSound

UV =Ultraviolet spectrum

VIS =Visible

WHO =World Health Organization

Chapter 1

Introduction

According to the World Health Organization [World Health Organization, 2011], between 2 and 3 million non-melanoma skin cancers and approximately 132,000 melanoma skin cancers are recorded every year of which 48,000 related to deaths [Lucas et al., 2006]. Skin cancer is among the numerous skin diseases that affect the life of million people worldwide. The World Health Organization (WHO) estimated that around 0.5 to 1% of the world population is affected by vitiligo. Skin diseases have often been ignored or given low priority in comparison to diseases with more significant mortality (HIV, tuberculosis) by international health authorities. Although certain skin diseases are not medicaly harmful and cause limited to no physical pain, they can have a strong psychological effect. The trends have changed with a global awerness that skin modification may be an early sign of more serious disease such as autoimmune disease, potentially affecting the general health. There is a growing awareness of skin disease condition worldwide [Kingman, 2005].

The visual assessment of different skin pathologies is a result of ambient light that enters the skin and is scattered and diffused within it. The re-emitted light carries important information about the physical and optical tissue parameters. Well trained dermatologists analyse the skin color and interpret the clinical pathologies based on their knowledge and experience. Imaging systems for skin analysis often try to mimic the eye analysis. Nowadays, digital imaging system are more and more available to the clinicians but it is mostly restricted to colour cameras. Such systems are limited in terms of spectral information. They do not take advantage of the skin/light interaction which occurs over the whole spectrum range.

To improve the subjective assessment made on color information, several optical acquisition systems have been developed to study the skin more objectively. Optical Coherence

Tomography (OCT), Magnetic Resonance Imaging (MRI), Confocal Scanning Laser Microscopy (CSLM) and Ultrasound (US) systems may provide extensive skin information but these technologies are costly, often cumbersome and not easily available to dermatologist. This is not practical for the explorative study of skin lesions on a daily basis. Several studies [McIntosh et al., 2001, Tomatis et al., 2005a, Baruah et al., 2000] point out the possible differentiation of skin variegation above specific wavelength values as compared to healthy skin, meaning that spectral information is an important tool of assessment. Based on this finding, the current classical technology does not cover both spectral and spatial information.

Currently, there is no system that can replace the diagnosis abilities of experienced clinicians. However the use of optical instruments increase the amount of complementary information to the dermatologist. It can provide information not detectable by the human eye and can lead to precise skin chromophore quantification.

As a result, the development of a technology, combining a large amount of skin information (both spectrally and spatially) and analysis of the skin information for retrieval of parameters, might increase the information available to the dermatologist. This influenced our research toward multispectral imaging system. Currently, multispectral imaging systems developed for skin lesions acquisition focus their studies on a single disease analysis, mostly melanoma with illumination at specific wavelengths. These systems omit to acquire large wavelength bands for the study of different skin diseases. We address this problem by developping an exploratory imaging system dedicated to dermatology.

1.1 Contribution of the thesis

The objectives of this thesis were to develop a camera that extends the limited capabilities of the human visual system, providing objective and reproducible data.

- Optical imaging system: development of a multispectral imaging system that acquires objective and reproducible skin data. The system reconstructs cube of skin reflectance which is is directly linked to the skin instead of color image that depends on the illuminant and environment conditions. The reconstruction capacity is validated on healthy patients from different skin populations.

- Parameter extraction: development of a method to retrieve skin parameters from reflectance spectrum. We use a combination of a model of light propagation based

on the Kubelka-Munk theory and an optimization technique based on Genetic Algorithm to extract five characteristic skin parameters.

- Application: test of the complete system on two skin diseases to generate skin parameter maps.

1.2 Organization

This thesis is organized as follows. Chapter 2 reviews the different non-invasive skin acquisition systems and compares their pros and cons to define a suitable basis for the development of our system. Chapter 3 gives a detailed description of our multispectral imaging system applied to dermatology. It acquires multispectral images and reconstructs reflectance cubes. The system is validated using data of healthy patients and comparison with a spectrometer system. A review of the different skin data analysis techniques is presented in chapter 4. It introduces the human skin, different skin light propagation models and some methods to retrieve skin parameters. Chapter 5 details the implementation of a model of light propagation and its optimization to retrieve different skin parameters. Finally, in chapter 6, we describe the validation of our technique to retrieve skin parameters based on healthy skin and apply our method to two skin diseases.

Chapter 2

Review of Skin Imaging Systems

The skin, covering 97% of the body, can be directly examined without excision. Diseases altering its appearance can be easily observed. Visual evaluation of lesions is the first and most common procedure made by dermatologists in daily practice. In this context, dermatologists mainly rely on the aspects of a skin lesion to determine whether it is benign or malignant. The evaluation is based on the distribution, size, shape, border, symmetry but mostly on the colour aspect of the lesion. Dermatologists evaluate the lesion condition based on a score and journal note; journal note and lesion photography are often the only means of follow-up to determine the evolution of the condition from a previous visit.

Most diagnosis based on colour is subjective as colour perception depends on the human visual response to the light and light interaction with objects. Human eye is composed of two different receptors, rods for dim light and cones for daylight. Rods are monochromatic, meaning they do not provide spectral information whereas there are three different types of cones, each of them having selective wavelength response. The cones are named L, M and S, each respectively centred at long (564 nm), medium (534 nm) and short (420 nm) wavelengths [Bowmaker and Dartnall, 1980] (see figure 2.1). The human eye does not have the same sensitivity for all the wavelengths [Dowling, 1996] and between individuals. The discriminant power is poor for the extremity of the spectrum but much higher in the wave range between of 490 and 550 nm.

Colour is sensed by the human eye which integrates electromagnetic spectrum of the visible range according to the three different spectral bands composing the cones. It is subjectively interpreted as a unique sensation but it is indeed a combination of wavelengths.

There is no spectral distribution information meaning that the eye can be affected by metamerism. To detail the metamerism, an example of colour comparison can be made

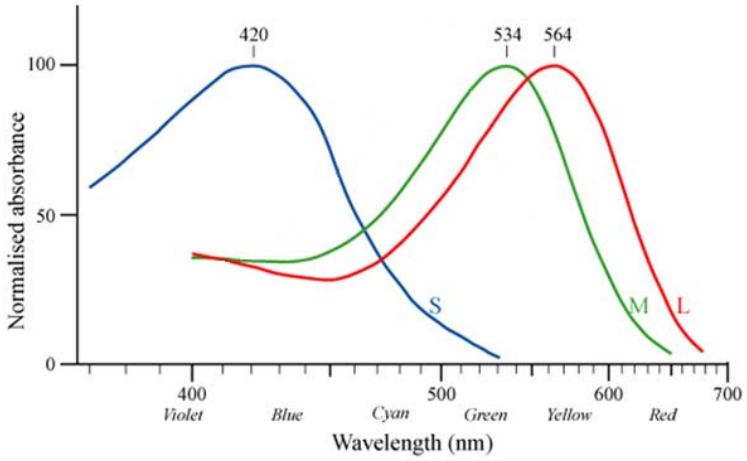

Figure 2.1: Normalized human photoreceptor absorbance for different wavelengths of light [Bowmaker and Dartnall, 1980].

using a yellow light and combined (a mixture of) red and green light producing yellow colour. The human eye will only see yellow and it is not able to discriminate the spectral information in the two cases. The amount of each wavelength reaching the cones produces in both cases the same perceived yellow colour. This effect can also arise under different illuminant (two skins with different chromophore distribution can look identical under one specific illuminant)(see figure 2.2).

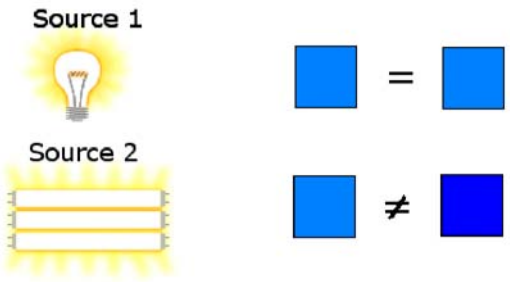

Figure 2.2: Example of metamerism: two patches match under one illuminant but appear different under another illuminant.

In the case of skin, colour is conditioned by the spectral energy (response) of the illuminant and the skin composition. The spectral response resulting from the interaction of the light with the skin is a combination of selective absorption and scattering of specific

light wavelengths due to the physical properties of chromophores composing the skin [Anderson and Parrish, 1981].

One pitfall of colour analysis is due to the spectral sensitivity curves of the three cones which overlap each other. Consequently, dermatological diagnoses that rely mainly on skin colour through visual analysis are limited due to the poor colour discrimination of the human eye and brain as well as the poor visual memory for comparisons at different times. Therefore, visual diagnosis of lesions made by dermatologist may not result in an absolute decision. When doubt arises for a lesion, skin diagnosis golden rule remains the histological examination of a skin biopsy which is an invasive technique that is costly and time consuming. It can also result in unwanted side effect such as scar and/or infection. Practitioners may benefit from faster and reliable mean of analysis that can enhance their diagnosis.

Nowadays, intensive researches aim to increase the amount of data available to the dermatologist by improving the diagnostic made from visual analysis, thus targeting to avoid unnecessary skin biopsy and delivering more objective assessment. One study, by Pearl *et al.* [Pearl et al., 2009], shows that accurate clinical diagnosis depends on the experiences of the clinicians and improves the diagnosis correctness from 53.3% to 65.0% after a period of one year. The aim of imaging system in dermatology is to acquire spatially distributed information for diagnostic purpose. One reason to employ non-invasive imaging technique is to add objective and quantitative assessments to dermatologist subjective impressions and qualitative descriptions of lesions. Such system can be adjunct to the eye in the diagnostic process or in some case even surpass its capacity. The benefits of moving toward new imaging technology are among others higher accuracy, repeatability, time invariant.

In the scope of this review, imaging technologies focus on non-invasive technologies that are easily available to dermatologist. These imaging techniques are limited to the ultraviolet (UV), visible (VIS) and near-infrared (NIR) electromagnetic spectrum. These technologies include dermoscopy under its various forms, spectrophotometry, multispectral imaging system and hyperspectral imaging system. Other non invasive imaging techniques such as Optical Coherence Tomography (OCT), Magnetic Resonance Imaging (MRI) and Ultrasound Imaging also exist for the analysis of skin lesions but are generally employed for research purposes rather than daily clinical analysis. The herein mention of these techniques is only for information purpose as we want to study system that can be easily available to dermatologists.

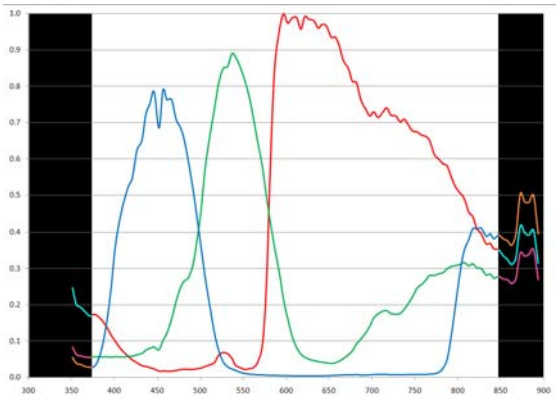

Figure 2.3: Example of spectral response: Nikon D80 CCD sensor. [Verhoeven and Schmitt, 2010].

2.1 Digital Imaging in dermatology

Conventional colour imaging devices define each pixel as a combination of the three primary colours using trichromatic model [Rowe, 2002], reflecting the sensitivity of the eye. These bands, when taken separately, are grey-level contrast images which correspond to large spectral bands (see figure 2.3) of their respective red, green and blue spectrum band (constrained to the visible spectrum). The perception with a trichromatic model is sufficient to characterize any colour in regards to the human eye.

With the cost decreasing and the resolution and capacity storage increasing over the last decades, digital imaging has been used more and more in dermatological practise. Digital imaging in dermatology aims to provide extra information to the practitioners such as clinical visualization (temporal monitoring), quantification and diagnostic classification. Digital images are acquired to provide baseline of the skin condition evolution. There is an improvement of dermatologist awareness of use of digital images in clinical practice [Perednia, 1991] and most dermatologists consider baseline photography useful in the follow-up of skin lesions [Nehal et al., 2002].

Digital photography offers a wide range of combination, with different configuration possible, with type of image sensor (CMOS or CCD), the spatial resolution (2,3,10 Megapixel), the colour resolution (8, 12, 16 or 32 bits), the colour space representation (RGB, CMY, HSI, L*a*b*, etc.), the lighting that can be added, the magnification (different lenses) and possible calibration. One problem with digital imaging is standardization as there are many technical factors influencing the image quality such as the camera sensor type, the resolution, the use of filters, the type of lighting. These multiple configurations

affect the diagnosis accuracy [Loane et al., 1997].

RGB cameras are easily available and practical to use. It is often used to record visual temporal information about a lesion. However, RGB colour cameras are conceived on the eye response to light meaning that it suffers from the same limitations. The large spectral bands offer very limited spectral information and set serious limitations in the detection and identification of tissue.

Clinical photography of skin lesions are affected by the type of illumination device equipping the camera. Different type of camera illumination device can be employed, ring-type electric flash, standard light source, fluorescent light among others. One pitfall arises with theses equipments because the quality of the reproduced images is different from the actual skin lesions seen by the human eye [Ikeda et al., 2003], possibly affecting the analysis. To standardized visual colour assessment, coloured reference samples are used (Munsell hue chart, MacBeth chart). These techniques, while improving the reliability of the colour designation, still suffer from illumination conditions which have to be kept similar to be useful.

Photography can help to some extent to compare current state of lesions with previous images acquired (see table 2.1). However, some limitations have to be taken into account as most digital camera are designed for user preference and the RGB signal does not correspond to objective colour information. When signal is represented by colour space, the colour space is defined under a specific illumination (i.e. D65 or D50 standard illuminant), meaning that images acquired under different illuminants may not reflect objective colour information. Digital photography brings the first quantification possible in term of RGB or other colour space leading to limited quantification.

	Pros	Cons
Digital camera	• Good spatial resolution • Storage capacity • Affordable	• Limited spectral resolution • Illumination sensitive • Wide choice of configuration

Table 2.1: Pros and cons of digital camera in dermatology.

Attempt to measure erythema and pigmentation using digital cameras seems to work properly [Yamamoto et al., 2008]. However there is limitation in the reproducibility of

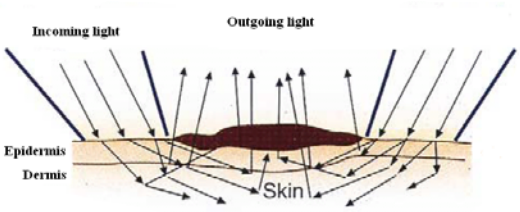

Figure 2.4: Transillumination of a lesion. This allows the visualization of sub-surface structures not seen with the unaided eye [Marghoob et al., 2003].

this study because the value acquired are camera and acquisition condition dependent (the distance between the skin and illumination). RGB sensors limitations arise due to the broad and overlapping spectral sensitivity of the three RGB sensors, affecting the unmixing accuracy of the method applied [Ruifrok and Johnston, 2001].

2.2 Dermoscopy

Dermoscopy is a non-invasive surface microscopy technique which is used for *in vivo* examination of the epidermis and papillary dermis [Soyer et al., 1987]. Dermoscopy can also be referred to as dermatoscopy, skin surface microscopy, *in vivo* cutaneous surface microscopy, epiluminescence microscopy. It is considered as a tool in between macroscopic clinical dermatology and microscopic dermatopathology. Dermoscopy brings new morphological criteria for the differentiation of melanoma compared to other melanocytic and non-melanocytic pigmented skin lesions. A dermoscope can be seen similar to a magnifying lens. It can contains extra features such as a built-in illuminating system, a higher magnification, the ability to observe structure up to the reticular dermis and record capability to follow-up patients from its digital version.

Description:

The principle of dermoscopy is transillumination which throws a strong light through an organ or part of skin as a mean of diagnosis of a skin area, generally lesions, seen through a high magnifying optics. This technique uses the fact that light incident on skin experiences reflection, refraction, diffraction and absorption. The physical properties of the skin are the source of these phenomena. It is briefly shown in figure 2.4. It allows visualization of subsurface anatomic structures of the epidermis and papillary dermis which would not be discernible to unaided eye.

The stratum corneum is rendered translucent with different techniques (oil and incident

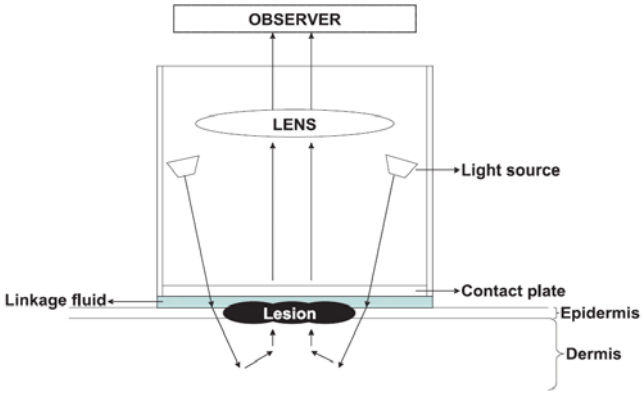

Figure 2.5: Optics of Dermoscope. The refracted light transilluminates the lesion while passing through it and is perceived as a distinct pattern [Nischal and Khopkar, 2005].

light magnification, polarized light, computerized systems, etc.). It allows the visualization of *in vivo* pigmented anatomic structures of the epidermis, dermoepidermal junction and superficial papillary dermis. In Figure 2.5, the principle of dermoscopy is presented. There is oriented light (at a certain angle, +/- 20) around the lesion which enters in the skin. Light is reflected, refracted, diffracted and/or absorbed, then part of the light is backscattered through the lesions, revealing the anatomic structures.

There are two main types of dermoscopy, there is conventional **Non-Polarized light Contact Dermoscopy (NPCD)**, **Polarized light Dermoscopy (PD)** (which can be divided into Contact (PCD) and Non-Contact Dermoscopy (PNCD)). An example of the obtained images using different types of dermoscopy is shown in figure 2.6.

For NPD, the technique requires a liquid interface to prevent surface reflection. It eliminates the surface scattering by minimising the change in refractive index at interface air/skin. Immersion liquid, such as mineral oil, water or alcohol, has a refraction index relatively equal to that of skin. Direct contact between the skin and instruments is made using a glass interface which has a refractive index (1.52) close to that of skin (1.55) [Nischal and Khopkar, 2005] and is enhanced when placed over immersion liquid-applied skin. The refraction index of the immersion liquid and the glass plate mounted on the dermoscope corresponds optically to the stratum corneum. This mechanism makes the stratum corneum translucent and reduces the amount of light reflected at the skin surface. It is considerably valuable as it reveals structure beneath the stratum corneum.

For Polarized light Dermoscopy, the incident light is polarized and a polariser (filter mounted in front of the lens) blocks the reflected light, allowing only light which has been

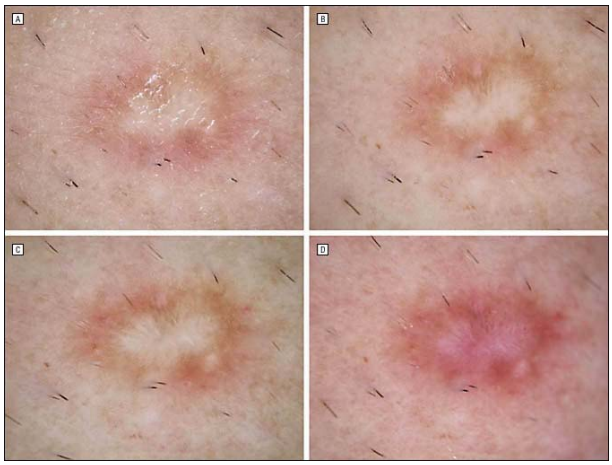

Figure 2.6: Images of a classic dermatofibroma obtained using 3 methods. A, Close-up clinical image. B, Non-polarized Contact Dermoscopic image. C, Polarized light Contact Dermoscopic image. D, Polarized Non-Contact Dermoscopy [Agero et al., 2006].

scattered within the skin to be viewed, leading to better visualization of pigmentation [Arrazola Peter, 2005]. Such dermoscope employs the property (see figure 2.7) that linearly polarized light (within the visible range) is partly reflected directly by the upper skin surface layer (stratum corneum) and partly scattered in the deeper layer of the skin tissue. Most of the polarized light conserves its state, while the light, diffused back-scattered, gradually becomes depolarized. The light emerging through the skin surface goes through the second polarized filter. Through cross polarization the lighting is polarized vertically and the lens horizontally. Thus, reflections on the skin are completely eliminated.

For PCD, a liquid interface and direct contact with skin surface is compulsory whereas for PNCD, there is no need of liquid interface neither direct contact with the skin. PCD and NPCD yield mainly similar patterns but have difference in vascular structures, colour variation, pigmented distribution which are complementary for both techniques. The different dermoscopy technique can be coupled with a digital camera. This dermoscope digital system allows monitoring and better follow-up of lesions.

Non-polarized versus polarized light and non-contact versus contact dermoscopy provides fairly different appearance of the examined lesions in regards to colour and visualization of vessels according to [Benvenuto-Andrade et al., 2007, Wang et al., 2008]. They also stated that most dermoscopic structures had a fair to perfect agreement with some exceptions.

Considering its advantages (see table 2.2), dermoscopy improves the diagnostic accu-

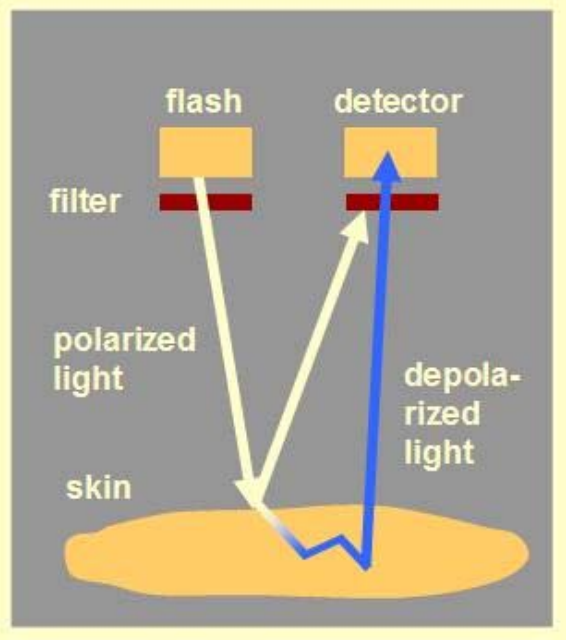

Figure 2.7: Schema of skin cross-polarization [WheelsBridge, 2008].

racy for pigmented lesions after a brief training period [Rigel, 1997]. According to [Argenziano et al., 2002] and [Lorentzen et al., 1999], dermoscopy has an impact on the clinical management of pigmented skin lesions. But in clinical setting, this improvement is not verified [Soon et al., 2003].

	Pros	Cons
Dermoscopy	• Good spatial resolution • Limited depth information • Affordable	• Limited spectral resolution • Illumination sensitive

Table 2.2: Pros and cons of Dermatoscopy.

2.3 Spectrophotometry

Among non-invasive imaging techniques used to help clinician, in-vivo optical spectroscopy is a technique that proves to be potentially useful [Bigio and Mourant, 1997]. A reflectance spectrum provides precise objective physical information compared to colour measurement which is a subjective information based on the human colour vision system. One major interest of spectroscopic approaches lies in the fact they have a high sensibility and acquires quantitative data. This allows the detection of skin condition at early stages before it is not even visible to the human eye and can also be applied to physiological assessment parameters, skin monitoring, and treatment evaluation.

The principle of spectrophotometry is based on the study of the interaction of molecules with electromagnetic radiations. The technique is influenced by the absorption, scattering and emission properties of the skin. Spectral emission of a tissue returns information about its histological, morphological and biochemical properties.

Basically, a spectrophotometer is a combination of a spectrometer and a photometer, the former is a system that emits light and the latter is a system that converts photon into an electrical/digital signal in between these two elements, a prism or similar optical equipment is used to disperse the re-emitted light from the skin into numerous wavebands. This setting forms the fundamental instrumentation required to perform spectrophotometry. Spectrophotometry measures the light intensity as a function of wavelength in the form of spectra. This type of measurement is directly linked to the physical light property over the entire spectrum (UV, VIS, VIS+NIR, NIR, IR) of a sample studied, meaning that it is not affected by metamerism condition or change of illumination as the measurement area is concealed from possible outside light perturbation. It has been demonstrated that measures of skin colour via spectrophotometry are reproducible, not affected by ambient lighting and independent of skin pigmentation [Corporation, 1998, Levine et al., 1991].

Different optical spectroscopic techniques can be employed such as diffused reflectance spectroscopy, fluorescence, Raman and multimodal spectroscopy.

2.3.1 Diffuse reflectance spectroscopy

Diffuse Reflectance Spectroscopy (DRS), also called elastic scattering spectroscopy, is a technique based on the mechanisms of wavelength dependent scattering and absorption properties of the skin but also on the skin architectural features. Elastic scattering refers to the interaction between photons and particles of the medium in which photons keep their initial energy. This phenomenon means that there is no modification of the photon

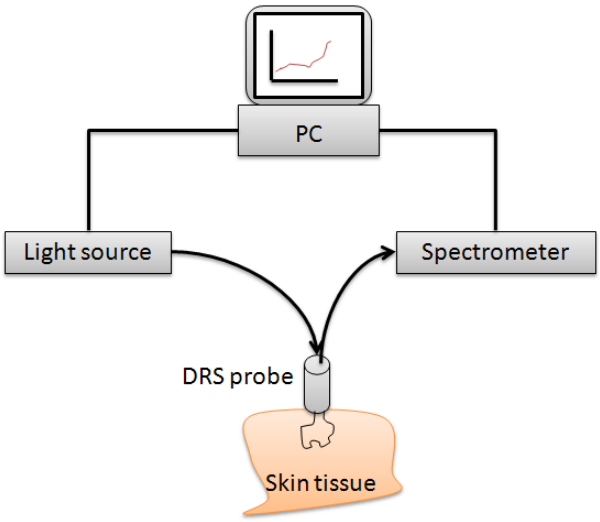

Figure 2.8: Diffuse Reflectance Spectroscopy system.

wavelength but changes in its propagation direction can occur. A light beam of wavelength λ going through an inhomogeneous medium can propagate itself in the medium following its initial direction, or be deviated once (simple scattering) or several times (multiple scattering) or can be absorbed. The scattering can be either Rayleigh scattering, in which dimension of the particles is much smaller than the wavelength of the incident beam or Mie scattering in which dimension of the particles is similar or superior to the wavelength of the incident beam. In case of Rayleigh scattering, the scattering probability decreases as $1/\lambda^4$, with λ, the wavelength value whereas in case of Mie scattering, the scattering effect will decrease less rapidly with wavelength.

Basic description of DRS uses a white light source (with broad bandwidth property) which is carried out by a bundle of multiple optical fibres to the probe head or integrating sphere (with diameter of 0.2 to 0.4 mm for fibre and 3 to 8 mm for integrating sphere), in contact with the skin. The light illuminates and penetrates the skin sample area. The incident light on skin sample is partly reflected, absorbed, affected by multiple scattering and re-emitted. A "reading" optical fibre/integrating sphere collects the diffuse light back to a spectrometer for acquisition, where the light will be converted into a digital signal in the form of a amount of light per wavelength (spectrum) (see figure 2.8).

Spectrometer detector is usually a linear array sensor where dispersed light is imaged on. The detectors are usually based on CCD silicon technology as it tends to be more efficient at some wavelength than others. The wavelength sampling is the relation of dis-

persed light over the size of the array detector. The dispersed light is split into wavelength by a diffraction grating. There are two possible positions for the dispersing element in the optical path. It can be located before the sample so the incident light illuminates the sample at a single waveband (monochromatic) and every band is acquired sequentially. It can and mostly is positioned after the sample to allow acquisition in a single shot. The sample is illuminated by a light source covering a large spectrum (polychromatic illumination) and the illuminated sample light is dispersed into the detector.

Spectrophotometer measures a ratio value (between 0 and 1 or 0 and 100%). The reflectance value is obtained after a calibration step which takes into account the intrinsic wavelength dependence of the detector as it has different efficiency over its wave-range. A spectrum is a ratio of reflected sample light divided by the reflected light from a reference white surface (called diffuser).

After illuminating the skin, two types of light are returned to the observer, specular light and diffused light. The former is determined mainly by the surface properties (hence containing limited skin composition information and representing 4 to 7% of the light reflected from the surface according to Anderson *et al.* [Anderson and Parrish, 1981] and Takiwaki *et al.* [Takiwaki, 1998]). The latter is a result of the scattering and absorption properties of the skin, called diffuse reflectance. The diffuse reflectance from the skin is linked to the ratio of the scattering (μ_s) and the absorption (μ_a) coefficients of the chromophores within the skin. Different skins yield different reflectance spectrum due to the unique chromophore composition of each skin but even spectra measured at different body locations on the same person can vary greatly. Healthy skin and disease tissues have different reflectance spectra, hence yielding important diagnostic information.

For this reason, diffuse reflectance should be measured instead of surface spectral reflectance which does not contain skin composition information. This type of measurement is achieved by choosing the right position/orientation of the light source to prevent direct illumination at the surface of the skin allowing only diffuse light to be measured. This aims to render the stratum corneum translucent similarly to oil/polarized light technique used in dermatoscopy.

An integrating sphere is used to produce a diffuse source of light (Lambertian illumination) and to collect diffuse light from the skin (figure 2.9). For illumination by optical fibres, the delivery fibres are often placed around the central collection fibre for homogeneous lighting.

Mehrube *et al.* [Mehrubeoglu et al., 2000] presents an "imaging" diffuse reflectance spectroscopic system which is a line of fibres which acquires the skin response from the

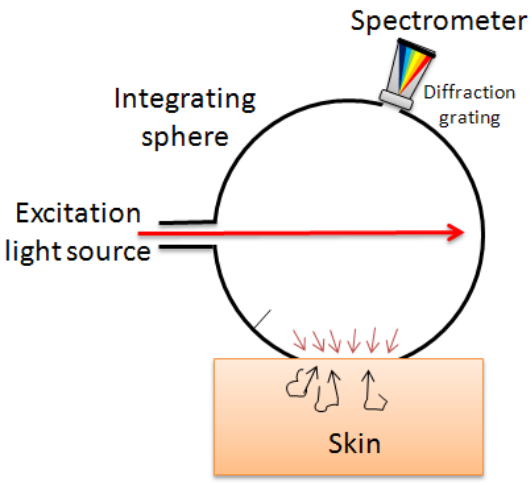

Figure 2.9: Diffuse Reflectance Spectroscopy using an integrating sphere.

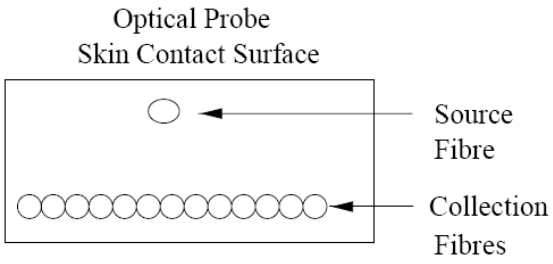

Figure 2.10: Fibre optic Diffuse Reflectance Spectroscopy by Mehrube *et al.* [Mehrubeoglu et al., 2000].

illumination by a single optical probe (see figure 2.10). The acquired data is a two-dimension image where the x axis represents the fibres location and the y axis is the spectral information. The image acquired is analysed in terms of texture information for classification of skin lesions.

The strong interest and research on diffuse reflectance spectroscopy resulted on the commercialization of several devices (Zeiss, Minolta, Spectral research). These devices are usually hand-held devices and return diffuse reflectance spectra but sometimes additional information such as L*a*b coordinates. However, they are often limited to the visible light spectrum.

Commercial spectrophotometer like Minolta CM-2600d is based on an integrating sphere probe to acquire reflectance spectra in the range of 360 to 740nm with a wave-

	Pros	Cons
Diffuse reflectance	• Strong signal intensity • Good signal to noise ration • Fast & easy	• Provides an average spectrum of an area • No spatial information

Table 2.3: Pros and cons of Diffuse Reflectance Spectroscopy.

length pitch of 10 nm. It can also provide simultaneously two types of spectral data, reflectivity measurements (SCI standing for Specular Component Included) and Scattered light measurements (SCE standing for Specular Component Excluded).

The main advantage of diffuse reflectance spectroscopy (see table 2.3) is the strong intensity of the signal (several orders of magnitude compared to fluorescence signal) which results in a good signal to noise ratio with a relatively moderate equipment cost. This technique is fast (from few milliseconds to few seconds) and easy to set-up, even commercial device are available. However, there is limited to no spatial information from a single measurement and the diffuse reflectance spectrum is generally the average of a skin area.

Diffuse reflectance spectroscopy has been widely used in dermatology, particularly for the study of skin pigmentation [Hajizadeh-Saffar et al., 1990]. Reflectance measurement can provide information about the light scattering properties of the skin [Dawson et al., 1980b,Garcia-Uribe et al., 2011]. It can be used as a tool to quantitatively measure melanin and haemoglobin content of the skin [Zonios et al., 2001] but also other chromophores (carotene, bilirubin, etc.) and to determine skin hyperpigmentation and hypopigmentation (pigmentation index) [Gniadecka et al., 1996], inflammation and erythema among other studies. In vivo measurement can be done to gather useful information to aid in the assessment and diagnosis of a variety of dermatological conditions.

Narrow-band spectrophotometry are spectrophotometer device designed specifically to measure melanin and haemoglobin pigments. Narrow-band spectrophotometry systems are based on the model developed by Diffey et al [Diffey et al., 1984]. Usually portable, these devices require measurements at specific wavelength (absorption coefficient of melanin and melanin), for example the Mexameter©MX 18 (Courage-Khazaka Electronic, Köln, Germany [CK electronic, 2011]) uses lights at three wavelengths whereas the DermaSpect (Cortex Technology, Hadsund, Denmark [Cortex, 2011]) only emits light at two wavelengths. Narrow-band spectrophotometry systems are limited in their application

due to fewer information returned by this technique and low sensitivity.

Absorption spectroscopy is a method derived from diffuse reflectance spectroscopy [Stamatas et al., 2004] and absorbance is a unitless quantity. This absorption spectroscopy method uses the Beer-Lambert law, linking the proportionality between the absorbed light intensity and the quantity of absorbent material. In dermatology, absorption of light is of great interest and can be approximated by the theory described by Dawson *et al.* [Dawson et al., 1980a]:

$$\rho_r(\lambda) = log_{10}\frac{1}{\rho_a(\lambda)} \tag{2.1}$$

where λ represents a wavelength, $\rho_a(\lambda)$ is the light absorption coefficient and $\rho_r(\lambda)$ is the light reflectance coefficient.

The different chromophore proportions are estimated from their distinctive optical absorption characteristics which take into account the tissue scattering effect [Nishidate et al., 2004]. The development of this absorption technique is based upon simple model of skin, generally described by optically homogeneous layers. The model is inversely applied to adjust the optical properties until matching calculated spectrum to the measured spectrum [Wang et al., 1995]. This technique aims to retrieve concentration of specific chromophores.

2.3.2 Fluorescence spectroscopy

Human vision works in a very limited region of the electromagnetic spectrum, from 390 to around 750 nanometres. A large amount of information is available from other parts of the spectrum. For example, by using ultraviolet light, fluorescence spectroscopy information can extend the amount of information of skin condition available.

Over the last decades, advance in numerous research fields has been possible thanks to fluorescence spectroscopy, especially in biomedical diagnostic. In this domain, fluorescence spectroscopy has been exploited for the analysis of various biochemical molecules but also for the analysis of in-vivo human organs. Fluorescence technique is probably the most used spectroscopic technique at the research and clinical level [Ramanujam, 2000]. It is used to localize lesions and quantify the photodynamic treatment [Wagnieres et al., 1998] by the detection of endogenous and exogenous molecules.

Fluorescence is a subcategory of photoluminescence which is linked to the electronic states of a photon or molecule and refers to the emission of light called “cold”, occurring at low temperature in opposition to incandescence. Fluorescence is a result of light ab-

sorption. The phenomenon is influenced by a variation of the external electromagnetic field.

Physical principle of fluorescence involves the fact that a molecule can only exist in a limited number of discrete energy state corresponding to given electronic configurations. The radiative transition is the crossing of a molecule from an energy state to another by absorption or emission of a photon. When absorbing a photon of specific energy, the molecule is set to one of its vibrational level of the electronic excited state, acquiring an exceeding energy in regards to its fundamental state. This exceeding energy will be released in the environment under specific form, non-radiative relaxation (fast phenomenon which does not generate light emission), and fluorescence emission (the energy is lost by the spontaneous emission of photons, this process occurs in the order of few nanoseconds). Fluorescence emission generates a response at a different wavelength than the wavelength of illumination.

Fluorescence emission can be a result of either autofluorescence (also named endogenous fluorescence) or exogenous fluorescence. In the former case (radiative transition), the energy is lost by the spontaneous emission of a photon corresponding to the transitions of vibrational states by the molecule. This radiative process has duration of the order of few nanoseconds.

The use of ***exogenous fluorophores*** is a method that requires the ingestion by the patient of fluorophores which are accumulated essentially in the cancerous tissue, resulting in the generation of fluorescence by irradiation at a wavelength corresponding to its absorption spectra. Its measurement is determined by the fluorescence intensity of the irradiated area. Disease area tends to have higher concentration of fluorophore than healthy tissue leading to easier localization of the area of interest. However, this method is invasive and has potential risk.

The ***endogenous fluorophores*** imaging method is based on the known response of fluorophores to a specific light excitation ranging from UV to visible. Fluorophores naturally present in the skin tissue are likely to emit a fluorescence (endogenous) called autofluorescence. The number of fluorophores that are excited and the importance of their respective contributions by the skin autofluorescence emission depend on the wavelength selected to illuminate the tissue. Such method requires prior knowledge about the chromophore fluorophore characteristics. It requires filtering the emission and the reception of the data acquired by a spectroscope .

A large number of endogenous fluorophores are presents in skin tissue [Vo-Dinh and Cullum, 2003] and example of absorption and fluorescence emission spectrum of several

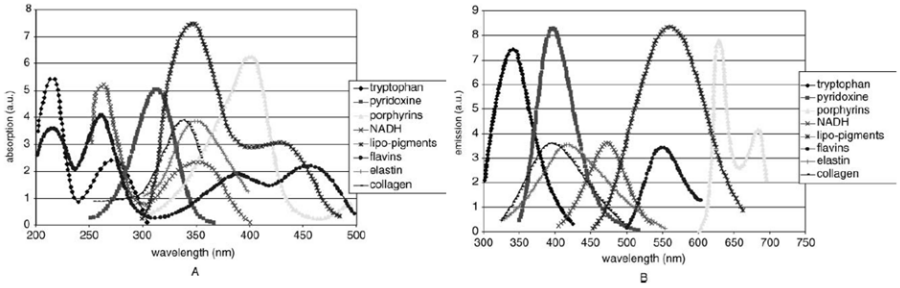

Figure 2.11: Absorption (A) and fluorescence emission (B) spectrum of several fluorophores present in tissue. (Adapted from [Wagnieres et al., 1998]).

	Pros	Cons
Endogenous Fluorescence	• No intake necessary	• Difficulty to extract information from multiple fluorophores • Weak signal intensity
Exogenous Fluorescence	• Strong signal intensity • One predominant fluorophore	• Fluorophore intake • Possible allergy • Limited selectivity

Table 2.4: Pros and cons of Fluorescence Spectroscopy.

fluorophore naturally existing in skin tissues is shown in figure 2.11.

This technique offers the advantage that the autofluorescence of healthy tissue versus disease tissues presents a strong difference of intensity and shape of the emission spectra. The tissue autofluorescence depends on several parameters which vary according to the nature (healthy vs. disease) of the tissue: concentration and spatial distribution of the fluorophores in the tissues, structure, pH [Ramanujam, 2000]. The autofluorescence intensity and spectral distribution are affected by the absorption and scattering optical properties of the skin. These properties, which are wavelength dependent, determine the penetration depth of the excitation light in the tissues and the fraction of fluorescence light collected.

Comparison of the pros and cons of the two types of fluorescence can be found in table 2.4. Autofluorescence spectroscopy tends to be more exploited than exogenous fluorophore techniques due to the constraint of the marker. The advantages of autofluorescence are its non-invasive technique and its spectral resolution that offers high sensibility in regards to the tissue biochemical composition. It seems contradictory but one drawback of autofluorescence arises from its large amount of information. The spectrum provides global information where amplitude variations are affected by the absorption from chromophores and fluorophores of the tissues. The acquired spectrum is a mix of several emission spectra and absorption spectra. The information need to be unmixed to be properly retrieved.

Fluorescence technique has the potential to perform real-time in vivo diagnosis directly on tissue, avoiding sample excision. It provides in vivo skin information [Gillies et al., 2000], which is an important information for dosimetry treatment but also for information on disease such as psoriasis, acne and non-melanoma cancer [Kollias et al., 2002] and hyperpigmentation [Kollias et al., 1997]. Fluorescence spectroscopy has been widely used in the analysis of cancer diagnosis.

2.3.3 Raman Spectroscopy

Raman spectroscopy is based on the phenomenon of inelastic diffusion of light which was experimentally observed by Raman and Krishnan [Raman and Krishnan, 1928] and depends on the vibrational energy level configurations of the biomolecule studied. The detection principle of Raman spectroscopy is a technique widely spread in biochemistry and biology where most of the molecules exhibit a Raman activity. Firstly used to study pure molecule in solution, Raman spectroscopy has been extended to cellular and sub cellular domain.

The Raman technique studies the vibrational transitions (wavenumber shift = 0 to 4000 cm^{-1}) from the process of inelastic scattering of light. The Raman effect is a result of the interactions of photons from a monochromatic light source with molecules of a sample. There are three possibilities of light scattering with only the last two being Raman scattering:

- No energy exchange after collision. The scattered photon has the same frequency as the incident photon. This type of scattering is called Rayleigh or elastic scattering (occurrence of approximately one over 10.000 photons).
- Energy exchanges arise between incident photons and the scattering molecules (from the photon to the molecule or vice versa). The scattered photon has either more or

less energy than its original electric state (incident photon). In Raman scattering, there are two types of scattering:

- When a molecule absorbs energy, the scattering is of **Stokes type**, the photon results in a lower energy which generate a Stokes line on the higher wavelength (red side) of the incident spectrum.
- When a molecule loses energy, the scattering is of anti-Stokes type, the incident photon is shifted to shorter wavelength (blue side).

The difference of energy ($1/\lambda$ in cm^{-1}) is measured as a difference between incident and scattered photons. A Raman spectrum plots scattered intensity as a function of the frequency shift (which is proportional to the energy difference). The wavenumber shift region between 200 and 2000 cm^{-1} is the most commonly used. A Raman spectrum is composed of several short wavebands, of 10 to 20 cm^{-1} spectral width. Each band characterizes a specific molecular vibration.

Raman spectroscopy detects the vibrational or rotational characteristic of molecules. Raman spectroscopy employs a monochromatic light that can be either in the near ultraviolet, visible and infrared range [Lawson et al., 1997]. Strong monochromatic light source is necessary as the Raman effect is weak (small occurrence), in the order of 10^5 weaker than the Rayleigh scattered component. The recorded frequency shift characterizes the molecule with which the photon collided. The spectrum obtained is characterized by a series of Raman bands which are linked to the various vibrational modes of the molecules. The signal resulting from this change of state is extremely weak and molecule concentration is proportional to the signal intensity. Moreover, the Raman peaks are relatively contained in short spectral bands.

Most biological molecules are Raman active. They have their own spectral signatures. It is therefore possible to quantify specific molecule from complex medium such as skin. Biochemical and structural modifications linked to the neoplastic transformation of tissues (mass of abnormal tissue) leads to a modification of the vibrational characteristics of molecule such as protein, lipids, generating a modification of the Raman spectrum. This modification reveals differentiation between skin tissues (see figure 2.12).

Raman spectroscopy is a promising techniques for biological tissues analysis for its real-time diagnostic capacity [Hanlon 2000] [Hanlon et al., 2000]. The use of Raman spectroscopy for diagnosis purpose is still at the research development stages [Choo-Smith et al., 2002, Pilotto et al., 2001]. It aims to provide non-invasive, real-time quantitative information.

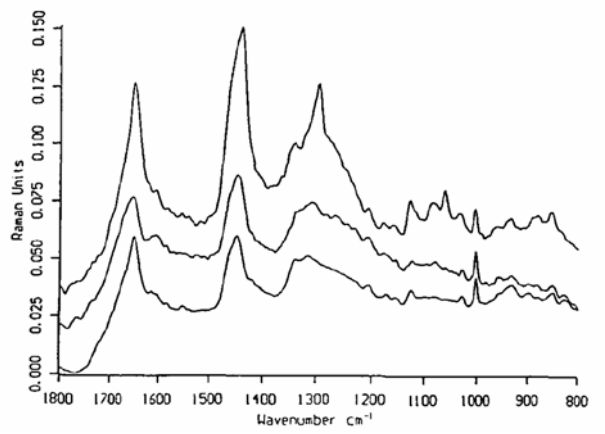

Figure 2.12: FT-Raman spectra of human stratum corneum (top), psoriatic plaque (middle) and callus tissue (bottom). Reproduced from [Edwards et al., 1995].

	Pros	Cons
Raman Spectroscopy	• No intake necessary	• Difficulty to extract information from multiple fluorophores • Weak signal intensity

Table 2.5: Pros and cons of Raman Spectroscopy.

The overall interest of Raman spectroscopy technique (see table 2.5) is that it provides rich information at the molecular and structural level as it gives information about the chemical tissue composition. The Raman effect is independent of the excitation wavelength used, which allows to eliminate unwanted phenomenon (such as fluorescence) by selecting an appropriate wavelength. Its main advantage results from a higher selectiveness compared to fluorescence. Its main disadvantage is linked to the difficulty to set-up an instrumentation clinically usable but attempt have been made using dual fibre probe [Myrick and Angel, 1990] or multiple fibre bundles [Ramanujam et al., 1996]. Also there is possible risk of noise in the acquisition process such as fluorescence signal when the monochromatic light is not carefully selected because the Raman signal is several orders of magnitude weaker.

2.3.4 Multimodal Spectroscopy

As seen from the spectroscopy techniques previously described, each specific spectroscopy technique provides complementary information on different aspect of the morphological and biochemical composition of tissues [Georgakoudi et al., 2003]. A fourth category called multimodal spectroscopy is the combination of at least two spectroscopy methods in order to gain additional information. However such techniques are only at laboratory development as no commercial system is yet on the market. Georgakoudi *et al.* also proposed bimodal [Georgakoudi et al., 2003] and trimodal [Georgakoudi et al., 2002] methods. Some works have been done using multimodal spectroscopy applied to in vivo diagnostic and discrimination of pathological states of biological tissues. Chang *et al.* [Chang et al., 2002] combines autofluorescence and diffuse reflectance to detect in-vivo pre cancerous lesions. They noticed an improvement of the specificity and sensitivity by combining the two techniques.

There has been increasing research of spectroscopy applied to skin. This technique grows rapidly with the development of commercial systems. The resulting applications are either for the measurement of reflectance or fluorescence which aims to quantitatively measure the composition of chromophores in the tissue or to assess the skin pathology.

2.4 Multispectral Imaging

A series of images acquired at different wavebands across the electromagnetic spectrum is called a multispectral image. It is represented by a series of monoband greyscale images. Decomposing the electromagnetic spectrum aims to capture information barely noticeable to the human eye and for some even invisible to it as this information is mixed between the three large spectral bands representing the trichromatic model.

It is known that skin has different properties related to the wavelength it is exposed. Moreover light of different wavelengths penetrates the skin at different depths. This property is of great interest for the evaluation of pigmented lesions under specific wavelength of light from Ultra-Violet (UV) to InfraRed (IR). A standard colour camera is composed of three channels (red, green, blue) but it is not suitable for skin spectral reflectance acquisition. Multispectral imaging system generally employs a grey level camera and acquires a sequence of images at different wavelength bands. Multispectral image data is useful for its extended spectral capacity, thereby reducing the effect of metameric mismatches that may occur with different illumination [Yamaguchi et al., 2008] and variability of the sensor spectral responses.

According to Nuhamara et *al.* [Numahara, 2001], digital imaging technology of high spectral quality is required in order to use images for diagnosis in dermatology. He recommends multispectral imaging technology to tackle the colour reproduction problem.

There are numerous techniques available to acquire spectrally resolved images. For these techniques, the spectral selective device can be inserted either in the illumination path (see figure 2.13(a)) or in the imaging path of light (see figure 2.13(b)).

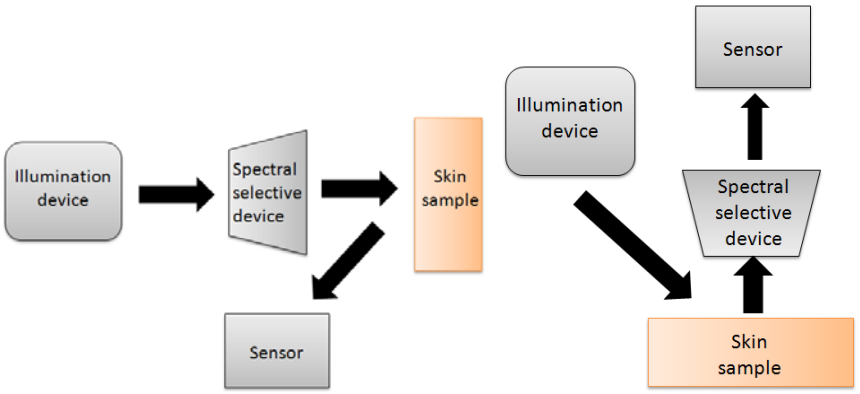

(a) Spectrally selective device in front of the illumination.

(b) Spectrally selective device in front of the sensor.

Figure 2.13: Possible position of the spectral selective device in the light path.

The motivation of MultiSpectral Imaging (MSI) is to go beyond the limited red, green and blue colour information available to the dermatologist. It aims to bring objective measurement of skin lesions. MSI combines the advantages of both spectrophotometer (spectral resolution) and digital camera (spatial resolution). MSI systems acquire three-dimensional data, two dimensional spatial information (x, y) and a spectral dimensional information (λ). The innovation with such acquisition devices is to provide spectral information for each pixel. The technology often requires calibration but the corrected information is a physical quantity, often the diffuse reflectance. Figure 2.14 illustrates the various approaches that can be employed for the acquisition of spectral data cube. The different technologies of MSI are divided into two categories: the spectral scanning and the spatial scanning techniques. The slit scan corresponds to the spectral scanning of the x line along the y axis. The plans named filters refers to the acquisition of an image at a wavelength λ while the point scan acquire spectrum for each x and y position of the scene.

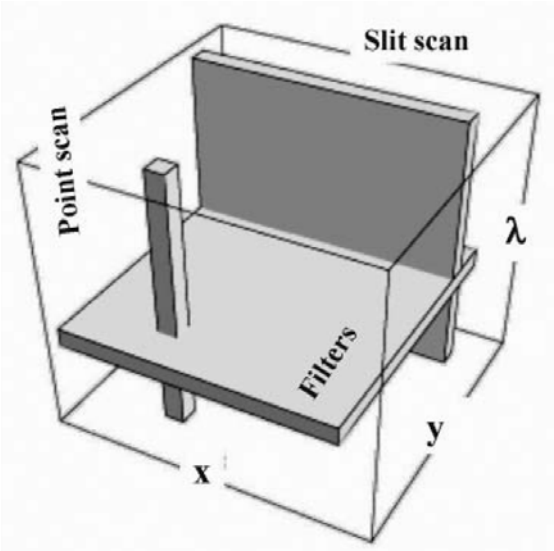

Figure 2.14: Illustration of various spectral cube acquisition processes, image from [Bearnam and Levenson, 2003].

2.4.1 Spectral scanning

Spectral scanning refers to the acquisition of spectral bands. The equipment consists of at least spectral imaging optics (filters) and a camera. The filters can be of two types, fixed filters or variable filters.

2.4.1.1 Fixed filters

One easy implementation of MSI is to use bandpass filters in the optical path of the system. The most common solution incorporates a set of bandpass filters into a filter wheel [Waggoner et al., 2001]. The recording is performed upon synchronized rotation of the wheel with the camera acquisition. The filters are successively placed in the optical path, performing the wavelength selection. This approach is flexible in regards to the large availability of filters with numerous specifications. Filters specification are fixed but they can have settings with different transmissions (depending on the wavelength of interest, the transmission is often superior to at least 70%), Full Width at Half Maximum (FWHM), central wavelength. So careful selection is required upon configuration. The advantages of this approach (see table 2.6) are its relatively low cost and the large selection available. However, it is not flexible in terms of filter specifications (apart from changing the filters) and in terms of number of filters slot available in the holding wheel.

	Pros	Cons
Filter wheel	• Low cost • High transmission value • Numerous filter specification	• Limited filter slot • Fixed configuration

Table 2.6: Pros and cons of Filter wheel systems.

Yamaguchi *et al.* [Yamaguchi et al., 2005] proposes a MSI system with 16 wavebands based on filter wheel applied to dermatology. The application focuses on inflammatory and immunologic disorder and use of MSI is proven to help differentiation between normal and abnormal skin. The system acquires a multispectral image in 10 seconds which is not suitable for daily practice. Vogel *et al.* [Vogel et al., 2007] also uses filter wheel to quantitatively assess tissue vasculature. Their system is composed of six narrow-band interference filters centred at 700, 750, 800, 850, 900 and 1000 nm.

2.4.1.2 Tunable filters

A tunable filter refers to a filter where the spectral transmission band can be shifted continuously along the electromagnetic spectrum at any wavelength λ within its defined spectral capability ranges. These filters can tune their spectral waveband electronically, modifying their waveband width and their central band. There are two types of tunable filters: Liquid Crystal Tunable Filter (LCTF) and Acousto-Optic Tunable filter (AOTF). Both tunable filters are polarization sensitive, affecting the transmission by at least half. This effect requires strong illumination.

Liquid Crystal Tunable Filters (LCTF) consists of a set of liquid crystal layers, each transmitting a number of different frequencies. Figure 2.15 presents the set-up of a LCTF which is based on Lyot filter. The device consists of a number of static optical stages, each containing a birefringence retarder stack between two parallel polarisers. The voltage tunes the retardance of each stage, affecting the band of constructive interference to yield the wanted wavelength.

The position of the bandpass can be easily tuned; however the bandwidth is fixed and characteristic of the device. The bandpass is wavelength dependent ranging from 10 nm at 550 nm to 16 nm at 700 nm. Currently the tuning time of commercially available LCTF

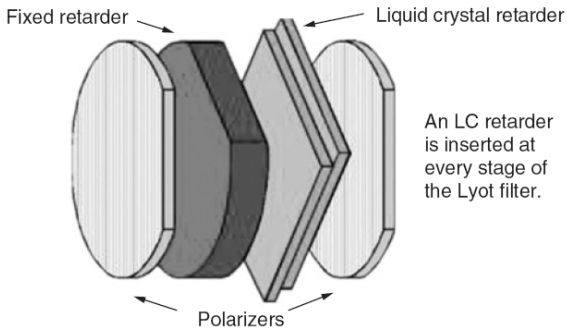

Figure 2.15: Different elements used for LCTF [Bearnam and Levenson, 2003].)

ranges from 50 to 75 milliseconds.

Acousto-Optic Tunable Filters (AOTF) are filters based on the interaction between a crystal lattice and an acoustic wave which are electronically controlled. AOTF works on the principle that an acoustic wave propagated through the crystal creates a grating obtained from alternatively compressing and relaxing the lattice. The modification of density changes the local index of refraction, acting as a diffraction grating to filter one wavelength. By modifying the acoustic wave frequency, the selected wavelength can be obtained from the resulting change of refraction index (see figure 2.16). The diffracted light wavelength is dependent on the acoustic frequency.

When multiple frequencies are affecting the crystal, a set of frequencies are simultaneously diffracted. In this condition, the filter can generate multiple bandpass at a time which makes it more flexible than LCTF which can only generate single bandpass. High-end AOTF offers the possibility to switch faster and to tune the wavelength, the bandwidth and intensity of the transmitted light.

The interests of both LCTF and AOTF (see table 2.7) are that they are not affected by mechanical constraints, image shift, speed limitation and vibration that are associated with the use of filter wheel. However, tunable filters have weak transmission (often in the order of 30%), requiring the use of strong illumination device to compensate this drawback. The disadvantages of AOTF are image shift, out of band rejection (wavelength leaking), also vignetting effect and weak transmission and bandwidth limited from 2 nm to 10nm.

A study by Shi *et al.* [Shi and DiMarzio, 2007] presents a multispectral system based on LCTF. The system has an 8nm bandwidth with transmission of only 25% to 35% for the range of 480 to 720 nm; the overall system is limited to acquisition in the range of 500 to 700 nm.

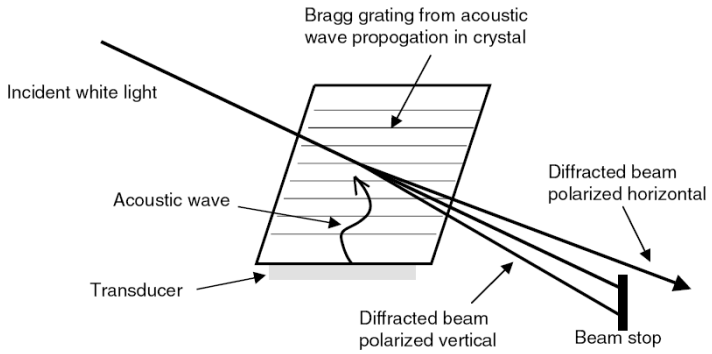

Figure 2.16: AOTF process [Bearnam and Levenson, 2003].

	Pros	Cons
Tunable filters	• Fast tuning time • Actively tunable bandpass • No mechanical constraints • No image shift (LCTF only)	• Limited transmission • Spectral leakage • Limited bandwidth selection • Vignetting effect

Table 2.7: Pros and cons of Tunable systems.

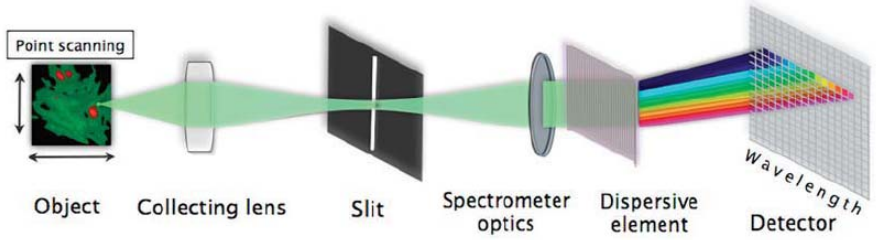

Figure 2.17: Point-scanning multispectral imaging system [Burton et al., 2009].

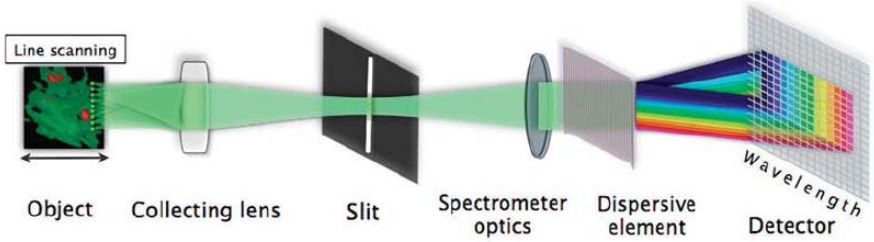

Figure 2.18: Line-scanning multispectral imaging system [Burton et al., 2009].

2.4.2 Spatial scanning

Spatial scanning, as indicated in its denomination, is acquisition of spectral information along a spatial dimension at a single time. Spatial information is obtained by scanning in spatial coordinates through the area of interest. Two techniques can be employed, single slit spectrometer and multi-slit spectrometer.

A **single slit system** scans a spectrum through x-y spatial coordinates. It is similar to spectrometer measurement but offers spatial dimension. It allows high spectral resolution but limited spatial resolution. Figure 2.17 describes the acquisition process for a single point scanning MSI system. A single spectrum is dispersed on a sensor and a data cube is obtained after scanning the object in both x and y direction.

A multi-slit system (also called push broom system) scans a line. It acquires an image onto a two-dimensional camera: spatial information is projected onto one axis and spectral information along the other one. Figure 2.18 describes the acquisition process for a line scanning MSI system. A spatial spectrum is dispersed on a matrix sensor (providing spectral information from a line in the area of interest) and a data cube is obtained after scanning the area of interest perpendicularly to the acquisition line.

Limits of these systems (see table 2.8) are due to the diffraction system employed

	Pros	Cons
Spectral scanning	• High spectral resolution	• Time consuming • Motionless object

Table 2.8: Pros and cons of Spectral scanning systems.

(prism, grating) and by the sensor wavelength sensitivity. These techniques are better suitable for motionless object.

Several research groups are currently working on the development of multispectral imaging system applied to dermatology. Such systems were initially developed in Italy by Marchesini [Marchesini et al., 1994] and other groups have since followed in UK [Moncrieff et al., 2002], US [Elbaum et al., 2001b] and also three commercial systems are available: Spectrophotometric Intracutaneous Analysis (SIA) scope [Cotton et al., 2001, Moncrieff et al., 2002], MelaFind [Elbaum et al., 2001a] and SpectroShade [Tomatis et al., 2005a, MHT Optics, 2011].

The main difference between the systems is their acquisition wave-ranges and targetted applications.

Melafind [Eosciences, 2011, Elbaum et al., 2001a] is an automated system providing a diagnosis. It is a system using multispectral illumination of clinical and dermoscopic images. The system is based on ten different, narrow-spectrum wavelengths (variable width in the order of 100 nm), from visible light to near-infrared spectrum (ranging from 430 to 950 nm). This system provides information on the absorption and scattering properties at different depths of lesions (see figure 2.19). It provides information not available by naked eye diagnostic. Its objectives are to be fully automated and to detect *in situ* melanoma. It is currently undergoing clinical trials in the USA and is awaiting FDA approval before being commercially available.

SIA system is considered as a skin chromophore imaging system. The system permits *in vivo* examination of a 12-mm diameter skin area which is captured at 8 different narrow spectra within 400 to 1000 nm range [Biocompatibles.com, 2011](see figure 2.20) and claims to measure up to 2mm beneath the skin's surface. The wavelength dependent images provide information about the concentration, distribution and position of skin chromophores such as collagen, melanin and haemoglobin. Siascope outputs graphs and images that requires interpretation to obtain a diagnosis.

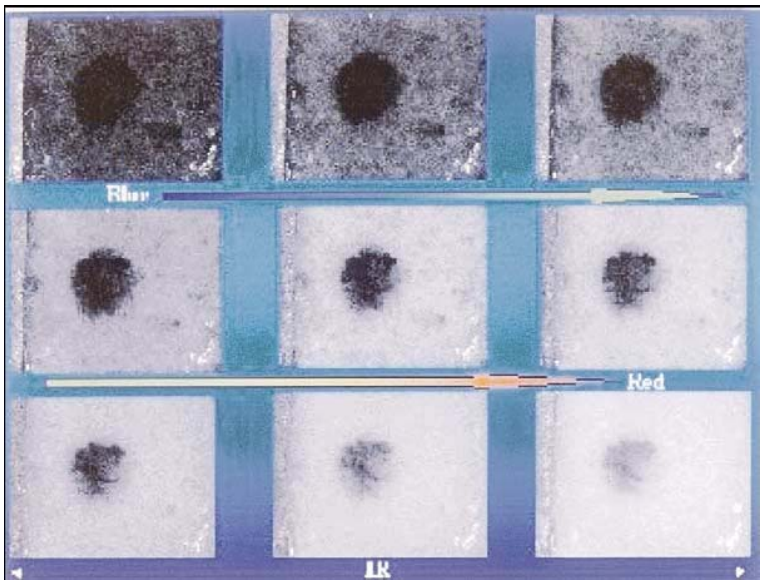

Figure 2.19: Each image in MelaFind is obtained with a different spectral illumination band, and therefore represents information from different depths in the lesions [Marghoob et al., 2003].

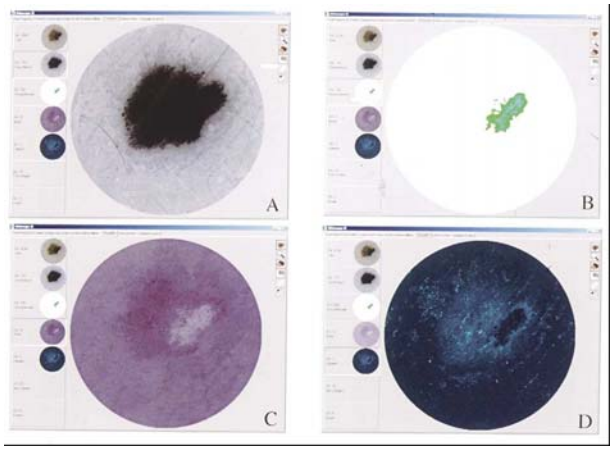

Figure 2.20: Siagrapgh of malignant melanoma. (A) Total melanin siagraph, (B) dermal melanin siagraph, (C) blood siagraph and (D) Collagen siagraph [Marghoob et al., 2003].

SpectroShade multispectral system acquires 15 wavebands ranging from 483 to 950 nm (with a bandwidth of 30 nm) and has mainly been used for melanoma studies [Tomatis et al., 2005a].

There are researches on several multispectral acquisition devices, based on monochrome camera with a Liquid Crystal Tunable Filter [Levenson et al., 2003] or a rotating filter wheel [Hill and Mancill, 1994, Tominaga, 1996, Yamaguchi et al., 1997]. Acquisition technique of multispectral images by light illumination modulation is a useful technique to obtain spectral reflectance information of an object [Martinez et al., 2002]. Several projects of multispectral imaging systems are still currently under development. Attempts have been made to acquire multispectral images from a single acquisition [Mathews, 2008, Yi et al., 2011] combining a CCD sensor with a diversity plate accommodating narrow bandpass optical filters. One application [Mathews, 2008] is oriented toward home-based health care for the detection of tissue abnormality [Yi et al., 2011]. Gomez *et al.* [Gomez et al., 2004] introduce a multispectral system based on Light Emitting diodes (LEDs) and integrating sphere. This system allows acquisition of up to ten different wavelengths from 472 to 940 nm. Their works focus on the suitability of their system to collect reproducible image and track evolution of skin diseases. Nakao *et al.* [Nakao et al., 1995] developed a real-time MSI system based on integrating sphere for mapping skin pigmentation. These techniques offer interesting multispectral capabilities however, they lack portability.

A new category, called HyperSpectral Imaging (HSI) system is currently investigated by several research groups, mainly in microscopy [Ornberg et al., 1999] [Rothmann et al., 1998] and also for *in-vivo* optical diagnosis [Vo-Dinh et al., 2004]. However limitations of HSI are generally their complexity, cost and acquisition time [Balas et al., 2001] which may be affected by camera displacement. MSI and HSI systems are different because MSI systems generally involve 4 to 20 spectral bands when HSI systems are capable of recording higher number of very narrow spectral bands (20 - 100) [Vo-Dinh et al., 2004]; hence the spectral resolution is higher for HSI.

Figures 2.21(a),2.21(b),2.21(c),2.21(d) are the decomposition into spectral bands of a skin lesion. The figures provide the different spectral channels given respectively by the eyes, a RGB camera, a MSI system and a HSI one. It highlights that the amount of spectral information about skin lesions is gradually increased from digital colour camera to HSI.

Most of MultiSpectral and HyperSpectral Imaging techniques require several exposures to acquire a data cube. Therefore, the acquired data have to justify the extra-time/cost

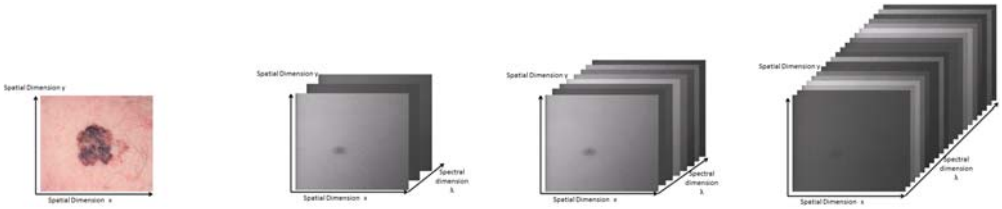

(a) Image seen by the eye. (b) RGB maps. (c) A multispectral image with 7 bands. (d) Hyperspectral cube.

Figure 2.21: Difference of spectral information.

in comparison to colour camera that acquires an image with a single exposure. When spectral acquisition is preformed successively, stacking together spectral data acquired even at short period of time might be affected by motion artefact. The justification is provided by the increased amount of information available about the skin reflectance not seen by the human eye.

Once a spectral image is acquired, several mathematical approaches ranging from spatial to spectral can be used to analyse the data. The analysis can be performed on the spectral image (corrected after calibration) or this image can be transformed from a spectral image to a reflectance cube. The state of the art of skin analysis techniques are presented in chapter 4. In the following chapter, we present our own imaging system for dermatological applications.

Chapter 3

Asclepios Acquisition System

Among the different techniques presented in chapter 2, each reveals specific skin information and they all have pros and cons. The classification of skin optical acquisition systems is divided into two categories: spectral and spatial. Two modalities arise from the previous state of the art, diffuse reflectance spectroscopy and multispectral imaging system, the former for its high spectral resolution and the latter for its spatial and spectral resolution (though lower than spectrometer). The analyses of skin lesions with these techniques have been mainly focused on melanoma [Tomatis et al., 2005b, Dominic and Moncrieff, 2001] and most of the systems neglect the possible analysis of other skin lesions.

Study by Tomatis *et al.* [Tomatis et al., 2005a] shows that cutaneous melanoma may have a different variegation above specific wavelength values as compared to non-melanoma, indicating that prospective study might have an impact on the diagnosis of several dermatological conditions. To allow prospective study of different skin lesions in daily clinical, a system must provide large spectral resolution, spatial information, reproducible acquisition, be practical to use and offering quantitative information about the skin.

Based on the principle of non-invasive light-tissue interactions [Van Gemert et al., 1989], we present the development of a new MultiSpectral Imaging (MSI) system combined to a neural-network based algorithm that reconstruct Reflectance Cube (RC) of cutaneous data. We detail the MSI characteristics and the reconstruction method employed. To conclude this chapter, we present the results of the reconstruction accuracy on synthetic colour patches and real skin data.

3.1 Objectives

Spectral characterization of numerous skin lesions is not a procedure widely performed but might prove to be potentially useful for diagnosis. In this chapter, our motivation is to develop a generic imaging acquisition system covering visible and near infra-red spectrum in order to measure optical reflectance of skin lesions. It aims to be a system for prospective study of different skin lesions in order to reveal possible lesion spectral signature.

Why a new system ? We can answer to this question by referring to the limitations of the human eye and current systems, either good spectral resolution but no spatial information (spectrometer) or improved spectral resolution with spatial information (MSI) or high spatial and spectral resolution (HyperSpectral Imaging) but long acquisition time.

Our motivation is to provide a system that acquires a multispectral image of the skin in the visible and near infrared wave range. This system must be suitable according to dermatological constraints: ergonomic design adapted to clinical environment and fast acquisition time. It must be easy to manipulate to allow comfortable acquisition. It aims to deliver diffuse reflectance spectra for every bidimensional skin area. The interest of such spectrum is to deliver information reproducible and independent of the acquisition conditions (ambient light, ...).

LE2I laboratory has been active in the development of the MSI prototypes for many years. Though, researches on the different systems have been mainly focused on the study of cultural heritage and agronomy measurement. Currently, the main multispectral imaging prototypes are composed of a camera associated with a motorized wheel holding a set of interferential filters in front of it (see figure 3.1). This type of multispectral camera has large size and is heavy, making it not pratical to hold and manipulate for acquisition on individuals. Also, it requires numerous calibration procedures [Mansouri et al., 2005b]. The calibration need to correct the positioning of filters in front of the lens, the induced difference of depth of field, the possible misalignement of filters with the sensor and necessitates to take into account the ambient light for every acquisition meaning that the system cannot be directly used in different environments.

This work is the continuation of a work initiated by Romain MARINELLI, apprenticeship engineer from the Engineering Institute ISTASE (University Jean Monnet, Saint Etienne, FRANCE). Following the initial design and development of a new system adapted to dermatological purpose, the first step is to evaluate the existing system developed and analyse the optimization to be made and the elements that can be used to fit the requirements. The second step consists of validating the system for dermatological applications

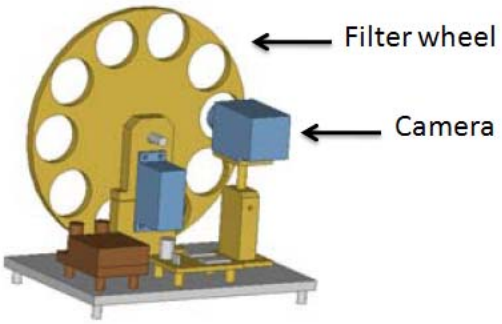

Figure 3.1: Presentation of a MultiSpectral Imaging prototype developed at LE2I where the wheel is positioned in front of the camera [Mansouri, 2005].

in real conditions.

3.2 ASCLEPIOS system

The system presented is called ASCLEPIOS, standing for Analysis of Skin Characteristics by Light Emission and Processing Of Image of Spectrum. The development of a portable integrated MSI system yielding reflectance cube is described. The multispectral system provides images of skin reflectance at several spectral bands (Visible + Near Infrared spectrum), coupled with software that reconstructs a reflectance cube from the acquired images. The reconstruction is performed by neural network-based algorithm. This yields to an increase of the spectral resolution without the need of an increase of the number of filters. Reflectance cubes are generated to provide spectral analysis of skin data which may reveal certain spectral properties or attributes not initially obvious in multispectral images.

The following parts present a description of the elements composing the system and followed by explanation of the neural network-based algorithm that reconstructs the cube from a multispectral image (see figure 3.2).

3.2.1 MultiSpectral Imaging system

A MSI system is generally composed of elements similar to colour acquisition system [Hardeberg, 1999b]. The main differences are that it has more than three channels and does not try to reproduce human colour vision system.

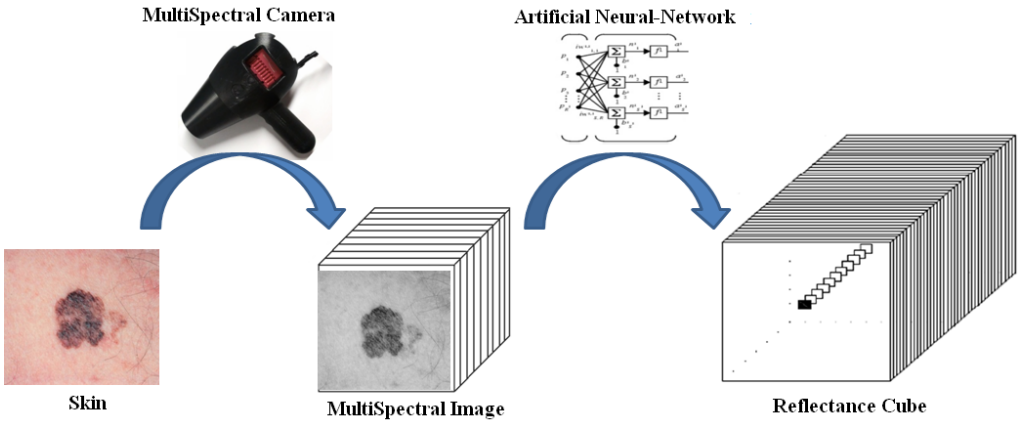

Figure 3.2: ASCLEPIOS system.

For MSI, two methods are usually employed to acquire spectral band images. One consists of placing a rotating wheel containing interference filters or a tunable filter In Front of the Camera (IFC). A second method is set by positioning the spectrally selective element In Front of the Illumination (IFI).

For ergonomic purpose, our acquisition system (see figure 3.3) is based on IFI and is decomposed in two parts: a light source compartment and a hand-held acquisition device, making the system more 'portable' to facilitate acquisition anywhere on the body. The design of the system is different from classical imaging system because it does not filter the incoming light but it filters the illuminating light source. Due to the clinical applications of the system, the IFI setting protect the system from external light which avoids the calibration for every acquisition made in a different environment as a result of the controlled illumation environment.

3.2.1.1 Spectral illumination

As we previously mentioned, for ergonomic and practical purposes, the illumination device is deported from the hand-held device into an illumination compartment. This compartment also houses the spectral selective device. This modification has the advantage to reduce the weight, the size of the hand-held device and reduce the number of calibration steps. This configuration provides light of different spectral wavebands. Each waveband light illuminates the skin which is the technique we used to produce multispectral images.

The choice of spectral selective device takes advantage of the knowledge gained from the several MSI systems developed by our laboratory. The choice of medium band interference

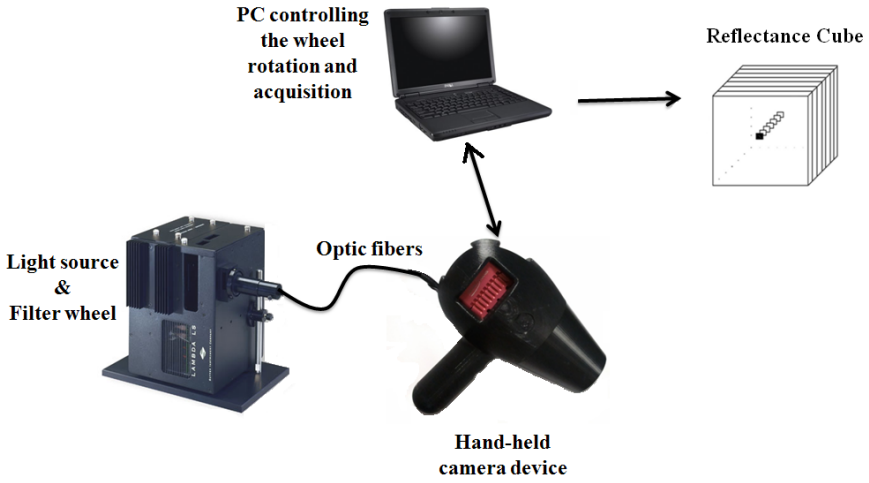

Figure 3.3: Description of the MultiSpectral Image System.

filters mounted on a rotating wheel for the spectral decomposition of the visible and near infrared wave range is due to the large offer available in terms of spectral bandwidth and transmittance. Methods using AOTF does not offer spectral bandwidth selection (fixed and depending on the wavelength) and have at best 50% transmittance. In addition to these limitations, the use of short band filters requires long acquisition time, increasing noise in the image.

The working range of the system should cover VIS+NIR. The light selected for our system is a Lambda LS Xenon Arc (Sutter Instrument). It is a 175 Watts light bulb with an output range from 340 nm to infrared light (see figure 3.4). The Lambda LS is pre-aligned to a liquid light guide connector to eliminate focusing and collimation problems. It offers a flexible direction of light output. Lambda LS lamp can accommodate a filter wheel within its compartment, reducing the number of components of the system in order to be easily transportable.

The spectral selective device is based on interference filters which are held on a filter wheel, housed in the lambda LS lamp. The filter wheel selected is a Sutter Instrument Lambda 10-3 (model LB10-NW) with 10 positions for 25 mm filters. It achieves switching times of 40 milliseconds between adjacent filters. The filter wheel controller is commanded by a laptop connected via an USB interface.

Therefore, we selected a set of ten medium bandpass interference filters from *CVI Melles Griot*. An interference filter is a multilayer thin-film device. It works similarly as first order Fabry-Perot interferometer where the air layer is replaced by a thin dielectric

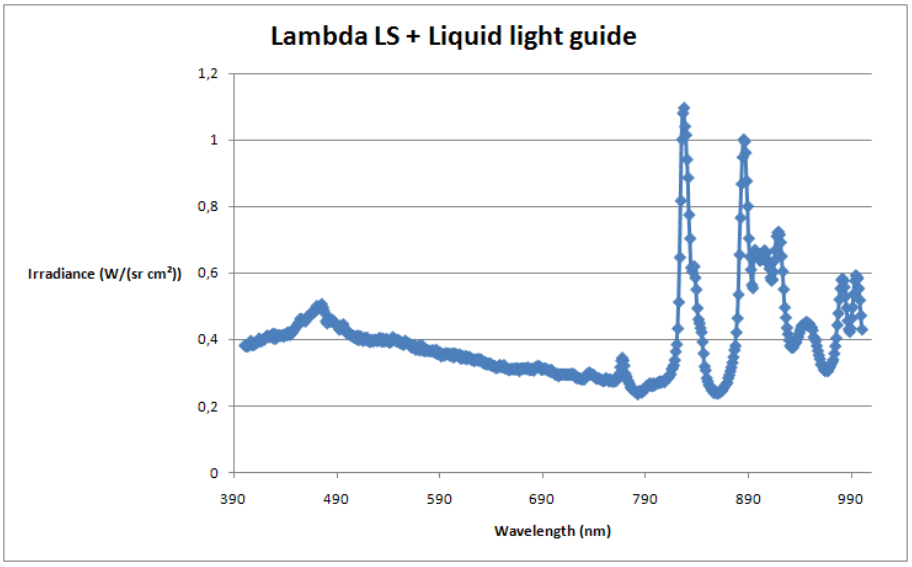

Figure 3.4: Irradiance of the Lambda LS Xenon Light and liquid light guide.

layer which the width determines the transmittance wavelength. The filters have been chosen to equally divide the spectral domain of interest (400 to 1000 nm) with FWHM of 80 nm and position every 60 nm at 420, 480, 540, 600, 660, 720, 780, 840, 900 and 960 nm. According to the filter characteristics, an overlay is necessary because the filter manufacturer guaranties a central wavelength tolerance of +/− 16nm. The filters have peak transmittances that range from 60 to 80% (see figure 3.5).

The system being used for prospective study, we did not perform a specific analysis to determine the number of filters to use, neither on their specific passband size in comparison to Preece and Claridge [Preece and Claridge, 2004] who study the selection optimization of spectral filters to recover human skin information only in the visible. They defined six filters from 450 to 700 nm to describe different elements of the skin (melanin, blood, papillary dermal thickness). However, each of these skin components has effect across the whole VIS+NIR range and every filter acquires information related to these parameters. The selected set of filters acquires skin component information and the following spectral reconstruction reduces the need of optimization as the waveband size does not affect the reflectance reconstruction accuracy [Imai et al., 2000].

The filter wheel gradually rotates to position each filter in the light path (between the light and the liquid light guide). The light at specific waveband is transmitted from the illumination compartment to the back of the hand-held device by the liquid light guide.

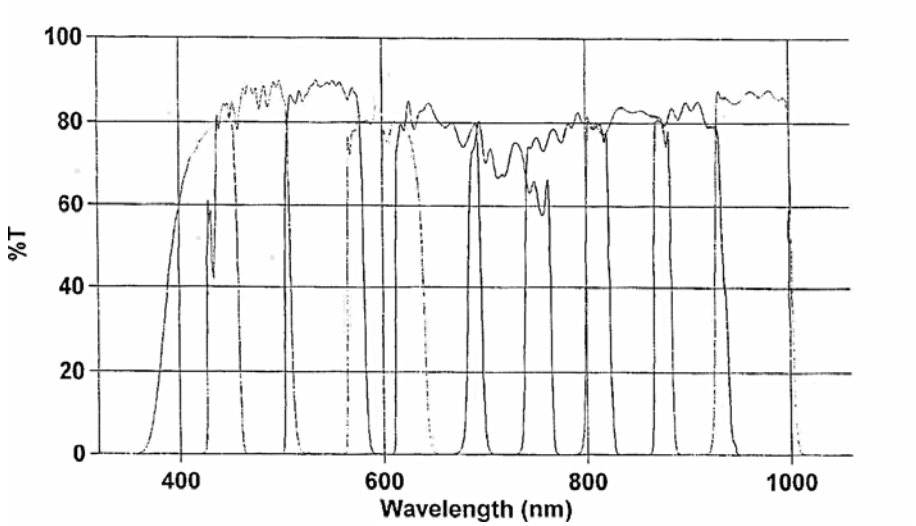

Figure 3.5: Spectral response of the set of 10 CVI Melles-Griot interference filters [Melles-Griot,].

3.2.1.2 Hand-held device - Camera and lens

The hand-held device is a light hair-dryer look-alike device. It is designed using CAD software to enhance the comfort of the handgrip and it is 3D-printed in light ABS plastic. The hand-held device is a light opaque device which is composed of a wireless trigger, a camera, a lens and liquid light guide. The extremity of the hand-held device is composed of a nozzle which sets a constant focus distance of 10 cm between the skin area and the camera.

The study range covers visible and near infrared domain. To match this requirement, we selected a camera with spectral response covering the wave range of interest. Our acquisition system is based on a CMOS camera offering a good sensibility in the visible and near infrared spectrum. The selected camera consists of a monochromatic CMOS digital sensor (Photonfocus Model MV1-D1312l-160-CL) with data coded on a 12 bit greyscale resolution and offers a 1.4 Megapixels resolution (1312 $\times$ 1082 pixels). The monochrome camera is based on a Camera Link© data transfer protocol, with acquisition rate of 108 frames per second at full resolution. We selected this camera for its extended spectral range covering from 350 to 1000 nm and especially for its excellent NIR response. Figure 3.6 shows the camera quantum efficiency as a function of the wavelength provided by the manufacturer [Photonfocus, 2010]. The Photonfocus camera has also the advantage to fit our portability constraint with its compact size of 60 $\times$ 60 $\times$ 45 mm and light weight of

265 grams. Camera Link© is a high-speed serial data transfer with data rate capabilities up to 2.3 Gb/s. A PCI Camera Link Image Acquisition card (National Instrument, model NI PCI-1426) is enclosed in a Magma ExpressBox to convert the PCI connector into a PCI Express cards for laptop usage.

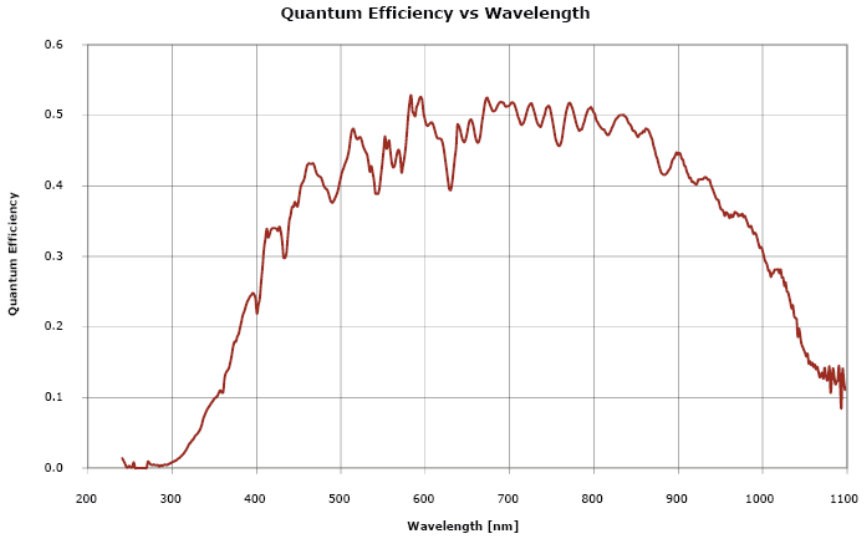

Figure 3.6: Spectral response of the PhotonFocus MV1-D1312-160-CL-12 [Photonfocus, 2010].

A C-mount lens (Linos model MeVis-C) is a C-mount lens developed for spectral range of 450 to 1000nm (VIS and NIR). The figure 3.7 presents the lens transmittance as a function of the wavelength. This lens is designed to provide excellent resolution, no brightness fall off or distortion across the full field. It delivers chromatic correction through the entire operating wavelength range.

The focusing and iris diaphragm are manually lockable. Tests have been performed to define suitable focusing and aperture for our dedicated dermatological application. Once the parameters selected, the configuration was locked to ensure reproducibility of the data over time. In the defined configuration, the lens provides an useful area of 32 $\times$ 38 mm with a depth field of 5 mm, yielding a spatial resolution of 33 $pixels.mm^{-1}$.

The parameterization of the exposure time is defined for a fixed aperture. It corresponds to the period of time during which the sensor receives light. This setting needs to be defined for each waveband due to the non uniform spectral response/transmittance of the different components of the system. The adjustment of the exposure time aims to gain most of the dynamic range of the camera without over exposition. The exposure

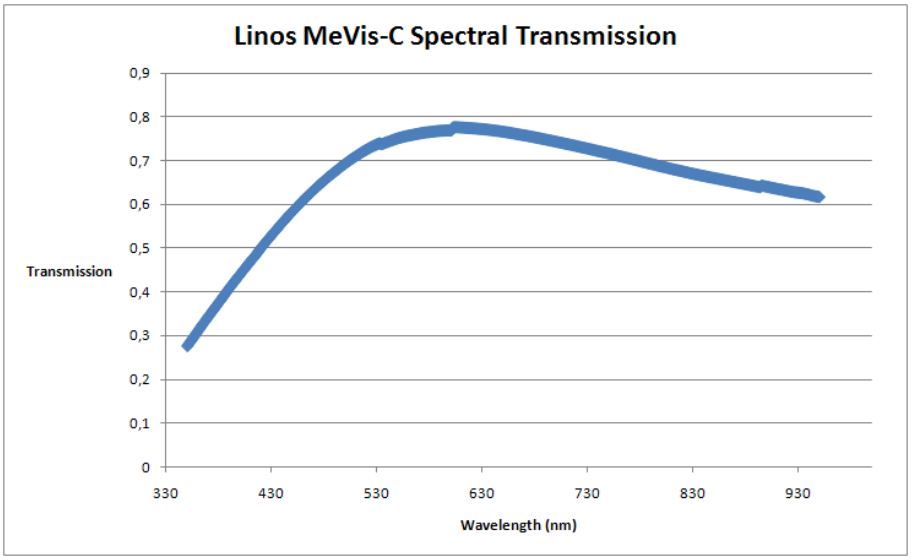

Figure 3.7: Linos MeVis-C Spectral transmission.

time for each waveband is selected by illuminating a reference Lambertian surface (Spectralon 99%) and increasing the exposure time before saturation of the sensor (by mean of histogram analysis).

The filter wheel controller and camera are provided with SDK (Software Development Kit) which allows development of external software to control the filter position/rotation, the camera acquisition, the exposure time and other parameters.

A C++ software controls the entire acquisition process. Considering the detailed configuration, the camera and liquid light guide are enclosed in the hand-held device protecting the acquisition of external light, thus the lesions are illuminated with light of a specific waveband. After positioning the hand-held device nozzle on the skin area under study, the user presses a wireless remote trigger located in the handle of the device. The pressure triggers the synchronised rotation of the filter wheel with the camera acquisition. The acquisition of a multispectral image composed of ten wavebands is performed in less than two seconds. The system is easily transportable as the whole equipment fits in a large suitcase.

Configuration of ASCLEPIOS system with controlled spectral illumination (protected against external light) and a fix set distance between the lesions and the camera allows the acquisition of sequential images over time for the detection of lesion changes [Vazquez-Lopez et al., 2003].

3.2.1.3 Calibration

The usual MSI optical path configuration using filter wheel In Front of the Camera has several drawbacks such as chromatic aberration, image registration due to the mechanical vibration of the system and dust or defects on filters are less noticeable when placed in front of the illumination. These drawbacks necessitate specific calibration [Folm-Hansen, 1999]. As we previously described ASCLEPIOS, IFI based systems offer normal CMOS calibration methods to be applied because there is no distortion problem in comparison to IFC method.

The aim of this section is to characterize the MSI system. The calibration purpose is to remove systematic noise introduced through the acquisition chain. Noise might cause a distortion of the real reflectance property of skin. Elimination of the noise is necessary to avoid possible incorrect reconstruction of spectra that could affect subsequent processing. Such effects are undesirable and need to be corrected. The calibration task is different for MSI system in comparison to single grey level one as the system acquires multispectral image meaning that each monoband image needs to be calibrated. This specificity is due to the fact that exposure time is different for each monoband image but also because dust or scratch might affect each filter.

A raw monoband image can be modelled as follow:

$$[R] = [O] + [U \times S] \tag{3.1}$$

where [R] is the raw image, [O] is the offset, [U] is the useful signal we want to extract and [S] is the sensor response. Using the cited modelled, it is necessary to calibrate, first the offset noise and then pixel gain.

The offset corresponds to the intensity values that the camera acquires when observing a black target. The offset frame is obtained by averaging multispectral images of a Spectralon© gray-scale standard target with 2% reflectance and is denoted [O] in equation 3.1 (it is noted O which stands for offset frame). This process sets the zero level of the camera sensor for every monoband image.

The [S] is in most cases characterized by uneven intensities in an image of a uniform surface. This effect is generally caused by non-uniform illumination, blemish on optical elements, difference of sensitivity within the sensor and vignetting. Flat-field correction is the technique that removes this effect. Its goal is to compensate any variation within the detector for a given amount of light. The acquisition of flat-field MultiSpectral Image is obtained by averaging MultiSpectral Image of a Spectralon© gray-scale standard target

with 99% reflectance across the visible and is denoted F and stands for the flat-field image.

The gain correction image is composed of specific coefficient for each pixel of each monoband image. The coefficients are obtained using the following formula:

$$[S] = \frac{[F] - [O]}{DR} \tag{3.2}$$

where F is the flat-field monoband image and DR is the Dynamic Range of the camera. In the case of ASCLEPIOS, DR is equal to 4.096, corresponding to 12 bits images.

The final correction of the raw image is applied using equation 3.2:

$$[U] = \frac{[R] - [O]}{[S]}. \tag{3.3}$$

The previous corrections suppose that the sensor has a linear response.

3.2.2 Reflectance cube reconstruction

A multispectral image is composed of the M monochromatic images (M being the number of filters used) where each pixel, which is a spatial sampling, carries spectral information in the form of a vector of scalar values measuring the electromagnetic radiation hitting the sensor, integrated on narrow wavebands.

The aim of reflectance cube reconstruction is to retrieve, from the camera signal, the spectrum in each pixel (linked to the physical property of the skin element). We call this mechanism spectral reflectance reconstruction. The difference between multispectral and hyperspectral cube comes from the fact that multispectral image have limited number of waveband images (4-20) in comparison to hyperspectral cube that have higher number of bands (20-100) with narrow width (1 to 20 nm) and that their bands are contiguous. HSI only increases the spectral resolution. Moreover, the acquired data, in both cases, contains the reflectance information of the subject acquired and the effects of the spectral response of the elements of the optical path. Whereas our reflectance cube reconstruction aims to only extract the reflectance information of the skin.

The reconstructed spectral volume of skin lesion provides a 3-dimensional volume (x,y,λ) where x and y are for spatial dimensions and λ for spectral dimension and is referred to as Reflectance Cube(RC). Figure 3.8 describes a reflectance cube which provides both spectral band image along the wavelength axis and a spectrum for a defined pixel.

According to Ribes [Rib és, 2003], there are three categories of spectral reconstruction

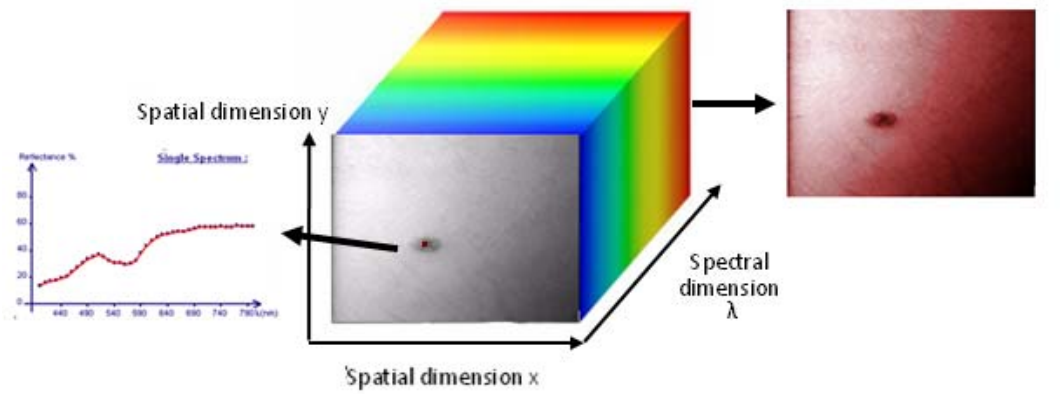

Figure 3.8: Reflectance cube description.

techniques based on different regularization method: interpolation, direct inversion and indirect inversion.

The former does not require any specific implementation to obtain reflectance spectrum while the two latter are based on the estimation of the spectral properties of the system elements.

Interpolation reconstruction method does not require knowledge of the spectral optical system response. The aim is to reconstruct spectrum directly by interpolating spectral information obtained from the acquisition. It considers filter as sampling function. It requires that the spectral response of the filters to be Gaussian at best, ideally as a Dirac. For a high quality reconstruction, it necessitates a high number of filters, thus increasing the acquisition time.

For direct inversion, it is required to individually characterize the spectral response of each element of the optical system. The characterization of each element being performed individually, it does not take into account the noise related to the acquisition conditions of an image. This leads to unstable operation. To correct this effect, it necessitate the use of approximation method to inverse the model such as smoothing [Neumaier, 1998], Hardeberg [Hardeberg, 1999a] or Wiener [Hardeberg, 1999a] regularization. Moreover, the reconstruction accuracy depends on the precision of the monochromator used for the characterization.

Indirect inversion reconstruction techniques do not require knowing the spectral response of the optical system. It aims to retrieve the spectral reflectance information using known spectral colour patches which are independent from the acquisition conditions. Non Negative Least Squares and Neural Network are among techniques of indirect inversion

reconstruction.

The hyperspectral cube is reconstructed using a neural network-based algorithm. While mostly used for classification purposes, it has been proposed by Mansouri *et al.* [Mansouri et al., 2005c, Mansouri et al., 2005d, Mansouri et al., 2005a] to reconstruct reflectance spectrum. The artificial neural network (ANN) is composed of two steps, learning and reconstruction step. In order to reconstruct spectra that are linked to the physical properties of the element being studied, the proposed method takes into account a model of light propagation, used to extract the reflectance information.

3.2.2.1 Spectral model

Figure 3.9 presents the model we use for decomposition of the spectral response of all the elements involved in the acquisition process. Such model aims at separating each element of the acquisition chain to remove unwanted information and to retain the reflectance information $r(\lambda)$ only.

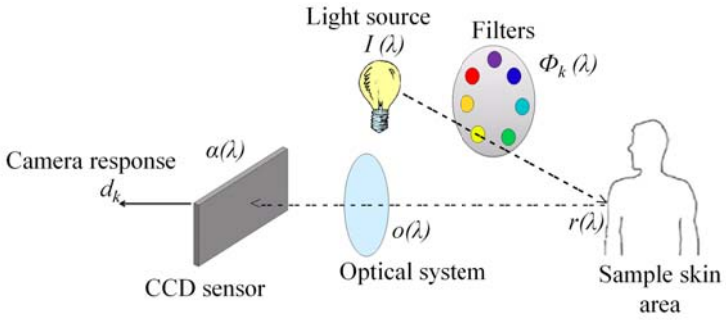

Figure 3.9: Synopsis of the spectral model of the acquisition process in a multispectral system.

By using this model, the signal d_k observed at the camera output, depending on the k^{th} channel, is given by the following equation:

$$d_k = \int_{\lambda_{min}}^{\lambda_{max}} I(\lambda)\phi_k(\lambda)r(\lambda)O(\lambda)\alpha(\lambda)d\lambda \tag{3.4}$$

where $I(\lambda)$ is the spectral radiance of the illuminant, $\phi_k(\lambda)$ is the spectral transmittance of the k^{th} filter, $r(\lambda)$ is the spectral reflectance of the skin, $O(\lambda)$ is the spectral transmittance of the optical system and $\alpha(\lambda)$ is the spectral sensitivity of the camera.

By considering a linear optoelectronic transfer function, $I(\lambda)$, $O(\lambda)$, $\phi_k(\lambda)$ and $\alpha(\lambda)$

can be substituted by the spectral sensitivity $S_k(\lambda)$ of the k^{th} filter (with k=1,...,K=10).

Then equation 3.4 becomes

$$d_k = \int_{\lambda_{min}}^{\lambda_{max}} r(\lambda) S_k(\lambda) d\lambda. \tag{3.5}$$

By sampling the continuous spectra λ to N regular intervals of wavelength, equation 3.5 can be rewritten in the form of a matrix:

$$d_k = r(\lambda)^t S_k(\lambda) \tag{3.6}$$

where $S_k(\lambda) = [s_k(\lambda_1)\ s_k(\lambda_2)\ \dots s_k(\lambda_N)]^t$ and $r(\lambda) = [\mathrm{r}(\lambda_1)\ \mathrm{r}(\lambda_2)\ \dots \mathrm{r}(\lambda_N)]^t$ are respectively the vector containing the spectral sensitivity of the acquisition system of the k^{th} channel and the vector containing the scene sampled spectral reflectance. ^{t} is the matrix transpose operator.

Using equation 3.6, first, the operator $S_k(\lambda)$ is retrieved. It characterises the spectral response of the system (including camera and illuminant); secondly, spectral reflectance curve for each pixel of the image is reconstructed using the operator $S_k(\lambda)$ and the MultiSpectral Image.

Considering this model, the reflectance spectra r is independent of the acquisition system and only depends on the skin characteristics.

3.2.2.2 Neural network-based spectral reconstruction

Following the model of light propagation, the reflectance spectra need to be extracted from the data. The reflectance spectra r needs to be estimated from the known camera response and the spectral sensitivity leading to an inverse problem. To reconstruct spectral reflectance spectra, Mansouri *et al.* [Mansouri et al., 2005c] suggested a robust method based upon neural network. Artificial neural networks overcome the problem that might occur with inverse problem such as slight variation in the input data (characterization of every element of the optical path) might alter the expected results. Moreover neural network has the advantage of being robust against noise. The choice of the artificial neural network-based algorithm for the reconstruction of reflectance spectra arises from the accuracy obtained by this method in comparison to direct inversion technique and interpolation reconstruction. Also, this process is working for ambient light condition, we want to apply it to our system and validate its effectivness with our new system configuration. Artificial Neural Networks (ANN) are modelled on the human brain. It

aims to mimic the function of biological neural networks. ANN models are composed of neurons which are linked to each other by synapses. These synapses have coefficients representing the weight of the connection. ANN learning process is accomplished by the adjustment of these weights yielding the neural network to output the appropriate results.

Neural network has the advantage of being robust against noise. For our system, the neural network task is to reconstruct reflectance cubes from multispectral images.

3.2.2.2.1 Learning process

ANN has to be configured, meaning that weights of the synapses have to be set to produce desired output for specific input during the learning process. Various methods exist to determine the correct weight of the different connections [Kröse and van der Smagt, 1996]. A Self-supervised learning is chosen to determine the correct weight of the different connections. Perceptron is a basic model of neural networks. It is a binary classifier where the output, which is function of the neuron activation, is either 0 or 1 for deterministic perceptron. Its aim is to establish an association between input and output but this limits the generalization capacity. Knowing that perceptrons give same response to same stimulus after training, the function that converts the activation into a response is modified. It is changed to give probabilistic response using Boltzmann distribution. Rather than outputting 0 or 1, this distribution delivers proportional response (restricted into the interval [0 1]).

Such perceptrons lead to the creation of associative memories, either hetero-associative or auto-associative. In case of auto-associative memories, stimulus is associated with itself and can be used to store stimuli. In case of hetero-associative memories, an input stimulus is associated to an output response whatever the size of the two vectors. The neural network employed in the spectral reflectance reconstruction uses hetero-associative memories due to its modularity in regards to the different sizes of the input and output vectors. Such neural networks have a capacity of generalisation meaning that a trained network can output expected data from input it has never seen before. In our application, it allows the reconstruction of spectra that has not been learned during the training stage. Such capacity improves the stability of the inverse problem.

The self-supervised learning method trains the network with provided input and known output. The learning process stops when the minimum of the validation error is reached. The rule of training applied is the Delta rule known as Widrow-Hoff rule which consists of continuous modification of the input connections weight ω_{ij} of the synapses in order to minimize the mean squared error of the neuron between an expected theoretical response

e and the observed one o of the neuron and is given by:

$$\omega_{ij}^{t+1} = \omega_{ij}^{t} + \eta(e_j - O_j)x_i = \omega_{ij}^{t} + \Delta\omega ij \tag{3.7}$$

where ω_{ij} is the intensity connection between the i^{th} input cell and the j^{th} output cell, e is the expected response, t is the number of iterations and η is the learning rate. When using neural network, it is known that the learning process has a strong influence on the output. Therefore, the learning set and the method have to be correctly chosen to avoid over-learning and to generalize best.

The learning process is performed using the GretagMacbeth ColorChecker© composed of 24 patches (see figure 3.10). The particularity of this ColorChecker comes from the fact that it represents primary. We use only the 16 colours patches of the chart which are colours encountered on natural objects and whose spectral properties of the patches are known. We employs white (99% reflectance), black (2% reflectance) and four neutral greys (20%, 40%, 60% and 80% reflectance) Spectralon© reflectance standards. The Spectralon© diffuse reflectance standards are highly Lambertian and calibrated over the range of 250 - 2500 nm and $+/-1\%$ over their respective spectrum. They provide higher reflectance qualities than the one from the GretagMacbeth chart and aims to potentially improve the learning process.

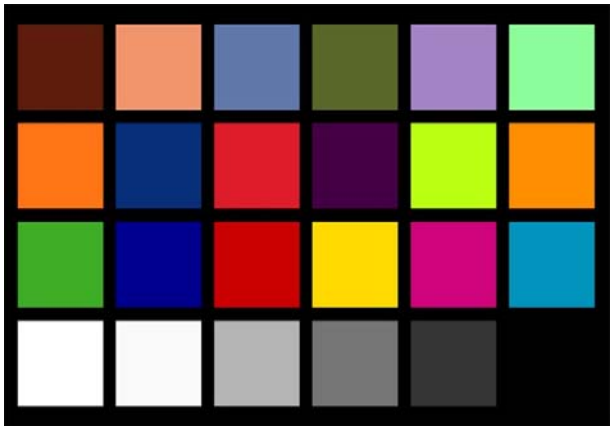

Figure 3.10: GretagMacbeth ColorChecker©.

Using equation 3.6, it is possible to characterise the system when the neural network learns a set of patches from the GretagMacbeth ColorChecker and by recording the camera response. This procedure involves acquisition, by a spectrophotometer, of the patches (with $p = 1, ..., P = 24$) of the Macbeth chart, providing N (N depends on the sampling

rate) values of the spectral reflectance curve for each patch p). It composes a learning matrix R (size [N x P]). The procedure also requires the acquisition by ASCLEPIOS of a multispectral image, containing K (with $K = 10$) gray-level values for each patch. The P patches are embedded in a matrix D (size [K x P]).

Both set of data (R , D) provides a set of corresponding pairs which are used by the neural network to perform a supervised learning, using matrix D as input and matrix R as expected output. The learning stops when it reaches the minimum of the validation error. Once learned, ANN outputs a coefficient matrix Q (called synaptic coefficient matrix) of size [NxK].

3.2.2.2.2 Reconstruction process

The neural network employed in the spectral reflectance cube reconstruction uses hetero-associative memories due to its modularity with regards to the different sizes of the input and output vectors, allowing reconstruction of reflectance spectra with higher sampling rate and spectral resolution than the initial multispectral image. From figure 3.9, the reflectance spectrum r of each pixel, from a multispectral image, is reconstructed using the camera response d and the result Q obtained from the ANN learning step (called coefficient matrix). The reconstruction associates a vector of K values obtained from the MSI to a vector of N values corresponding to the sampled spectral reflectance(figure 3.11).

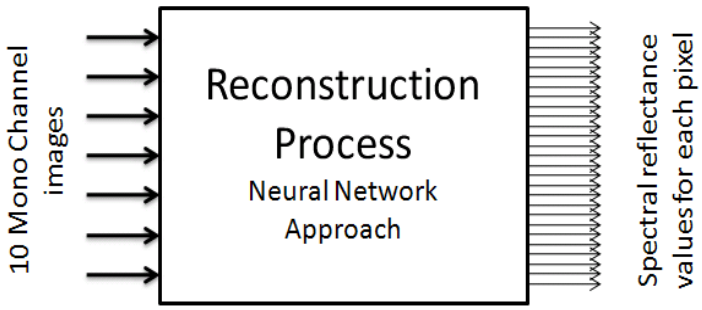

Figure 3.11: Reconstruction process for a set of images.

Using matrix notation, the expression of the neural network spectral reflectance reconstruction leads to

$$O = Qx \tag{3.8}$$

where x is the vector (size [Kx1]) containing the multispectral input values for one pixel,

Q (size [NxK]) is the coefficient matrix and O (size [Nx1]) is the reconstructed reflectance spectra for this pixel.

The reconstruction of a reflectance cube is fast and simple as the operation is a product between the coefficient matrix and the camera response. The implemented reconstruction function is flexible and allows different sampling rates for different wave-range sizes (within the system wave-range capability 430 to 970 nm) using the advantages of the hetero-associative memories.

3.2.3 ACLEPIOS software control

A C++ software was specially developed for the system. It is designed with tab look-alike windows; the software is composed of three tab buttons corresponding to the three main capabilities offered by the system: MultiSpectral Aquisition, Reflectance Cube Reconstruction and Processing.

The first tab allows the acquisition of a multispectral image (see figure 3.12. It controls and commands the whole acquisition process: the rotation of the wheel, the modification of the camera exposure time for each waveband, the acquisition and saving of the multispectral images into a database. The software contains a built-in database offering listing of acquisition made for every patient to be easily retrieved and it contains all the patient information (name, birthdate, gender, comment). After one acquisition, the user can select the body location where the acquisition was performed (aims to simplify patients' follow-up). The acquisition tab displays the acquired multispectral in a set of miniature images allowing rapid overview of the MSI.

The Reflectance Reconstruction tab enables the reconstruction of a reflectance cube. The user can manually indicate minimum and maximum reconstruction wavelength and its resolution or select the default reconstruction (430 - 780 nm with a resolution of 10 nm). This tab provides three modes of spectral display: single spectra, average spectra and spectro-spatial display (see figure 3.13).

The third tab is set-up to contain the different processing that will be performed on the reflectance cube.

3.3 Results and validation

The aim of the system is to reconstruct reflectance cube of cutaneous data with high quality. Therefore, we will first present the results from the calibration procedure: the linearity analysis of the sensor, the non-uniformity illumination correction and the effect of

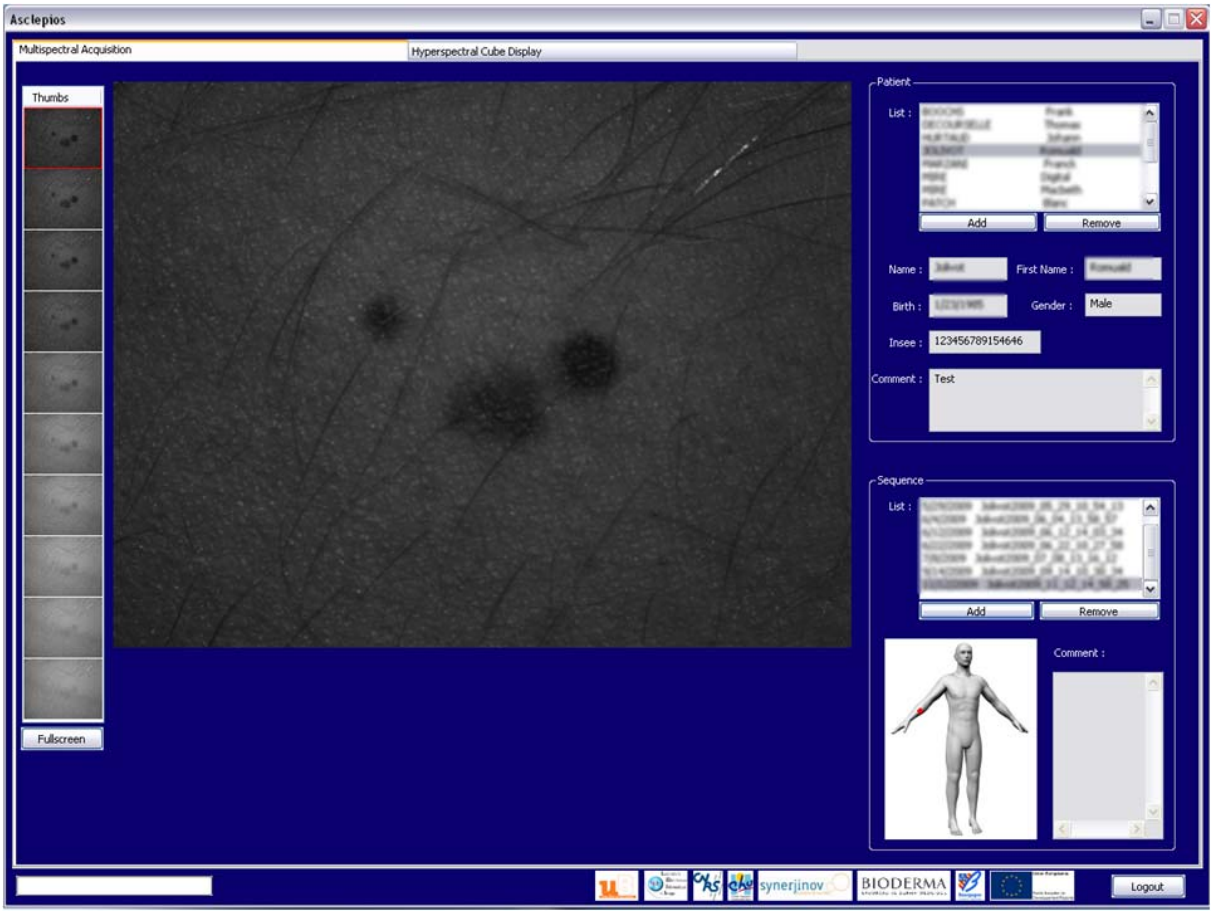

Figure 3.12: Screenshot of ASCLEPIOS software: Multispectral Acquisition tab.

the calibration on the reconstruction accuracy based on known spectral patches. Secondly, the validation of the overall system (acquisition of multispectral image and reconstruction of reflectance cube) will be performed on real skin data.

3.3.1 Calibration results

As detailed in the calibration section, the image modelling and correction suppose that the sensor has a linear response. The sensor linearity is studied to verify that the sensor response is linear in regards to a linear increase of incoming light. This process is assessed using six calibrated Spectralon© Gray-Scale Standards. These six grey scale reflectance standards range respectively 2%, 20%, 40%, 60%, 80% and 99% reflectance. The Spectralon© gray-scale standards have certified reflectance data which allow the calcula-

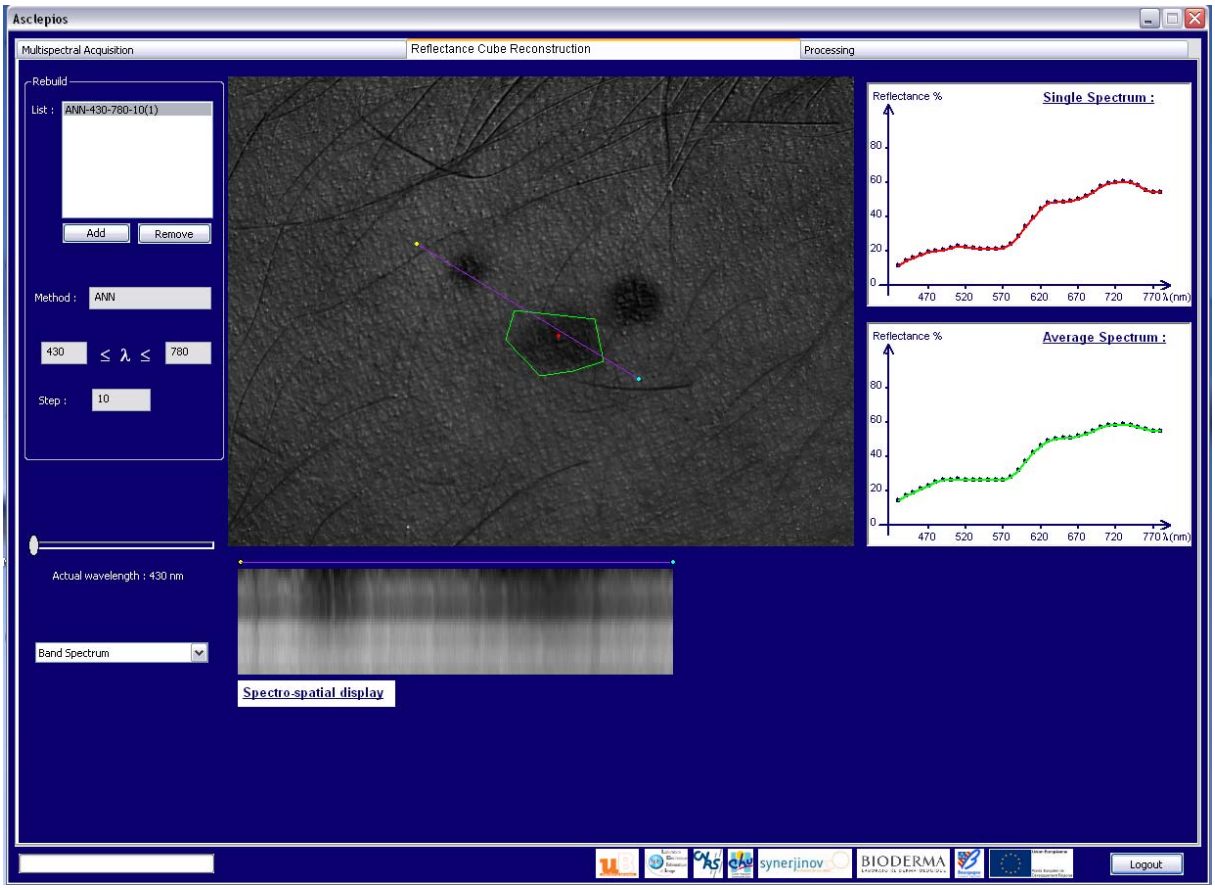

Figure 3.13: Screenshot of ASCLEPIOS software: Reflectance Cube Reconstruction tab.

tion of the theoretical grey-level that the camera should obtain.

A multispectral image is acquired for each grey-scale reflectance standard. These acquisitions provide the camera response. The calculation of the image average grey-level for each reflectance standard allows comparison with the theoretical data.

The results (figure 3.14) show that the camera response is nearly linear. The linearity of the sensor is indicated by the coefficient of regression R^2. It is calculated from the theoretical Spectralon data versus the measured one using ASCLEPIOS. The average R^2 obtained from the ten patches is 0.95. The sensor is considered linear thus the calibration can be applied as described.

The results obtained after calibration (according to equation 3.3) show a significant improvement of the image illumination uniformity in comparison to the original image (figure 3.15(a)). Also, it is important to have a large set of white acquisition as any dust

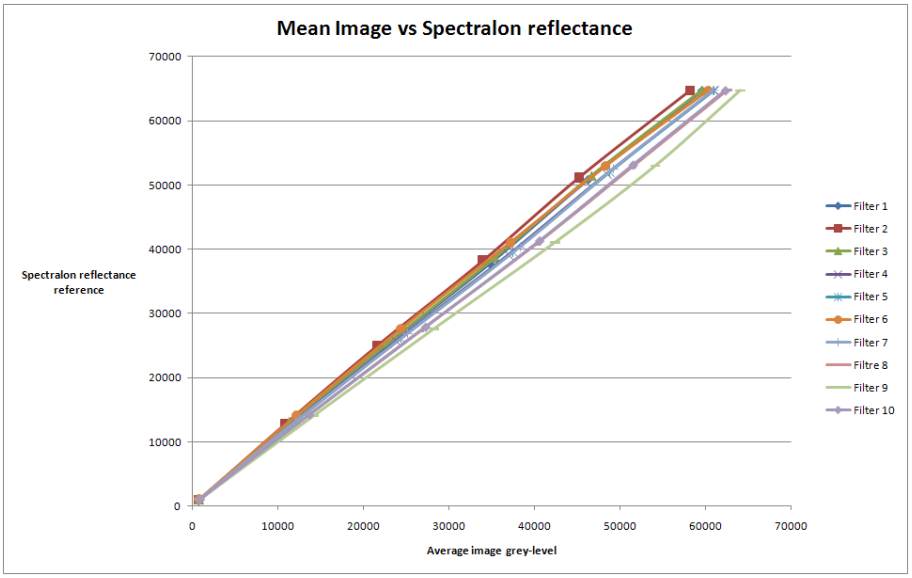

Figure 3.14: Camera linear response.

on the white balance target will have a noticeable impact on the averaged images.

The usefulness of the calibration is presented by comparing theoretical spectra obtained by spectrophotometer with reconstructed spectra from raw multispectral images and calibrated multispectral images.

To evaluate the performance of the calibration on the reconstruction of reflectance cube, three different metric scales are employed: the Root Mean Squared Error (RMSE), the Goodness of Fit Coefficient (GFC) and the Reconstruction Percentage (RecP).

The RMSE calculates the mean of Euclidean distance values between two spectra. Reconstruction is good when RMSE is close to zero. RMSE is calculated using the following formula:

$$RMSE = \frac{1}{N} \sum_{j=1}^{N} \|R_m(\lambda_j) - R_r(\lambda_j)\|^2 \tag{3.9}$$

where $R_m(\lambda_j)$ is the spectrum value measured with the spectrophotometer at wavelength λ_j and $R_r(\lambda_j)$ is the reconstructed spectra value at wavelength λ_j and N the number of samples.

The GFC is based on the Schwartz inequality and is calculated using the following formula:

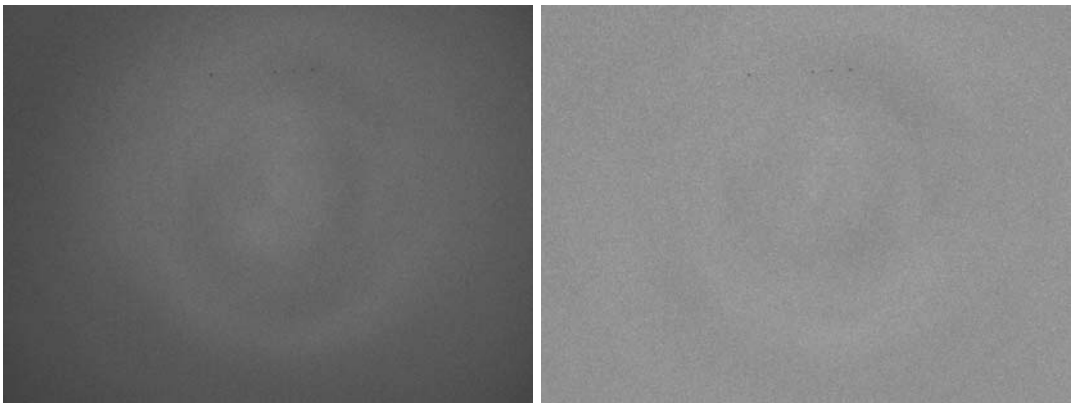

(a) Raw image (b) Calibrated image

Figure 3.15: Patch 9 of the GretagMacbeth ColorChecker acquired at 700 nm.

$$GFC = \frac{\left|\sum_j R_m(\lambda_j) R_r(\lambda_j)\right|}{\left(\sum_j \left[R_m(\lambda_j)\right]^2\right)^{1/2} \left(\sum_j \left[R_r(\lambda_j)\right]^2\right)^{1/2}}. \tag{3.10}$$

This criterion has the advantage to be bounded between 0 and 1, providing an easy interpretation. According to Hernandez *et al.* [Hernández-Andrés et al., 2001], the reconstruction is good if the GFC is above 0.99 and perfect if higher than 0.9999.

The RecP is a criterion which evaluates the distance between two spectra. It requires a higher precision for the spectrum part having low amplitude. A good reconstruction will be close to 100%. It is defined by:

$$RecP = 1 - \frac{\sum_{j=1}^{N} \|R_m(\lambda_j) - R_r(\lambda_j)\|^2}{\sum_{j=1}^{N} \|R_r \lambda_j\|^2} \tag{3.11}$$

Two sets of data were employed to validate the reconstruction. The first set is composed of the 24 patches of the GretagMacbeth ColorChecker© chart used during the learning process (see figure 3.10). The comparison is made between reconstructed spectra from the mean of the entire cube and spectrum acquired by the spectrophotometer (Table 3.1).

There is a strong improvement of the RMSE value (around 5 times better). GFC values are of similar order for uncalibrated and calibrated reconstruction. The average RecP proves to be higher for calibrated reconstruction. These results reveal a better

	GFC		RecP		RMSE	
Patch	No Calibration	Calibration	No Calibration	Calibration	No Calibration	Calibration
1	0,998103	0,998261	0,989971	0,998103	6,912576	2,855818
2	0,999304	0,999645	0,999231	0,999304	113,368883	2,291387
3	0,996783	0,997050	0,988120	0,996783	13,011755	5,686798
4	0,996362	0,993440	0,804207	0,996362	1,556516	13,712461
5	0,998668	0,999063	0,972184	0,998668	8,028323	23,145156
6	0,998882	0,999181	0,990200	0,998882	38,256325	10,318672
7	0,999594	0,999643	0,994944	0,999594	85,268149	10,582024
8	0,998900	0,999111	0,990469	0,998900	24,405763	8,086233
9	0,998389	0,998317	0,982192	0,998389	35,185789	24,735305
10	0,999309	0,999529	0,991685	0,999309	27,923215	7,635670
11	0,999578	0,999666	0,999331	0,999578	60,226801	0,836917
12	0,999368	0,999424	0,997977	0,999368	105,748586	4,775769
13	0,989582	0,989377	0,977869	0,989582	28,497951	6,295558
14	0,996411	0,997722	0,994044	0,996411	19,742834	1,658153
15	0,999317	0,999418	0,996130	0,999317	60,273816	7,464494
16	0,999860	0,999820	0,999632	0,999860	127,142400	1,369009
17	0,998902	0,999408	0,996899	0,998902	106,412589	9,089311
18	0,997003	0,997210	0,983862	0,997003	56,159532	10,095998
19	0,998734	0,998778	0,995815	0,998734	163,231494	28,199192
20	0,999296	0,999427	0,996509	0,999296	161,012269	10,075844
21	0,998909	0,998848	0,992822	0,998909	39,691119	8,184043
22	0,997760	0,996923	0,931148	0,997760	12,323021	14,129804
23	0,992849	0,993134	0,969202	0,992849	13,484009	2,342869
24	0,986473	0,979704	0,968232	0,986473	0,669882	8,025245
Average	0,997431	0,997970	0,979758	0,997907	54,522233	9,232989
Standard deviation	0,003309	0,002398	0,004506	0,041072	50,176413	7,279429

Table 3.1: GFC, RecP and RMSE of the 24 patches of the GretagMacbeth ColorChecker© and the overall average and standard deviation.

reconstruction of the learned patches when calibration is applied. Visual analysis of the calibration reveals a clear improvement of the reconstruction after the calibration is applied (see figure 3.16)

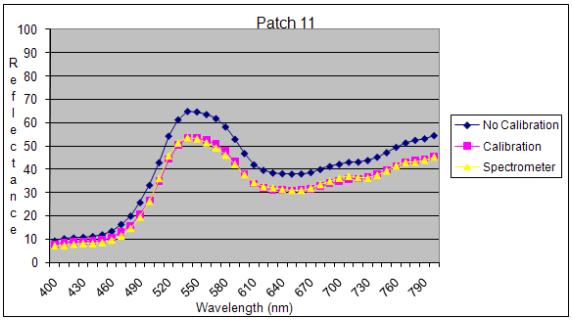

(a) Patch 11.

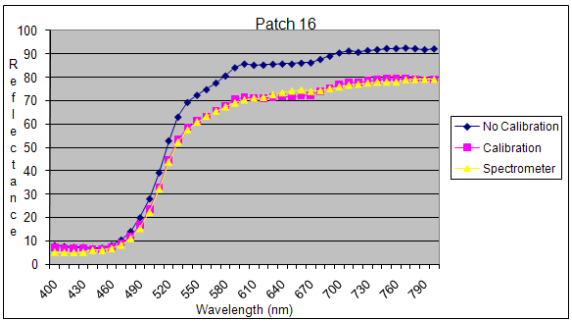

(b) Patch 16.

Figure 3.16: Effect of the calibration on patch 16 of the GretagMacbeth ColorChecker©.

To validate the calibration effect, a comparison is made between the set of 14 skin-tone colour patches and 10 random patches, from the digital ColorChecker© SG (see figure 3.17), reconstructed by ASCLEPIOS without calibration and with calibration having for reference spectra of the patches recorded by the spectrophotometer (see tables 3.2 and 3.3).

According to table 3.2 and 3.3, the results clearly show that a better spectral reconstruction is obtained when MSIs are pre-processed by the calibration method. RMSE is improved three times better once calibration is applied for skin-tone patches. RecP is clearly enhanced after calibration in both cases whereas GFC is slightly improved. We can notice a limited decrease in the reconstruction accuracy of the patch from the Digital ColorChecker© SG. This effect might result from the high reflection of the targets due to

	GFC		RecP		RMSE	
Skin Patch	No Calibration	Calibration	No Calibration	Calibration	No Calibration	Calibration
D7	0,99012	0,99223	0,87153	0,95251	473,37375	115,30838
E7	0,99374	0,99610	0,91809	0,97183	540,10274	136,02033
F7	0,99383	0,99361	0,89949	0,92943	357,61033	214,94931
G7	0,97708	0,98289	0,80967	0,91064	269,61052	80,56024
H7	0,99739	0,99793	0,91003	0,95606	334,00011	127,63971
I7	0,98071	0,98015	0,87101	0,90208	187,93503	120,88996
J7	0,99179	0,99235	0,88623	0,93374	367,23336	168,18069
D8	0,99805	0,99822	0,91138	0,95969	357,17170	124,85098
E8	0,99511	0,99551	0,93836	0,97115	335,36489	126,57464
F8	0,99641	0,99616	0,93059	0,95608	262,44676	142,71022
G8	0,99619	0,99606	0,90372	0,93983	371,37990	192,24276
H8	0,99652	0,99740	0,89488	0,95760	423,00330	123,06111
I8	0,97388	0,97987	0,82069	0,89484	128,73045	54,67885
J8	0,99383	0,99481	0,88407	0,94381	466,15736	167,32940
Average	0,99105	0,99238	0,88927	0,94138	348,15144	135,35690
Standard deviation	0,00790	0,00648	0,03714	0,02454	111,22439	41,36722

Table 3.2: GFC, RecP and RMSE of the 14 skin-tone patches of the Digital ColorChecker© SG and the overall average and standard deviation.

	GFC		RecP		RMSE	
Random Patch	No Calibration	Calibration	No Calibration	Calibration	No Calibration	Calibration
B4	0,98017	0,98118	0,89983	0,93544	311,39355	162,10931
B5	0,97382	0,96616	0,88904	0,88152	229,36164	239,69186
B7	0,89484	0,91392	0,41571	0,57242	119,23648	40,78820
C5	0,98357	0,98119	0,91904	0,94182	264,65742	158,44259
C8	0,95790	0,95878	0,84885	0,94182	167,70394	95,63027
K5	0,99829	0,99828	0,92345	0,95500	455,47935	224,74547
K9	0,98528	0,98652	0,93891	0,96927	69,07988	26,50522
L3	0,99242	0,99138	0,98395	0,97867	61,54563	67,82036
L4	0,99663	0,99665	0,96876	0,98904	100,43601	28,65605
L6	0,99606	0,99667	0,98988	0,99053	50,10596	38,31577
Average	0,97542	0,97707	0,87529	0,91555	168,62292	108,27051
STD	0,03289	0,02579	0,17820	0,12478	131,20041	82,00365

Table 3.3: GFC, RecP and RMSE of 10 randomly selected patches of the Digital ColorChecker© SG and the overall average and standard deviation.

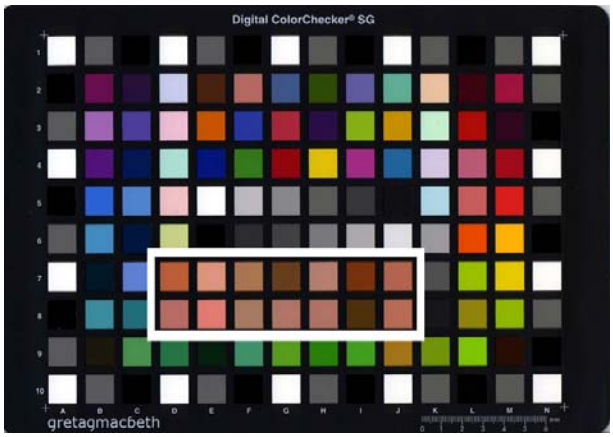

Figure 3.17: Digital ColorChecker© SG with skin-tone patches highlight.

its semi-gloss texture.

These results confirm the usefulness of the calibration for reconstruction of hypercubes (see figure 3.16).

The finality of ASCLEPIOS system is the reconstruction of reflectance cubes of cutaneous data. Therefore, a technique to characterize a MSI system is carefully designed to calibrate efficiently the system in order to remove systematic noise-related problem. The protocol takes into account offset errors and gain correction. The calibration is specific to every monoband image of a MSI. It eliminates noise related to time exposure which is different for each monoband but it also eliminates vignetting problem linked to the lens or filters, non-uniform illumination. The effect of calibration improves the reconstruction of reflectance cubes. The calibration proves to remove systematic noise which is of great interest to avoid possible incorrect reconstruction of spectra that could affect subsequent processing.

3.3.2 Validation on healthy skin data set

In the previous section, we have demonstrated that ASCLEPIOS system can reconstruct reflectance cube with high quality using the Macbeth Chart and the Digital Macbeth Chart. The Artificial Neural Network can reconstruct with high accuracy spectral reflectance of a wide range of colours, such as blue, green, purple covering most of the reflectance range of the visible spectrum. For general purpose, these results are sufficient. However, skin spectrum represents only a limited reflectance range of the electromagnetic spectrum. The system being designed for dermatological application, we need to validate

SPT Type	Fitzpatrick Scale point	Sun Response History
I	0-7	Always burns, never tans
II	8-16	Always burns, tans minimally
III	17-25	Burns minimally, tans gradually and uniformly
IV	25-30	Burns minimally, always tans well
V	Over 30	Rarely burns, tans darkly
VI	Over 30	Never burns, tans darkly

Table 3.4: SPT distribution.

the precision of the reconstruction of skin data, as the difference between two skin spectra might be very limited with only a slight variation.

3.3.2.1 Method

The aim of reflectance cube reconstruction is to retrieve skin information from the reflectance spectrum with aims to increase the amount of information available to the dermatologist for diagnosis purpose. To validate the accuracy of the reconstruction of reflectance cube of cutaneous data, a study on healthy participants from different skin tones has been performed. The validation on a skin data set of healthy participants was performed during a six months research exchange program at Universiti Teknologi Petronas (Tronoh, Malaysia) with the collaboration of Hermawan NUGROHO (PhD student) under the supervision of Professor Ahmad FADZIL MOHAMAD HANI.

The classification of the different skin tones is based on the Fitzpatrick Skin PhotoType [Fitzpatrick, 1975] (SPT) which classify a person's complexion and tolerance to sunlight. According to the Fitzpatrick scale (see table 3.4), human skin can be divided into six categories, SPT I for very white skin (never tans and always burns) to SPT VI for black skin (never burns). Fitzpatrick skin typing system is a self-reported skin type questionnaire, where people grades their tendency to burn and ability to tan after un-protected sun exposure. The number of points obtained from the questionnaire classifies the person into the Fitzpatrick SPT. Several SPT have been analyzed to quantify the reconstruction accuracy of ASCLEPIOS for a wide range of skin spectrum.

Three acquisitions (by a commercial spectrophotometer CM 2600d and by ASCLEPIOS) were collected from each participant of the study; two data were acquired from facultative skin colour and one from constitutive skin colour. Facultative skin colour is skin area affected by the environment (sun, hormones) and it impacts the original appearance of the skin colour over time whereas constitutive skin colour is determined by genetics.

For facultative colour, one sample from the back of the hand, one sample from the face is acquired. For constitutive skin colour, one sample from the lower back is acquired. The purpose of different body locations is to record a difference of skin chromophore composition between these samples. This is due to the fact that the face and the back of the hand are supposed to be more exposed to the sun than the lower back. Melanin production is linked to sun exposure (UV). These two body locations are expected to have higher melanin concentration and therefore it should have a different skin reflectance spectrum.

The aim is to observe a difference within each participant between exposed (facultative skin colour) and non-exposed (constitutive skin colour) area.

In this study, using the wave-range flexibility offered by the Artificial Neural-Network, three reconstruction configurations are selected, one reconstruction from 430 to 780 nm, another one from 430 to 850 nm and a third one from 430 to 950 nm. The objective of testing different wave-ranges is to select the best configuration for accurate reconstruction for visible light range (due to the limitation of the CM-2600d).

The study involves 150 recruited healthy (with no known skin disease) participants of different skin tones. The acquisition was conducted at University Teknologi PETRONAS (Malaysia). The population covers five out of the six SPT groups, no participant of type I SPT were available for the study.

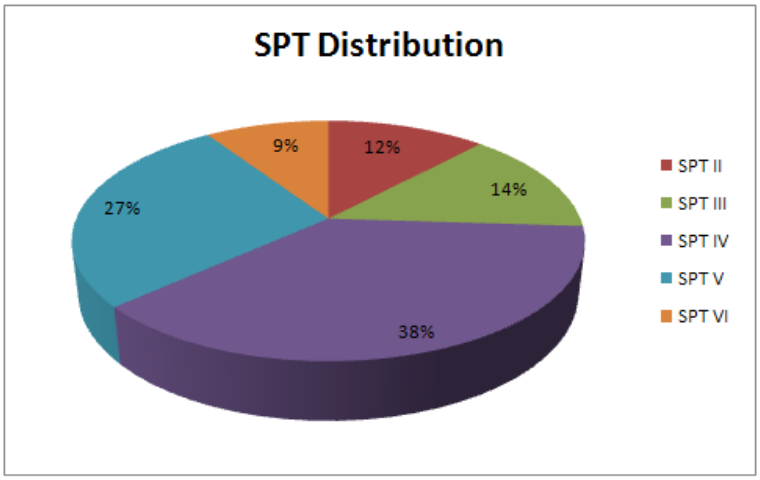

Figure 3.18: SPT distribution.

The distribution within the different SPT is shown figure 3.18. The population is mainly composed of undergraduates and postgraduates students ranging from 18 to 28 years old with an average age of 22.6 years and a standard deviation of 4.2 years (see table

3.19(b) for age distribution and table 3.19(a) for sex repartition). A majority of male responds to the research study.

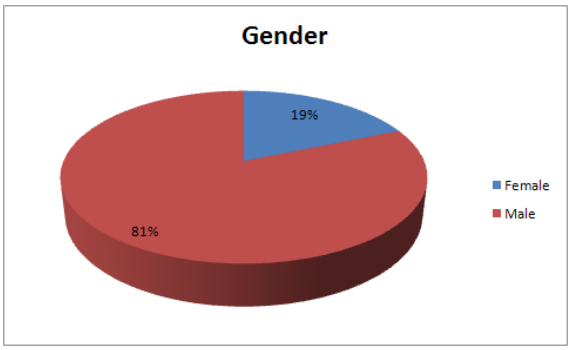

(a) Gender distribution

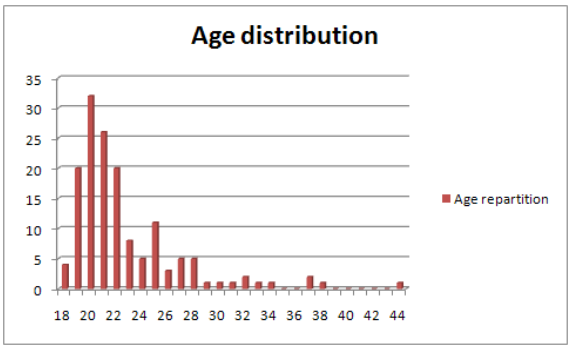

(b) Age distribution

Figure 3.19: Participant demographic distribution.

Attention was paid to ensure that the handheld device was properly in contact with the skin to avoid external light leaking into the system. During acquisition of participant data, care was taken between every acquisition that the nozzle part in contact with the skin was cleaned with an alcoholic swab.

The study protocol requires the consent of the participant. The participant needs to answer a two parts questionnaire, first the participant answers questions about his/her skin condition: do he/she use facial product or make-up, have known skin disease and whether his/her lower back is exposed to the sun. The second part is the Fitzpatrick questionnaire which classifies a skin phototype according to its reaction to the sun.

Inclusion criteria	Exclusion criteria
• Have been informed of the nature and the aims of the study and have given their written informed consent • Aged 18 years and above	• Participant refuses consent • Presence of dermatological disease, which could interfere with the interpretation of the data • Lower back exposed to the sun (not constitutive skin)

Table 3.5: Participants - Inclusion / Exclusion criteria.

3.3.2.2 Results

The data obtained from the spectrophotometer is a spectrum from 360 nm to 740 nm with a step of 10 nm. The reflectance cube is reconstructed from 430 to 780 nm for the first reconstruction, from 430 to 850 nm for the second one and from 430 to 950 for the third one, all with a step of 10 nm. Each cube is averaged to provide an average spectrum.

To evaluate the accuracy of the reconstruction, the spectrophotometer data is selected as reference spectrum to compare with the averaged reconstructed spectrum. Due to the spectral limitation of the spectrophotometer Minolta CS2600d (360 nm to 740 nm with a 10 nm step), comparisons are calculated from 430 to 740 nm for all data. The accuracy of the reconstructions is quantified by the calculation of three different metric scales, the Goodness of Fit Coefficient (GFC), the Reconstruction Percentage (RecP) and the Root Mean Square Error (RMSE).

The results are divided into six groups (see table 3.6). The first five sets of rows concern the average of each SPT (SPT II, III, IV, V and VI) according to their locations (hand, face and back) and reconstruction wave-ranges (450-780, 450-850 and 450-950 nm). The last row of table 3.6 is the averaged GFC, RecP, RMSE of all the data (regardless of their SPT) for each location and reconstruction wave-ranges. In table 3.6, 780, 850 and 950 refers respectively to their reconstruction range, all starting from 450.

The average of all the data reveals that the GFC, RMSE and RecP for the hand, face and lower back is higher for reconstruction range from 430 to 780 nm. It is also important to notice that the values of other reconstruction (430 to 850 nm and 430 to 950) are all superior to 0.9967 for the GFC. According to Hernandez *et al.* [Hernández-Andrés et al.,

2001], reconstruction with GFC higher than 0.99 is considered good.

The GFC result for each specific SPT group shows that reconstruction for SPT II and III appears to be better in the reconstruction range of 430 to 850 whereas reconstruction for SPT IV, V and VI obtains better results in the range of 430 to 780. Similar conclusion arises for the RecP values and the RMSE. Data for SPT IV, V and VI have flatter spectrum due to higher concentration of melanin and their reconstructions have better quality in the range 450-780 nm. This might be due to the limitation of the learning process in the NIR which only contains information from the grey-level Spectralon patches because the Gretag Macbeth chart is only valuable in the visible range (patches tend to have a flat shape after 780 nm).

SPT II	Hand 780	Hand 850	Hand 950	Face 780	Face 850	Face 950	Back 780	Back 850	Back 950
GFC	0,9977	0,9977	0,9970	0,9963	0,9964	0,9958	0,9963	0,9965	0,9957
RecP	0,9842	0,9846	0,9838	0,9776	0,9777	0,9694	0,9793	0,9809	0,9724
RMSE	18,87	18,30	18,91	32,23	32,11	44,42	35,15	32,67	47,93
SPT III	Hand 780	Hand 850	Hand 950	Face 780	Face 850	Face 950	Back 780	Back 850	Back 950
GFC	0,9980	0,9980	0,9974	0,9972	0,9973	0,9966	0,9974	0,9975	0,9967
RecP	0,9852	0,9856	0,9821	0,9797	0,9674	0,9677	0,9847	0,9848	0,9745
RMSE	12,78	12,37	20,02	22,08	37,31	38,22	20,88	20,74	34,54
SPT IV	Hand 780	Hand 850	Hand 950	Face 780	Face 850	Face 950	Back 780	Back 850	Back 950
GFC	0,9976	0,9975	0,9970	0,9972	0,9972	0,9966	0,9975	0,9976	0,9969
RecP	0,9792	0,9788	0,9749	0,9802	0,9797	0,9727	0,9781	0,9775	0,9612
RMSE	16,30	16,67	17,55	20,84	21,32	27,74	21,06	21,53	37,15
SPT V	Hand 780	Hand 850	Hand 950	Face 780	Face 850	Face 950	Back 780	Back 850	Back 950
GFC	0,9971	0,9968	0,9963	0,9971	0,9970	0,9965	0,9980	0,9979	0,9972
RecP	0,9814	0,9793	0,9807	0,9836	0,9839	0,9790	0,9765	0,9767	0,9548
RMSE	15,61	16,94	15,67	13,22	13,05	15,71	15,53	15,31	29,45
SPT VI	Hand 780	Hand 850	Hand 950	Face 780	Face 850	Face 950	Back 780	Back 850	Back 950
GFC	0,9972	0,9961	0,9962	0,9977	0,9969	0,9967	0,9975	0,9962	0,9961
RecP	0,9842	0,9797	0,9790	0,9860	0,9726	0,9775	0,9631	0,9691	0,9251
RMSE	4,89	5,92	6,35	4,44	8,51	6,80	7,81	7,03	16,20
ALL SPT	Hand 780	Hand 850	Hand 950	Face 780	Face 850	Face 950	Back 780	Back 850	Back 950
GFC	0,9975	0,9973	0,9968	0,9971	0,9970	0,9965	0,9975	0,9974	0,9968
RecP	0,9817	0,9807	0,9790	0,9813	0,9782	0,9738	0,9773	0,9778	0,9590
RMSE	14,86	15,33	16,50	18,77	21,40	25,97	19,77	19,42	33,71

Table 3.6: GFC, RecP and RMSE for each location and reconstruction range of the average data of each SPT and averaged of all data.

The results can be visually assessed with figure 3.20(a) and figure 3.20(b) which respectively show the average data per SPT acquired from the back of the hand for the

spectrophotometer and ASCLEPIOS.

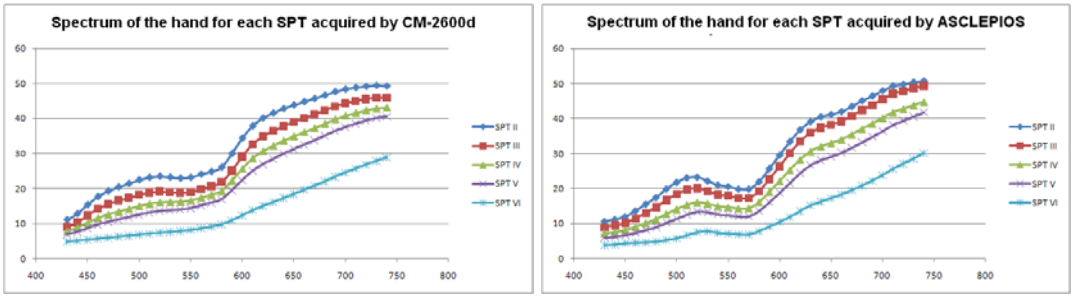

(a) Spectrophotometer data from back of the hand.

(b) ASCLEPIOS data from back of the hand.

Figure 3.20: Comparison of spectrometer and ASCLEPIOS data for all SPT from the back of the hand.

The shapes of the curve from ASCLEPIOS are in good accordance with the curves obtained from the spectrophotometer. It can be clearly seen from figure 3.20(a) and figure 3.20(b) that both graphs show correlation with each other.

Difference between constitutive and facultative skin colours is obtained by both systems. Figures 3.21(a) and 3.21(b) show respectively the average SPT III data acquired from the lower back (constitutive skin colour) and the back of the hand (facultative). The constitutive skin colour has higher spectral reflectance compare to the facultative one.

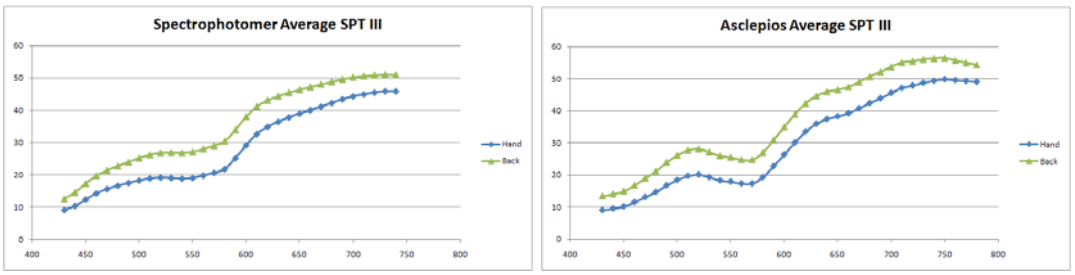

(a) Average SPT III at two different locations acquired by CS2600d

(b) Average SPT III at two different locations acquired by Asclepios.

Figure 3.21: Difference of spectral information at two locations.

The difference of spectrum shape between areas exposed to the sun against area non-exposed to the sun can also be visually assessed. This revelation means that quantification of skin chromophores is possible with the two systems. However, with a spectrophotometer,

two acquisitions are required because it does not provide spatial information whereas with ASCLEPIOS and its reflectance cube, only one acquisition is necessary (multiple spectra from a single cube). Both numerical and visual analysis of the results reveals that the reflectance cube can be accurately reconstructed

This study validates the capacity of ASCLEPIOS system to accurately reconstruct reflectance cube of cutaneous data, which provides more information than conventional spectrophotometer, which provides only the average spectrum of an area. Such reflectance cubes provide both spectral and spatial information. It seems that our system is able to discriminate different skin area following their chromophore concentrations, within the same cube.

3.4 Future works

The future improvement on the technical side of the system may be the implementation of polarizing filter to remove high reflection effects due to high sebum concentration and in case of study of wet skin lesions. Another modification would be linked to the illumination device. New light source based on Texas Instruments' Digital Light Processor (DLP) technology offers a fast programmable and variable light source. This light source is variable in terms of intensity and spectral resolution and two systems cover visible (380-780 nm) and near infrared (760 - 1600 nm) spectral range. This technology could be used to directly acquire reflectance cube of data. A postdoctoral fellow is currently on the development of the new generation of ASCLEPIOS based on the recently acquired DLPs light source. On the reconstruction side, study could analyse the potential learning and reconstruction process in the near-infrared region to use the full capacity of the spectral domain of ASCLEPIOS. The learning process is limited to the visible range because the Gretag Macbeth chart is not certified for NIR range. Only Spectralon patches are certified in VIS and NIR but only provide limited spectral information (plateau shape). To extend the reconstruction process in the near infrared, it requires developing a chart which permits learning of characteristic spectrum in the VIS+NIR. This chart may be based on different materials with known spectral information.

3.5 Conclusion

In this chapter, we described the development of a contact MSI system for dermatological applications: ASCLEPIOS. We defined the motivations of the development of this sys-

tem. The different specifications are detailed and the choice of the elements composing the system is described. The calibration steps are presented and allow reproducible acquisition over time. ASCLEPIOS system acquires MSI and has the capacity to reconstruct reflectance cubes. This step is based on a neural network algorithm. This reconstruction process is explained and validated with the reconstruction of colour patches. The system has also been validated on the acquisition and reconstruction of cubes from a set of 150 healthy participants (at 3 different body locations) covering five of the six Fitzpatrick skin phototypes with reconstruction quality over 99.96% for the GFC metric scale.

The system is exclusively devoted for dermatology applications and is elaborated for *in vivo* imaging of skin lesions. It is intended to reveal extra information for the spectral characterization of skin lesions.

Our system is innovative compared to actual system thanks to the combination of a MSI and a spectral reflectance reconstruction algorithm. To meet our requirements and improve the system, (1) we developed a system to acquire data independent of the condition of acquisition (reproducible) and (2) we coupled the system with a reconstruction algorithm which provides reflectance spectrum independent of the optical path, increasing the spectral capacity of the system and assuring the reproducibility of the acquisition to allow skin lesions follow-up and comparison throughout the time.

The system provides a reflectance cube of cutaneous data. Analysis of the cube offers three possible processing, spatial and spectral one or both combined. Spatial processing refers to the analysis of one or several spectral bands using image processing tools. The spectral processing designates study of a single or multiple spectra for a defined spatial location by signal processing techniques.

In the following chapter, we detail the current state of the art of skin data analysis to set the ground for skin data analysis by ASCLEPIOS.

Chapter 4

Review of Skin Data Analysis

Skin is an external organ which has attracted many researches. In a large variety of fields such as medicine (dermatology), cosmetics industry and/or realistic image synthesis, human skin reflectance model is an important tool as researchers require accurate models of light propagation in skin.

Such model can bring valuable information about the skin composition. To extract information, it is necessary to have a description of the human skin complex composition and its optical properties are important in the development of model of light propagation.

Despite being a subject of great interest for different fields of research, there is no single model of skin reflectance spectra. Each field tends to focus on specific aspect, their models concentrate on some skin characteristics, i.e. quantity of melanin and blood concentration, other focus on erythema pigmentation whereas other focus on the rendering.

In van Gemert *et al.* [Van Gemert et al., 1989], it is stated that "*at present, a rigorous theory is far from being available, partly because skin is irregularly shaped, has fair follicles and glands, is inhomogeneous, multilayered, and has anisotropic physical properties. So any fruitful attempt to understand skin optics requires a considerably simplified model for skin*". Although this statement is from 1989, it still holds nowadays.

The following chapter first presents the human skin, then the presentation of models of light propagation in skin is detailed and finally, the different processing that allow extraction of skin information from image and/or spectra.

4.1 The Human skin

The description of human skin physiology and anatomy is aimed at setting the basic knowledge about human skin to understand the concept of light propagation model in it.

4.1.1 Physical aspect of human skin

4.1.1.1 Skin anatomy

The structure of human skin consists of three main layers from the surface: epidermis, dermis and subcutaneous fat [Anderson and Parrish, 1981].

The **Epidermis** is the outer surface layer of the skin. It can be decomposed into five sublayers (most of the models consider only one layer to model the light interaction): stratum corneum, stratum basale, stratum spinosum, stratum granulosum and stratum lucidum. It is listed from the outer superficial layer to the deeper layer. Its thickness is around 0.1 mm on average [Anderson and Parrish, 1981] but it may vary according to its body location. The external sublayer (know as the stratum corneum) is composed of dry dead cells without organelles and filled with keratin fibres. The epidermis main effect on the light is absorption due to its principal component the melanin. Epidermis is considered as an optical filter.

The **Dermis** is the layer between the epidermal layer and hypodermic layer. It is thicker than the epidermis, approximately 0.6 to 3 mm thick [Anderson and Parrish, 1981]. The dermis main functions are the thermoregulation, mechanical resistance and nourishing of the epidermis. This intermediary layer is composed of elastic collagen fibres, blood vessels, nerves, lymph vessels, hair follicles and sweat glands but the principal molecules with interesting optical properties are the haemoglobin, carotene and bilirubin. It is composed of two sublayers, papillary dermis (with principal function of thermoregulation) and reticular dermis (which gives the skin its strength and elasticity).

The **subcutaneous fat** (also referred to hypodermic) is the deepest layer of the skin. The thickness of this layer is on average 4 to 9 mm [Anderson and Parrish, 1981]. It is composed of connective tissues, fat cells and blood vessels.

Skin being a non-homogeneous dielectric material, its micro-anatomical complexity makes quantitative analysis of the skin optical properties difficult to model.

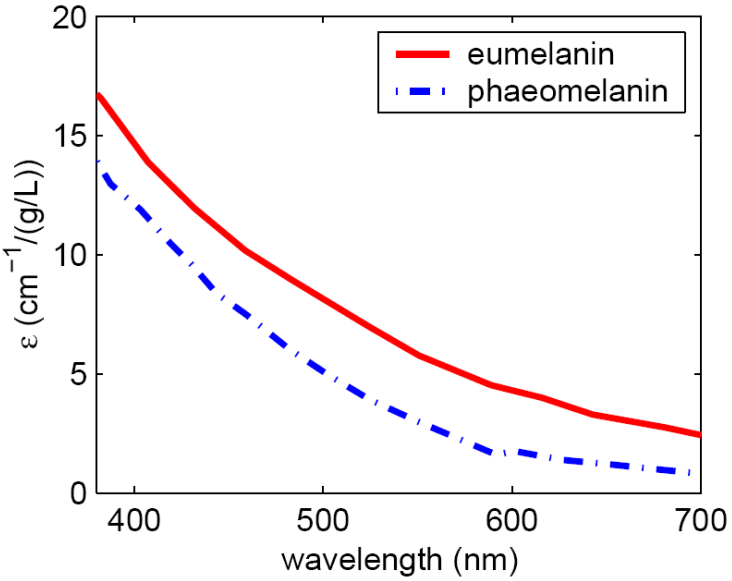

Figure 4.1: Optical absorption spectra of melanin (eumelanin and pheomelanin) [Prahl, 1988].

4.1.1.2 Skin optical properties

Skin is composed of various types of chromophores which are light-absorbing chemical compounds. Two important chromophores are *melanin* and *haemoglobin* because they play important part in the appearance of normal skin as they absorb light particularly in the visible wavelength range [Anderson and Parrish, 1982, Young, 1997].

Melanin is the major chromophore of the epidermis which occupies the top 50-100 μm. This chromophore is produced in the stratum granulosom and is also in the stratum spinosum. The epidermis superior layers do not contain melanin. Melanin is produced by melanosomes when exposed to UV light. There are two types of melanin: eumelanin and pheomelanin (see figure 4.1. The former has a brown/black colour whereas the latter has a red/yellow colour. Concentration ratio of eumelanin and pheomelanin varies between individuals. Its physiological function is to protect the skin by absorbing and scattering ultraviolet light. Skin colour depends on the fractions of the volumes of melanosomes, mostly with eumelanin. For light Caucasian skin, the fraction is between 1.3 and 3%, in well-tanned Caucasians and Mediterranean's, the percentage increases to 11 to 16 % and in dark coloured African skin, it can reach up to 45% [Jacques, 1998a].

Haemoglobin is a chromophore of red colour found in erythrocytes and is found in

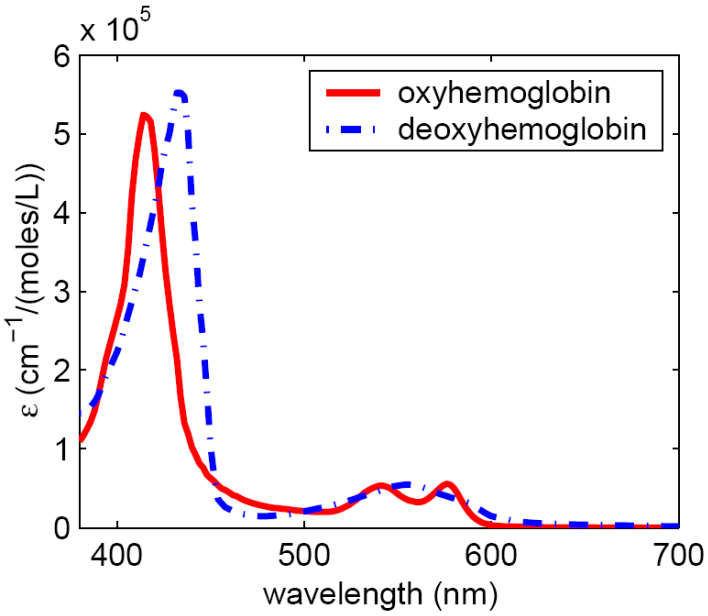

Figure 4.2: Spectral molar extinction coefficient curves of the oxy/deoxy-haemoglobin [Bowmaker and Dartnall, 1980].

the microvascular network of the dermis, typically 100-500 μm below the skin surface. It carries oxygen through vessels and capillaries. It is called oxy-haemoglobin when it contains oxygen, otherwise, it is called deoxy-haemoglobin [Prahl, 1988] (see figure 4.2).

Both melanin and haemoglobin strongly absorb light in the ultraviolet (UV) and visible ranges but have low absorption properties in the near-infrared.

4.1.2 Optical scattering and absorption parameters

Two phenomena happen in the skin, absorption and scattering. The former is mainly caused by two types of chromophores: melanin and haemoglobin, the latter is mainly induced by fibres, cells and cellular organelles.

When light interacts with human skin, photons are absorbed and scattered by the skin tissues. The measurement of re-emerged light after multiple scattering produces reflectance spectrum. The diffuse reflectance spectrum is determined by the absorption and scattering skin properties.

The skin reflection can be described by several properties. At angles of incidence that are close to normal ($\approx 90°$), only 5% of the incident light is directly reflected at the surface

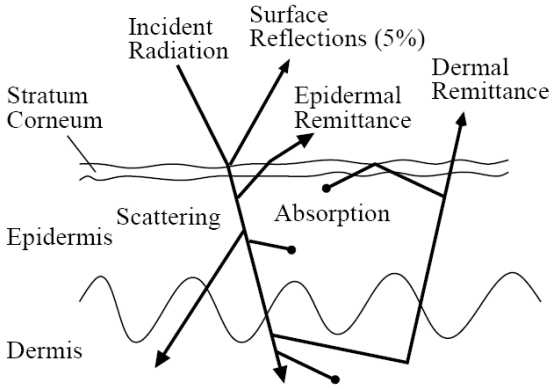

Figure 4.3: Representation of the major optical pathway of the light in human skin [Störring et al., 2000].

of the skin, this is due to the change of refractive index between the air (n_{air}=1.0) and the medium ($n_{stratum}$=1.55). This is described by the Fresnel's equation [Wyszecki and Stiles, 2000]. The rest of the incident radiation light (95%) is entering the skin where absorption and scattering occur within the layers. Figure 4.3 represents the optical pathway of the light in human skin.

The scattering and absorption properties of the skin layers require to be quantitatively represented in order to model light transport within the skin. Both scattering and absorption coefficients are wavelength dependent.

The absorption phenomenon corresponds to the energy attenuation of a photon due to the absorption by a particle or a group of particles. Each skin layer is composed of several chromophores; the absorption coefficient of a layer is function of the molar concentration and the absorption coefficient of the molecules present in the layer. Meglinski *et al.* [Meglinski and Matcher, 2002] have defined the equation of the absorption coefficient for a single layer:

$$\mu_a(\lambda) = \sum_{i=1}^{m} \left(\mu_a^{(i)}(\lambda) C_i \prod_{j=1}^{i-1} (1 - C_j) \right) + \mu^{(0)}(\lambda) \prod_{j=1}^{i-1} (1 - C_j) \tag{4.1}$$

where C_i is the volumic fraction of the i^th molecule, m the total number of molecules in the layer, $\mu_a^{(i)}$ the absorption coefficient of the i^th absorber and $\mu^{(0)}$ is the absorption coefficient of the medium without absorber. The different values of the Meglinski skin model are presented in table 4.1.

k	Name of layer	C_{Blood}	C_{H_2O}	$\mu_s(mm^{-1})$	g	n
1	Stratum corneum	0	0.05	100	0.86	1.5
2	Living epidermis	0	0.2	45	0.8	1.34
3	Papillary dermis	0.04	0.5	30	0.9	1.4
4	Upper blood net dermis	0.3	0.6	35	0.95	1.39
5	Reticular dermis	0.04	0.7	25	0.8	1.4
6	Deep Blood net dermis	0.1	0.7	30	0.95	1.38
7	Subcutaneous fat	0.05	0.7	5	0.75	1.44

Table 4.1: The parameters used in the calculation of the absorption coefficients of the blood contented layers of the skin and in the model of the human skin.

The scattering phenomenon is linked to a change of direction of a wave after its interaction with one or several elements of the medium. The wavelength dependency is due to Mie (scattering theory is valid for all possible ratios of particle diameter to wavelength) and Rayleigh (elastic scattering of light by particles much smaller than the wavelength of the light) scattering where Rayleigh scattering dominates in wavelength below 650nm and Mie scattering have a stronger impacts above 650nm [Jacques, 1996]. The values of the reduced scattering of the epidermis and dermis are considered equal and are the sum of the Rayleigh and Mie scattering. Figure 4.4 shows that skin scattering is very close to the sum of Rayleigh and Mie scattering. The Rayleigh scattering is defined as:

$$\mu_{s,Rayleigh}(\lambda) = (2 \times 10^{12})\lambda^{-4} \qquad [cm^{-1}] \tag{4.2}$$

The Mie scattering is defined as:

$$\mu_{s,Mie}(\lambda) = (2 \times 10^{5})\lambda^{-1.5} \qquad [cm^{-1}] \tag{4.3}$$

The reduced dermis/epidermis scattering can be approximated by:

$$\mu_{s',epidermis}(\lambda) = \mu_{s',dermis}(\lambda) = \mu_{s,Rayleigh}(\lambda) + \mu_{s,Mie}(\lambda) \qquad [cm^{-1}] \tag{4.4}$$

One can notice from table 4.1.2 that as the wavelength becomes longer, the incident light reaches deeper into the skin. According to this table, a model taking into account several skin layers seems adequate to correctly model the skin reflectance spectra as modelling a single layer would lose the relation between wavelength and depth.

Figure 4.5 shows the spectral reflectance curves of human skin [Anderson et al., 1981, Wyszecki and Stiles, 2000]. The two spectral reflectances for Caucasian skin are

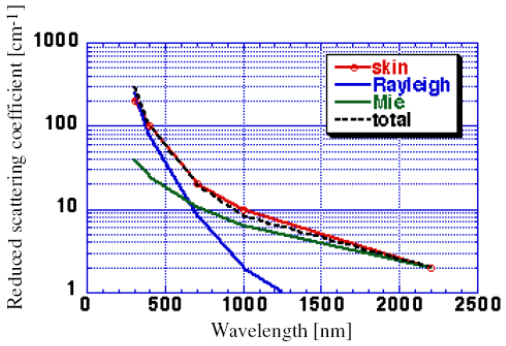

Figure 4.4: Relation between the reduced scattering coefficient, Mie Scattering and Rayleigh scattering [Jacques, 1996].

Wavelength / nm	Depth/μ m
400	90
450	150
500	230
600	550
700	750

Table 4.2: Relationship between depth of penetration of incident light and wavelength in the case of Caucasian skin [Anderson and Parrish, 1982].

higher than the one for dark skin due to a lower melanin concentration [Störring et al., 2000].

4.2 Light propagation models in the skin

Light propagation model in the skin is a very complex task and understanding the light/tissue mechanism in turbid medium (skin) allows its analysis and interpretation.

The light reflected from a surface is generally modelled by the Dichromatic Reflection Model [Klinker et al., 1990]. It describes the light L reflected from a point on a dielectric, nonuniform material (see equation 4.5). This light L is combination of L_{Surf}, the surface reflection (specular, approximately 5% for skin medium) and the light L_{Body} (95%). The body reflection is the light reflected from the material body (diffuse). It penetrates into the materials where it is scattered, partially absorbed at specific wavelength and remitted out of the material.

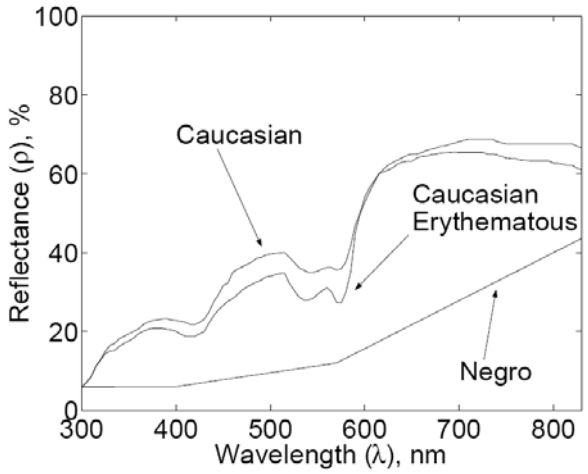

Figure 4.5: Spectral reflectance curves of human skin for normal Caucasian [Anderson and Parrish, 1981], erythematous Caucasian (sunburn) [Anderson and Parrish, 1981], and dark Negro Skin [Wyszecki and Stiles, 2000].

$$L = L_{Surf} + L_{Body} \tag{4.5}$$

Light entering the tissues interacts with its components, this interaction (absorption and scattering) alters the spectral composition of light in a specific way.

Light propagation in skin tissue is dominated by four physical phenomenon of interaction with matter: the reflexion, refraction, scattering and absorption. These phenomena are characterized by the interaction of photons with molecules present in various layers of a propagation medium [Sinichkin et al., 1996]. By combining equation of these phenomena and the known scattering and absorption properties of the main molecules composing the skin tissue, several models of light propagation in the tissue have been developed.

The most common models of light propagation in skin are briefly presented here and include the Radiative transport Equation, Monte Carlo simulation, Kubelka-Munk model and the modified Bear Lambert law. The different light propagation models, presented here, use different optical model and different skin tissue parameters, the reason behind this, is the complex non-homogeneous structure of the skin that some models simplified.

4.2.1 Radiative Transfer Equation model

The Radiative Transfer Equation (RTE) is commonly employed to model light propagation in scattering media, such as neutron propagation in nuclear reactor or also gas in the

atmosphere. This model is defined as an approximation of the Maxwell equations when undulatory phenomena (waves) are not considered.

Despite this simplification, the implementation of this technique, in the case of light propagation in space is impossible because of the complexity of the problem, and therefore it is rarely directly used to simulate light propagation under this current form.

The light propagation, after multiple scattering in turbid media, is not considered as a wave but instead it is expressed as the average energy it contains. The classical way to describe the light as an electromagnetic field is replaced by a measure of specific intensity $I(r, \hat{s}, t)$ which is expressed by:

$$dP = I(r, \hat{s}, t) d\omega da \tag{4.6}$$

where dP is the light power at time t propagating along the direction r to collide with a particle at the section da directed in a cone of solid angle $d\omega$.

The cone of solid angle $d\omega$ is oriented along the unit vector $\hat{s}$ normal to the surface area da. $I(r, \hat{s}, t)$ correspond to the light power (quantity of photons) per unit area per unit solid angle. This simplification is valid only if the wavelength is much lower than the size of the diffracting elements of the media.

The light energy propagation can be characterized by the following parameters: the scattering coefficient (mu_s), the absorption coefficient (mu_a)) and the phase function. The attenuation coefficient is defined as the addition of the absorption and scattering coefficient. The notion of attenuation coefficient mu_t is defined as:

$$mu_t = mu_s + mu_a \tag{4.7}$$

In RTE model, it is considered that only one type of particles is responsible for the scattering and absorption. For RTE, the phase function is approximated by the Henyey-Greenstein function and is modified to include the attenuation coefficient.

The RTE is considered being the most correct equation to describe the propagation of light in skin. Based on the Boltzmann equation, it considers the light propagation as a photon flux which can be locally absorbed or scattered by the biological medium. It is defined as:

$$\hat{s}.\overrightarrow{\nabla}(r, \hat{s}) = -(\mu_a + \mu_s) I(r, \hat{s}) + \frac{\mu_a + \mu_s}{4\pi} \int_{4\pi} p(\hat{s}.\hat{s}') I(r, \hat{s}) d\Omega' \tag{4.8}$$

A finite solution to the RTE is not easily obtained because of its integral-differential

form. However, RTE solution can be approximated. RTE is applicable when limited to simple conditions and slab geometries. Accuracy can be improved by adding robust methods (discrete coordinate).

4.2.2 Monte Carlo method

Monte Carlo (MC) method was first developed by Metropolis and Ulam [Metropolis and Ulam, 1949] to simulate physical processes using a stochastic model. Monte Carlo method, in a general view, searches to evaluate the macroscopic behaviour of a system from a statistical study of its microscopic behaviour. The objective of MC method is to translate a deterministic problem using probabilistic technique and the law of large numbers. It is a stochastic approach by opposition to determinist approach. This intuitive approach favours the analogy with physic reality. This method considers light as a very large set of photons and by randomly simulating the random free path of photons in a turbid medium, it is possible to converge to a steady state of the energy distribution in space after a number of iterations related to the optical properties of the medium.

MC simulations are commonly used to model light propagation in skin tissue for modelling light. In these simulations, each model adopts similar statistical approaches of the processes of interaction between photons and skin layers, but differs from others according to its structural characteristic and its chromophore composition. For skin tissue, this robust method allows the evaluation of the reflected light energy (called reflectance) which is directly linked to light energy absorbed by the different skin layers.

Typically in MC simulation, the main concept is the random walk where a photon path is recorded throughout a medium. A photon is injected into a scattering medium, it propagates in it based on the knowledge of parameters such as mu_s, mu_a and the phase function. MC model statistically computes the optical pathways of each photon in an iterative manner. For accurate results, it requires to perform numerous computation of the photon migration (often in the order of millions iteration), meaning that many photon histories are required and it is computationally expensive and therefore very time consuming and another disadvantage is the noise introduced by the stochasticity. Analytical methods are often preferred but at the expenses of restricting assumptions.

4.2.3 Kubelka Munk model

Kubelka and Munk [Kuberla and Munk, 1931] developed a theory originally based on a simple relationship between the scattering and the absorption coefficient of layers of

paint and its overall reflectance. The Kubelka-Munk (K-M) theory describes the radiation transfer in diffuse scattering media by applying energy transport equations. It is a special case of the radiative transfer equation. Kubelka-Munk developed equations that allow the quantitative studies of absorption, scattering and luminescence in diffuse scattering media. The Kubelka-Munk theory(applied to skin) assumes that the sample possesses inhomogeneities which are small compared with the sample thickness, that the incident radiation is diffuse and that regular reflection occurring at the boundaries of a sample can be neglected. The K-M model is widely used, for example in [Anderson et al., 1981], [Krishnaswamy and Baranoski, 2004], [Igarashi et al., 2007] and in [Cotton, 1997].

> *The Kubelka-Munk theory is one of the most popular and simplest approaches for computing light transport in a highly scattering medium [Igarashi et al., 2007].*

The Kubelka-Munk theory based models, used in tissue optics (also called flux models), employs K-M equations which relate tissue optical properties to measured reflectance and transmittance. Despite the fact that most of the models are based on the two-flux K-M theory, there are models expanding the original formulation to add more coefficients and/or flux.

Kubelka-Munk model is based on the three interactions an incident light ray can encounter at the surface of a medium: reflection, absorption and transmission. KM model divides the light flux passing through a material into two fluxes going in opposite directions.

The equation relating the energy variation of these fluxes on an infinitely small distance dX are known as the Kubelka-Munk (K-M) equations:

$$-\frac{dI}{dX} = -(S+K)I + SJ, \tag{4.9}$$

$$-\frac{dJ}{dX} = -(S+K)J + SI. \tag{4.10}$$

where I is the light intensity inside the sample going downward (transmitted), J is the light intensity going upward(backscattered), S and K are respectively the scattering coefficient and absorption coefficient per unit thickness and x is the distance surface/interaction area.

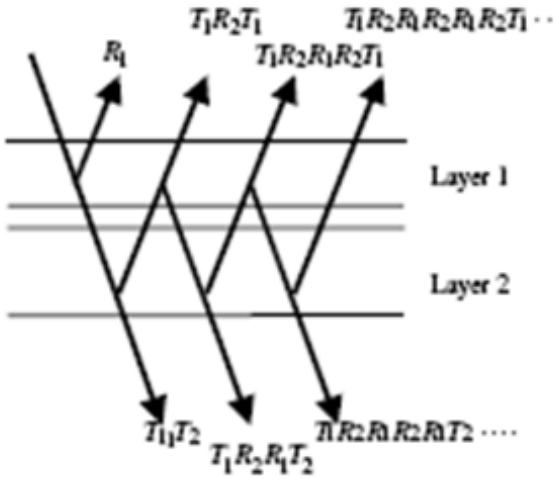

Figure 4.6: Energy separation according to Kubelka-Munk model.

These can be rewritten to express S and K as a function of reflectance R and transmittance T:

$$\frac{K}{S} = \frac{1 + R^2 - T^2}{2R} - 1. \tag{4.11}$$

When the thickness of the medium is very large, the transmittance T is close to 0 leading to:

$$\frac{K}{S} = \frac{(R-1)^2}{2R}. \tag{4.12}$$

By extending the model to two layers, the total reflectance $R_{1,2}$ and total transmittance $T_{1,2}$ can be calculated by rewriting equations 4.9 and 4.10:

$$R_{1,2} = R_1 + T_1T_2R_2(1 + R_1R_2 + R_1^2R_2^2 + \ldots) = R_1 + \frac{T_1T_2R_2}{1 - R_1R_2}, \tag{4.13}$$

$$T_{1,2} = T_1T_2(1 + R_1R_2 + R_1^2R_2^2 + \ldots) = \frac{T_1T_2}{1 - R_1R_2}. \tag{4.14}$$

For a n layered system (see figure 4.6), the model can be extended from the two layer model where the total remitted and transmitted light is calculated. The n layered system results in values for $R_{12\ldots n}$ and $T_{12\ldots n}$ written as :

$$R_{12\ldots n} = R_{12\ldots n-1} + \frac{T^2_{12\ldots n-1} R_n}{1 - R_{12\ldots n-1} R_n}, \tag{4.15}$$

$$T_{12\ldots n} = \frac{T_{12\ldots n-1} T_n}{1 - R_{12\ldots n-1} R_n}. \tag{4.16}$$

The described system of equations permits the computation of the total remitted and transmitted light from a n layered system with arbitrary complexity if the thickness and composition of the layers are specified.

The Kubelka-Munk theory is flexible. The K-M model allows expansion of the model to several layers and/or adding more coefficients and several papers present extension of the original model. The K-M models have an analytical form and it offers rapid skin optical parameters determination using inversion procedures. However, its apparent simplicity and speed are obtained at the expense of lower accuracy [Tuchin, 2000] compared to MC methods. It also can be expended to Near-Infrared range according to Cotton [Cotton, 1997].

The results of the theoretical model of light interaction with a multi-layer optical system provide a good investigation tool. The model can recover a number of parameters characterising skin structure, including amount of epidermal melanin, dermal blood, papillary dermal thickness from standard colour and infrared images. According to the authors of [Cotton, 1997], the model can serve as a powerful simulation system for medical applications, and can generate explanations of why skin diseases manifest themselves through some specific appearances (including malignant melanoma, port wine stains, nevi, wound healing, etc).

4.2.4 The Modified Beer-Lambert Law model

The Beer-Lambert law is used in [Meglinski and Matcher, 2003], [Shimada et al., 2001a], [G.N. Stamatas, 2008] and [Tsumura et al., 2003]. This technique tries to account the spectral distortion induced by multiple scattering via a linearised equation relating the general tissue attenuation -ln(I/I_0) to the tissue absorption coefficient μ_a:

$$A = -\ln\left(\frac{I}{I_0}\right) = \mu_a \sigma \rho + G \tag{4.17}$$

where ρ is the spacing between the source and the detector and σ is a scaling factor taking into account the path lengthening effect of the random walk experienced by photons as they propagate through the multiple scattering medium. G is an offset term determining either

the tissue-probe geometry or the scattering (according to Twersky's multiple-scattering theory [Twersky, 1962, Twersky, 1970]); it depends on μ_s, the scattering coefficient. Equation 4.17 is a linear relationship between -ln(I/I_0) and μ_a helps to estimate the relative concentration of chromophore in the skin. According to [Meglinski and Matcher, 2003], equation 4.17 can be rewritten for N chromophores as:

$$A = a + b\lambda + \sum_{i=1}^{N} C_i \epsilon_i(\lambda). \tag{4.18}$$

G is of the form $a + b\lambda$ and μ_a being the sum of absorption coefficients for each chromophore determined by the absolute concentration C and specific absorption coefficient ϵ of each chromophore. Then, equation 4.18 for a, b and C_i can be solved by measuring A with a minimum of $N+3$ wavelengths using multi-linear regression [Press et al., 1992].

The modified Beer-Lambert, using absorption properties of skin layers (blood, water, melanin and chromophores content) can simulate skin reflectance spectra.

4.3 Methods for retrieving skin component information using the previous models

In this section, we present methods to retrieve skin chromophore composition based on model of light propagation from diffuse reflectance spectrum. The difference between the models is characterized by the type of light propagation model employed and the number of layers and chromophores chosen by the authors. The study is concentrated on the analysis of visual reflectance spectra.

Shimada *et al.* [Shimada et al., 2001b] employed a modified Beer-Lambert law as a model for light propagation in skin. The skin is defined as a three layers structure (epidermis, dermis and subcutaneous fat). The model considers three skin components: melanin, blood and a component grouping all the chromophores in skin apart from melanin and blood. A multiple linear regression analysis was applied to estimate melanin and blood concentration. To validate their model, skin phantom with known properties were fabricated. This requires only a short calculation time. However, this model is limited in terms of parameters and shows errors in visible wavelength extremity for the estimation of melanin.

Douven and Lucassen [Douven and Lucassen, 2000a] present a method for the retrieval of optical properties of skin from diffuse reflectance. The simulated reflectance spectra are based on a diffusion approximation analytical model which is a simplification of the

radiative transfer equation. The skin model is composed of five layers with two main chromophores (melanin and blood). Comparison between simulated and acquired diffuse reflectance spectra was performed using a fitting based on the Monte-Carlo method.

Meglinski and Matcher [Meglinski and Matcher, 2002] present a model of light propagation in tissue as it takes into account a large number of subdivisions of the principal skin layer with their different molecular characteristics. The model studies the propagation of photon in a series of cutaneous layers with totally different optical properties according to their molecular properties. It decomposed the skin into seven layers and several chromophores such as blood, blood oxygen saturation, water volume and other chromophores. The Monte Carlo model simulates light propagation in the visible and near infrared region. Multi-linear regression analysis fits the data and can retrieve quantitative information of skin chromophores of interest. This model is one of the most widely used for the study of light propagation in skin tissue.

Doi and Tominaga [Doi and Tominaga, 2003] presents a model to describe the human skin colour and to estimate the surface spectral reflectance. The human skin is modelled by two layers (epidermis, dermis). Reflectance estimation was defined using the Kubelka-Munk theory with five weights parameters: melanin, oxy-haemoglobin, deoxy-haemoglobin, carotene and bilirubin and it provides also the skin surface reflectance. The estimated reflectance was fitted with the measured values using least square method to retrieve five parameters.

Claridge *et al.* [Claridge et al., 2006] developed a physics-based model to retrieve skin parameters from multispectral images. The skin is decomposed into three layers (epidermis, papillary dermis and reticular dermis). The light propagation model is based on the Kubelka-Munk two-flux equation. Abnormal skin is taken into account in the model and is outlined for diagnostic analysis. The system outputs four parametric maps, total melanin, dermal melanin, thickness of the papillary dermis and blood one.

Verkuysse *et al.* [Verkruysse et al., 2005a] present a method to retrieve skin parameters using library-based fitting. The skin model uses a simple two-layered geometry (epidermis, dermis) and the light propagation is simulated using diffusion equation analytical solution. The method does not concentrate on the selection of optical properties but rather on the possibility of using library based fitting procedure. The library is generated using nine skin parameters for a total of around nine millions spectra. The fitting procedure tries to match a measured spectrum to a simulated one. The library search is divided into two: a global and then a local search. This technique seems always matching the best fit, however, the skin parameter values are often unrealistic data.

In the following chapter, the data processing developed to extract information from reflectance cubes generated by ASCLEPIOS is presented.

Chapter 5

Human skin optical properties retrieval

The development of methods to assist diagnosis of skin pathology is based on objective assessment of skin characteristics. Skin diffuse reflectance is of great interest as it contains important information about the skin physical and chemical properties. The spectral reflectance shape is a result of interaction between light and the complex medium which is the skin (due to the many chemical constituents, their quantities and varying structure of the skin [Van Gemert et al., 1989]). The absorption/scattering effects modify the re-emerge light and deliver information regarding the optical properties of the medium under study. The study of the reflectance can be correlated with the biochemical and morphology composition to reveal information about the skin condition.

The interest of the previously reconstructed reflectance cube is the retrieval of skin component parameters from each spatial area by mean of spectral analysis. Analysis of this reflectance cube can provide non-invasive evaluation of skin condition through the 2-D mapping of relative meaningful skin chromophore concentrations [Vogel et al., 2007].

There exist two main categories to analyse human skin reflectance spectrum.

One category is based on statistical analysis of the reflectance spectrum. Several researches base their skin parameters retrieval by multivariate methods such as partial least squares regressions [Zonios et al., 2001] Support Vector Machine (SVM) [Prigent et al., 2010b], Blind Source Separation (BSS) [Prigent et al., 2010a] or Independent Component Analysis (ICA) and Principal Component analysis (PCA) [Tsumura et al., 2003] to determine the concentration of skin chromophores. However these methods mostly lack the integration of the geometrical and optical skin information. These techniques as-

sumed that skin reflectance is a linear combination of different source component spectra weighted by their mixing quantities. The techniques are based on composition assumption. Generally, melanin and haemoglobin are assumed to be the two main components of the skin. They do not have *a-priori* information about the skin concentration and scattering. This category of analysis can be affected when the skin composition is different from the assumption. These methods remain uncertain.

Another category refers to the analysis of reflectance spectra by means of physical models of light transportation that are based on the optical properties of skin (scattering and absorption). Different light propagation models have been developed such as model based on Monte Carlo simulations, Kubelka-Munk and the modified Beer-Lambert Law (methods introduced in section 4.2). The main motivation to use light propagation model to estimate skin parameters is related to the physical basis of the model of light propagation. The properties of the model are obtained from the availability of *a-priori* knowledge of the skin absorption spectra and scattering properties. The parameter estimation problem is assimilated as an optimization problem. Therefore, using this information to retrieve skin parameters means that it requires solving an inverse problem. The analysis is performed by inversing the model to match a real reflectance spectrum with simulated spectrum generated by a model of light propagation. Several optimization approaches have been developed to estimate skin parameter quantities from measured reflectance spectra such as least-squared library search, Levenberg-Marquardt and genetic algorithm.

Our interest is to exploit the reflectance cubes acquired by ASCLEPIOS to provide dermatological analysis about the skin content. Using the knowledge of the skin absorption and scattering properties, we propose a method based on a physical model of light propagation coupled with an optimization technique. The interest of such analysis focuses on the *a-priori* knowledge of the parameters to retrieve as they are defined in the model. The technique aims to be used for general analysis and was selected because it offers the advantage of being based on a model with a physical meaning. It is in opposition to statistical methods which require assumption of the retrieved parameters. This is potentially a problem in case of disease with total lack of a skin component assumed.

In this chapter, we present a skin optical model according to its skin layers, absorption and scattering properties, followed by an extended description of the Kubelka-Munk model of light propagation. Then, we detail the Genetic Algorithm used to optimize the inversion of our model.

5.1 Skin optical model

Human skin reflectance varies between individuals due to the variation of the physiological skin composition (among different skin phototypes) and within body location for each individual. The aim of skin analysis is to retrieve the different parameter's composition (melanin, haemoglobin concentration, layer thickness) based on a model of light propagation. A model of light propagation simulates reflectance by taking into account absorption and scattering properties of the skin and aims to vary accordingly to real skin reflectance. The selection of a model is based on the achievability to reproduce real skin spectrum using a set of characteristic parameters including skin lesions (diseases, scars) which also affect the physical and/or chemical skin structure. Developing a model intents to objectively quantify skin parameters for diagnosis and follow-up process.

Several skin models have been developed with various numbers of skin parameters and different numbers of layers (2 [Kim and Moscoso, 2005], 3 [Svaasand et al., 1995], 5 [Douven and Lucassen, 2000b], 7 [Meglinski and Matcher, 2002] and even 22 layers [Magnain et al., 2008]). However, regardless of the sophistication of the models, of the numerous chromophores and layers composing the skin, it is accepted that the human skin appearance, in terms of colour and reflectance spectrum in the visible domain, is mostly a result of melanin and haemoglobin concentration (with melanin the main epidermis constituent and haemoglobin, the main dermis constituent) [Anderson and Parrish, 1982, Young, 1997]. Most of the models are developed in the diagnostic-therapeutic window (500 to 950 nm).

Following this assessment, we selected a model with two layers optically homogeneous, the upper layer is the epidermis and the dermis being the lower one. The model defined for our explorative study of the skin is based on the five principal parameters affecting the skin reflectance: melanin concentration, epidermis thickness, blood concentration, blood oxygen saturation and dermis thickness. The following section characterizes the optical properties (absorption and scattering) of the mentioned parameters. A brief description of the epidermis and dermis chromophores optical properties will complete the previous skin description made in section 4.1.

5.1.1 Epidermis optical properties

The epidermis, in the visible range, absorbs and propagates light. The absorption is performed by the main chromophore contained in the epidermis, the melanin [Jacques, 1998b]. It exhibits strong absorption in the violet region of the spectrum and its absorption

is attenuated accordingly to the wavelength increase (see figure 5.1).

The epidermis absorption property is mostly due to the melanin and lightly by the baseline absorption coefficient. The melanin absorption level varies depending on the volume fraction of melanosomes per unit and ranges from 1.3% for lightly pigmented skin to 45% for darkly pigmented skin [Jacques, 1998b]. The melanin spectral absorption coefficient is approximated by:

$$\mu_{a.melanosome}(\lambda) = 6.6 \times 10^{11} \lambda^{-3.33} \ [cm^{-1}]. \tag{5.1}$$

The epidermis and dermis skin layers are not only composed of their main components (melanin, haemoglobin). Other intrinsic constituents of these two layers also affect the light. The effect of carotene, keratin and collagen are neglected in the retrieval process because of their single absorption coefficients do not affect the reflectance significantly in the visible domain in comparison to the one of melanin and haemoglobin. The combined absorption of the different neglected skin components is taken into account by Jacques *et al.* which defines an equation for the baseline absorption coefficient free of the major chromophores which is similar for these two layers [Jacques, 1998b]:

$$\mu_{a.baseline}(\lambda) = 0.244 + 85.3 \exp \frac{-(\lambda - 164)}{66.2} \quad [cm^{-1}]. \tag{5.2}$$

For simplification purpose, epidermis and stratum corneum are regarded as a single layer because the stratum corneum light absorption is low and transmit light uniformly in the visible wave-range [Anderson and Parrish, 1981].

The optical absorption coefficient of the epidermis $\mu_{a.epidermis}$ is expressed as a function of the wavelength and depends mostly on the volume fraction of melanosome and lightly on the baseline skin absorption coefficient:

$$\mu_{a.epidermis}(\lambda) = f_{mel} \ \mu_{a.melanosome}(\lambda) + (1 - f_{mel}) \ \mu_{a.baseline}(\lambda) \ [cm^{-1}]. \tag{5.3}$$

where λ is the wavelength in nanometres and $\mu_{a.melanosome}$ is in cm^{-1}. The f_{mel} refers to the volume fraction of melanosome in % and $\mu_{a.baseline}$ is the baseline absorption in cm^{-1}.

5.1.2 Dermis optical properties

The dermis, in the visible range, absorbs and propagates light. The dermis thickness ranges from 0.6 to 3 millimetres. The absorption is performed by the main chromophore contains in the dermis, the blood [Jacques, 1998b]. Within the red blood cell, the haemoglobin is a major absorber and it is decomposed into oxy-haemoglobin (HbO_2) and deoxy-haemoglobin (Hb) components. The values of absorption coefficient for the deoxy- and oxy-haemoglobin were obtained from the Oregon Medical Laser centre website [Prahl, 1999] (see figure 5.1). Oxy-haemoglobin absorption spectra have two absorption peaks at around 542 and 578 nm, revealing the characteristic 'W' shape. The volume blood fraction varies between 0.2 to 7% (see table 5.1). Due to simplification, blood is considered evenly distributed within the whole dermis layer.

The total haemoglobin absorption spectrum is defined as:

$$\mu_{a.blood}(\lambda) = \mu_{a.oxy}(\lambda) + \mu_{a.deoxy}(\lambda) \ [cm^{-1}]. \tag{5.4}$$

The oxygen saturation level of blood typically ranges from 0.25 to 0.9 [Meglinsky and Matcher, 2001]. The relative oxygen saturation can be estimated using the concentration of oxy and deoxy-haemoglobin by the following equation:

$$R_{SO_2} = \frac{C_{HbO_2}}{C_{HbO_2} + C_{Hb}} \ [\%]. \tag{5.5}$$

The dermal absorption coefficient $\mu_{a.dermis}$ is expressed by:

$$\mu_{a.dermis}(\lambda) = f_{blood}(C_{HbO_2}\mu_{a.oxy}(\lambda)) + f_{blood}(1-C_{HbO_2})\mu_{a.deoxy}(\lambda) + (1-f_{blood})\mu_{a.baseline}(\lambda) \ [cm^{-1}] \tag{5.6}$$

where λ is the wavelength in nanometres. f_{blood} is the volume fraction of melanosome in %. C_{HbO_2} is the concentration of oxy-haemoglobin in blood. $\mu_{a.oxy}$ and $\mu_{a.deoxy}$ refer respectively to the absorption coefficient of the oxy-haemoglobin and deoxy-haemoglobin in cm^{-1}. $\mu_{a.baseline}$ is the absorption coefficeint of the skin baseline in cm^{-1}.

Subcutaneous layer is ignored because its main function is light absorption and mostly contains fat [Shimada et al., 2001a] and limited visible light reaches this layer.

Water is the body main constituent. However its absorption is insignificant in the visible domain. Its absorption is stronger in the NIR(see figure 5.1). It provides very limited effect on the reflectance spectrum despite modifying its concentration. Therefore, water concentration was not added in the skin model.

The physiological values to be estimated are constrained between realistic upper and

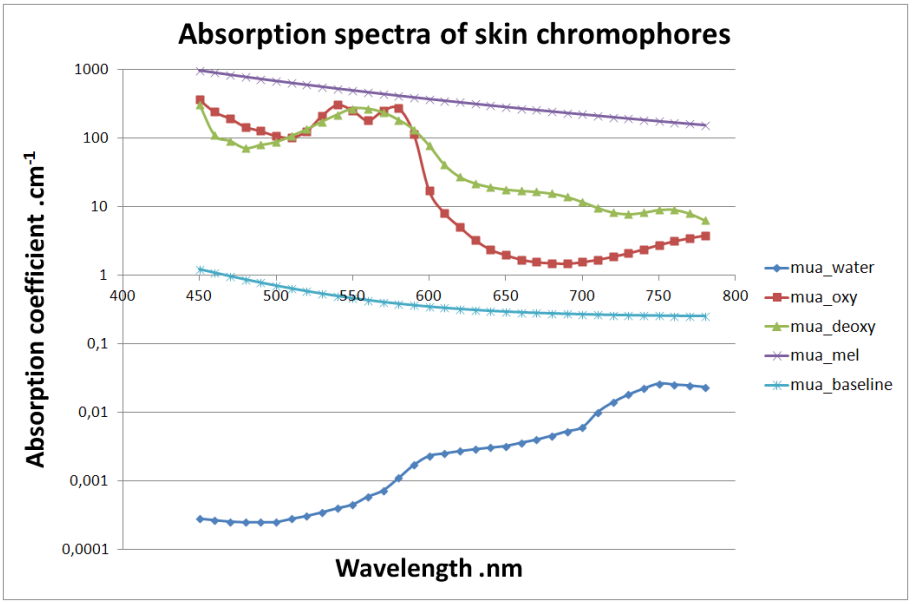

Figure 5.1: Absorption spectra of the main skin chromophores: melanin, oxy-haemoglobin, deoxy-haemoglobin, water and skin baseline.

Skin parameter	Range	Reference
Melanin concentration	1.3 to 45%	[Jacques and McAuliffe, 1991]
Epidermis thickness	0.015 - 0.15mm	[Anderson and Parrish, 1981, Doi and Tominaga, 2003]
Volume blood fraction	0.2 - 7%	[Meglinsky and Matcher, 2001, Kim and Moscoso, 2005]
Oxygen Saturation	25 - 90%	[Meglinsky and Matcher, 2001]
Dermis thickness	0.6-3mm	[Bashkatov et al., 2005, Anderson and Parrish, 1981]

Table 5.1: Skin parameters.

lower limits and are summarized in table 5.1. These data are reported from the literature.

5.2 Kubelka-Munk model of light propagation

The Kubelka-Munk (KM) model [Kuberla and Munk, 1931] was originally developed to model the reflectance and transmittance of layered painted surface from simple relationship between the scattering and the absorption coefficient. This model is one very popular for the computation of light transport in highly scattering medium. It has been extended to skin by different groups [Anderson et al., 1981, Krishnaswamy and Baranoski, 2004, Igarashi et al., 2007, Cotton, 1997]. In section 4.2.3, the general KM model was presented in term of interaction between two layers but no information was given on the determination of

the transmittance and reflectance of the skin for a single layer.

The interest of the Kubelka-Munk model is mainly due to its simplicity and particularly to the formula linking the coefficients of absorption and scattering from a measured diffused reflectance. This method is chosen for its flexibility toward the selection of a skin model, allowing rapid implementation of models with various numbers of skin parameters and skin layers. The model is based on the propagation of light between layers into two directions (forward and backward) and considers the skin as parallel slate.

To use Kubelka-Munk theory, assumptions need to be made. We consider that the skin consists of a finite number of layers and assumes that each layer is homogeneous in terms of optical properties (absorption and scattering coefficients) and that they have constant thickness. It assumes that the size of particles of a layer are small compared to the layer thickness. The model considers that the medium is irradiated by lambertian illumination and the light re-emitting from each layer after scattering is similarly distributed uniformly.

The principle of the K-M model was briefly explained in section 4.2.3 for the total reflectance of a n-layers medium. We detail the Kubelka-Munk model in terms of reflectance and transmittance for a single layer. It can be calculated based on the thickness of the layer d_{layer}, the layer absorption coefficient $\mu_{a.layer}$ and the layer scattering coefficient $\mu_{a.layer}$. Both absorption and scattering coefficient are function of the wavelength.

The equation to calculate the reflectance `R` and transmittance `T` for one layer defined by Kubelka-Munk are expressed by:

$$R_{layer}(\lambda) = \frac{(1-\beta(\lambda)^2)(\exp K(\lambda)d_{layer} - \exp -K(\lambda)d_{layer})}{(1+\beta(\lambda))^2 \exp K(\lambda)d_{layer} - (1-\beta(\lambda))^2 \exp -K(\lambda)d_{layer}} \tag{5.7}$$

and

$$T_{layer}(\lambda) = \frac{4\beta}{(1+\beta)^2 \exp Kd_{layer} - (1-\beta)^2 \exp -Kd_{layer}} \tag{5.8}$$

where K is the backward flux variable of one layer expressed by:

$$K_{layer} = \sqrt{\mu_{a_{layer}}(\mu_{a_{layer}} + 2 \times \mu_{s_{layer}})} \tag{5.9}$$

and β is the forward flux variable of one layer expressed by:

$$\beta_{layer} = \sqrt{\frac{\mu_{a_{layer}}}{\mu_{a_{layer}} + 2\mu_{s_{layer}}}} \tag{5.10}$$

The coefficient $\mu_{a_{layer}}$ and $\mu_{s_{layer}}$ in equation 5.9 and 5.10 refers respectively to the absorption coefficient and the scattering coefficient (detailed in section 4.1.2) of a skin

layer and d_{layer} is the layer thickness.

The total reflection of a two layer medium is defined by the following equation:

$$R_{total} = R_{12} = R_1 + \frac{T_1^2 R_2}{1 - R_1 R_2}, \tag{5.11}$$

and

$$T_{total} = T_{12} = \frac{T_1 T_2}{1 - R_1 R_2}. \tag{5.12}$$

The model allows fast computation of the total reflectance and transmittance of a medium based on the absorption and scattering coefficient and thickness of each layer.

The five biological parameters used to simulate a reflectance spectra can be represented by an input function denoted:

$$p = (f_{mel}, D_{epi}, f_{blood}, C_{oxy}, D_{dermis}). \tag{5.13}$$

The simulated reflectance spectrum is expressed by:

$$R_{sim}(\lambda) = f_{KM}(f_{mel}, D_{epi}, f_{blood}, C_{oxy}, D_{dermis}). \tag{5.14}$$

where R_{sim} is the simulated reflectance spectrum calculated using the KM equation 5.7 and f_{KM} is a function containing the parameters of the model.

The reflectance spectrum is calculated on a wave-range from 450 to 780 nm with a step size of 10 nm.

5.2.1 Forward model: testing parameters variation

Following the defined parameters from table 5.1, The KM two layers model is tested by generating reflectance spectra where each one of the main components of our model is varying within its biological defined range from the literature. For every parameter variation analysis, four fixed parameters are set at constant values to provide easy interpretation of the variation effect(see table 5.2). The aim of the forward model testing is to generate reflectance spectra and to evaluate individually the effect of the modification of one of the five parameters that are adjustable.

5.2.1.1 Epidermis thickness

Figure 5.2 shows the effect of the increase of the epidermis thickness layer. The reflectance decreases as proportionally to the increase of the thickness due to higher absorption from

Skin parameter	Symbol	Fixed value
Melanin concentration	f_{mel}	0.2%
Epidermis thickness	D_{epi}	0.015 cm
Volume blood fraction	f_{blood}	2%
Oxygen Saturation	C_{oxy}	60%
Dermis thickness	D_{dermis}	0.2 cm

Table 5.2: Fixed skin parameters for the reflectance analysis individual parameter effect.

the melanin component. The reflectance shape is affected by the increase of D_{epi} because less light reaches the dermis layer, leading to a gradual dissappearance of the haemoglobin 'W' pattern.

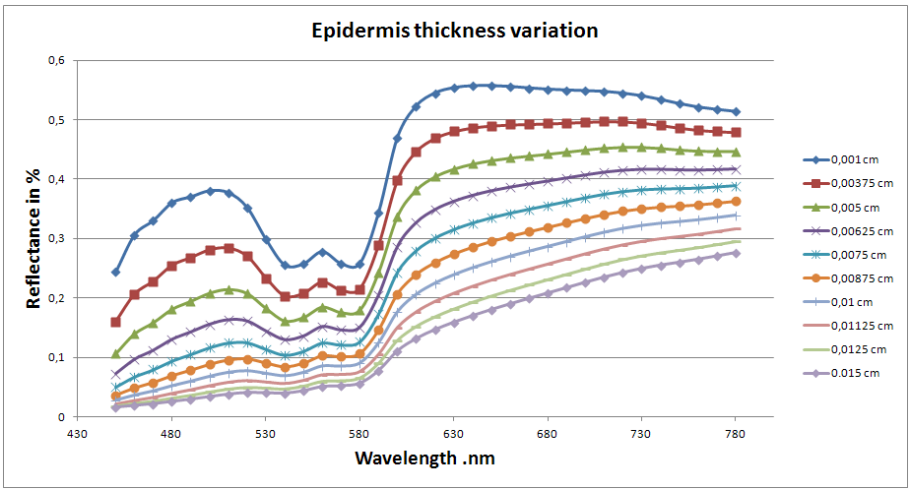

Figure 5.2: Reflectance with variation of the epidermis thickness from 0.001 to 0.015 cm.

5.2.1.2 Melanin

The variation of the melanosome volume fraction ranges from 1.3% to 45% (from lightly pigmented to highly pigmented skin). Figure 5.3 shows that the increase of melanosome volume inversely decreases the reflectance curves. High reflectance refers to fair skin people whereas low reflectance is obtained for darker skin individual. The haemoglobin characteristic absorption shape is highly attenuated for high concentration of melanosome which is a result of high absorption by the melanin, leading to limited amount of light reaching the dermis.

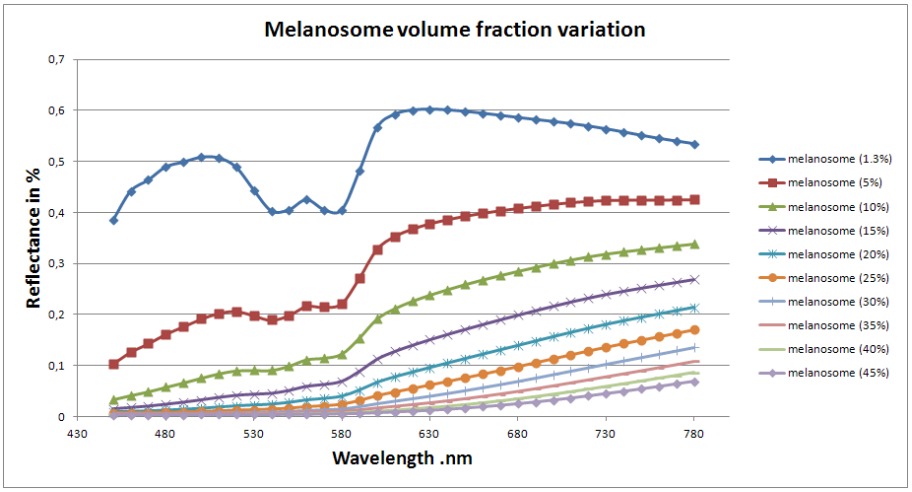

Figure 5.3: Reflectance with variation of the melanosome volume fraction from 1.3 to 45%.

5.2.1.3 Dermis thickness

The variation for the dermis thickness ranges from 0.5 to 3 mm. In comparison to an increase of the epidermis thickness which lowers the reflectance spectra, an increase of the dermis thickness leads to an increase of the reflectance due to its scattering nature from the collagen fibers.

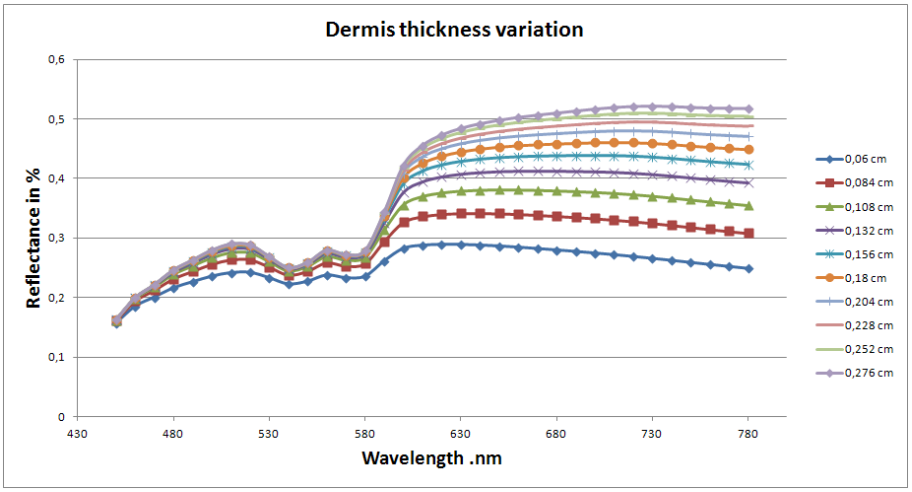

Figure 5.4: Reflectance with variation of the dermis thickness from 0.06 to 0.3 cm.

5.2.1.4 Blood volume fraction

The variation of the blood volume fraction shows a strong influence in the 500 to 600 nm range (see figure 5.5). High blood concentration has the effect to lower the reflectance spectra in the characteristic region, revealing the 'W' shape of the haemoglobin.

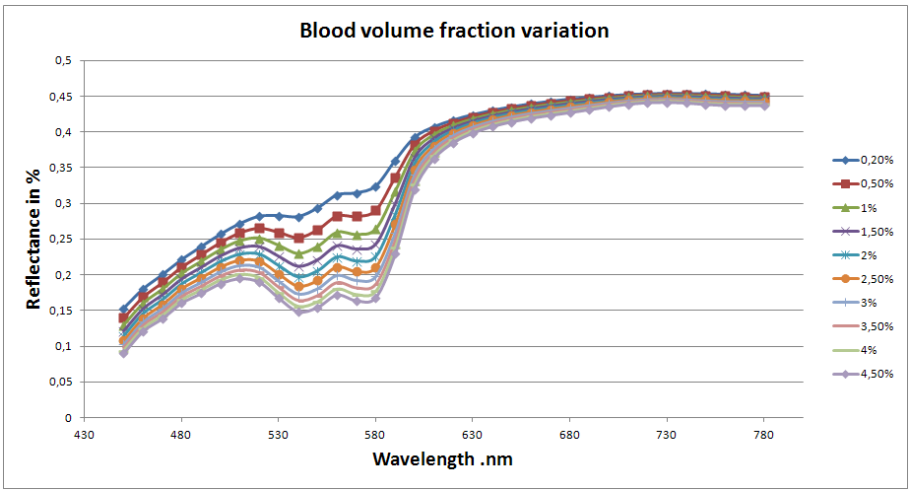

Figure 5.5: Reflectance with variation of the blood volume fraction from 0.2 to 7%.

5.2.1.5 Relative oxygen saturation

The relative oxygen saturation only affects the characteristic signature of the haemoglobin in the 530 to 580 nm (see figure 5.6). Despite its low effect on the reflectance spectra, the relative oxygen saturation is influenced by the surrounding area of the measure. Such information is of interest for diagnosis purpose and therefore is included in the model.

The figures show the behaviour of the reflectance spectra when one parameter evolves through its valid range. The variation of each parameter from the model seems to reproduce reflectance spectra in accordance to measured spectra. The result from the forward model indicates that a two-layered medium, with five flexible parameters, seems an appropriate skin model.

5.3 Genetic Algorithm for inverse problem optimization

The main objective of our method is not the analysis of the direct model (i.e. the effect of the parameters on the simulated reflectance spectrum). For diagnosis purpose, it is useful

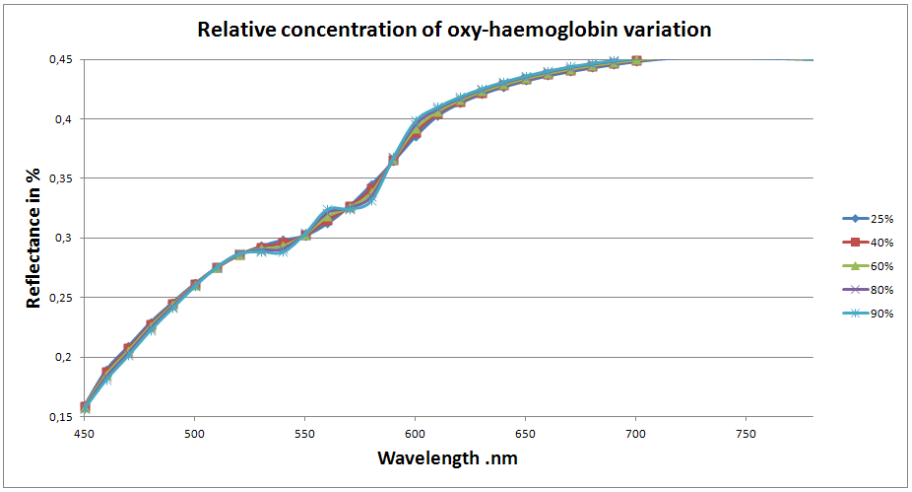

Figure 5.6: Reflectance with variation of the blood volume fraction from 25 to 90%.

to depict the concentration of the different skin parameters from acquired spectra.

We previously presented a model of light propagation based on a two-layers skin medium simulated using the Kubelka-Munk theory. The model generates reflectance spectra using five physiological parameters that can vary. From our research, the ASCLEPIOS system provides reflectance spectra. We need to extract information from these spectra. It requires solving an inverse problem to obtain skin parameter concentrations. This inverse problem is nonlinear due to the complex structure, in terms of scattering and absorption properties, of the two layers skin model.

Inversion procedure aims to retrieve biochemical and optical skin properties from non-invasive measurement. The inversion means to reverse the model of light propagation in which parameters are input to generate a reflectance spectrum. The inversion of our model aims to retrieve these five parameters by matching simulated spectra generated by the model with measured one. This technique necessitates generating simulated spectra and finding the one which matches the measured one, thus obtaining the parameters. This procedure can be performed manually by modifying the parameters until a similar spectrum is obtained, however this task is time consuming [Svaasand et al., 1995]. Search and optimization problems, such as parameter estimation in inverse skin light propagation model, require an optimization criterion. This criterion is generally a degree of similarity between a measured spectra and a simulated spectra by a model based on a set of estimated parameters. The goal of the optimization process is to retrieve a set of parameters which maximises the degree of similarity.

There exists many techniques of search and optimization, such as library search, least-square fitting, Genetic Algorithm to mention some.

Method based on library search requires building a library which needs to calculate spectra for a large number of skin parameter combinations and store the simulated spectra. The retrieval of the skin parameter is performed by fitting measured spectra with spectra from the library. According to Verkruysse *et al.* [Verkruysse et al., 2005b], their method based on a library search is capable of quickly and accurately find skin parameters from a library of nine million spectra. The spectra fitting procedure is based on a two steps search: a global and a local one. However, their method only works on simulated spectrum while only retrieving unrealistic values on measured data. To avoid such scenario, our model limits the range of values to physically plausible one, therefore avoiding the possibility of finding unrealistic values.

Another method to solve non-linear least squares model is the Levenberg-Marquardt Algorithm (LMA) [Gill et al., 1981]. It is based on Gauss-Newton algorithm and gradient descent method. This method is usually employed for minimizing a function from a space of parameters. Yudovsky *et al.* [Yudovsky and Pilon, 2010] solved their inverse problem to retrieve skin parameter using LMA. The LMA is a popular method for curve fitting algorithm, our current problem, but the major drawback of LMA is its solution which only finds local minimum and not global minimum. Thus this method was discarded for our analysis.

Among the different existing techniques of search and optimization, our interest focused on Genetic Algorithm (GA). GA is a metaheuristic method that optimizes a problem through iterative improvement of a candidate solution with a quality measurement. For some problems, it is hard to find an exact solution. The difficulty does not arise due to the complexity of the problem but rather from the excessive size of the search space. As a result, it is unthinkable to test every solution to find the best one. Search of a global solution using GA is done on a population of candidates rather than a single candidate. The strengths of GA are its capacity to explore large search space (through mimic of natural evolution) and most importantly, its strength against becoming trap into a local minimum (by introduction of random search). GA does not necessitate calculating derivatives and neither needs a continuous fitness space. The effect of the different parameters may result in several local optima (due to the effect of each parameter) where GA is more likely to find global optimum in comparison to other methods.

Attempts using GA to retrieve skin parameters of a Monte Carlo for Multi-Layered (MCML) media have been tested by Zhang *et al.* [Zhang et al., 2005] and a hybrid version

of it was developed by Choi [Choi, 2010]. Both prove the usefulness of the GA, but they also retrieve unrealistic values mainly due to the non constraint of the search space.

5.3.1 Introduction to Genetic Algorithm

In this section, a general overview of the Genetic Algorithm is presented by first, briefly referring to its roots, the Darwin's theory of evolution [Darwin, 1859]. We present general overview of the Genetic Algorithm applied to search and optimization technique, followed by the description of the GA steps. Finally, the adaptation of the GA for our application is presented.

To synthesise the Darwin Theory, the concept which is roughly imitated for the conception of GA is based on the idea that the apparition of species adapted to a medium is the consequence of the conjunction of two phenomena: natural selection imposed by the medium (individuals the most adapted to the medium survive and reproduce themselves) and undirected variations of the genetic material of the species (by pseudo-random variation of the parameters of some individuals). It is these two principles which are implied by the GA.

The concept of Genetic Algorithm has been introduced by Holland [Holland, 1975] for the computer science and artificial intelligence field but it has also being extended to other domains (Business, engineering,...). GA are explorative algorithms based on the mechanism of natural selection and genetic. Explorative algorithm considers the principal of survival of the fittest individual and the exchange of pseudorandom information. GA are one of the few optimization methods to optimize several criterions simultaneously.

5.3.2 GA overview

GA requires a representation of the solution space and a fitness function to evaluate the population of individuals. The evolution of the population is roughly based on an iterative three steps process: selection, crossover and mutation.

Using GA, solutions (also named individual, phenotype) to a problem need to be represented as a genome (or chromosome). The chromosome contains the function parameters. The algorithm starts the evolution by initially generating a population of random chromosomes. Each individual from the population is evaluated by a fitness function (for each iteration) and only the individuals with high fitness values are given more probability to reach the new population of the next iteration (selection process). Most individuals from the population undergo reproduction operations (mutation and crossover) to generate a

new population of individuals. This process terminates either after a number of iterations or after the population reaches an expected fitness level. The aim is to move a set of individuals adapted to the medium representing the global optimum solution.

5.3.3 GA steps

Genetic algorithm can be decomposed in several steps: encoding, population generation, fitness function, selection, genetic operation. Among these step, there are two critical components of genetic algorithm which are highly problem dependent, the encoding of the chromosome and the fitness function.

5.3.3.1 Coding

Coding is an essential aspect which consists of the representation of potential solutions (called chromosomes) by a set of parameters. A chromosome is divided into genes. A gene is the representation of a single parameter of the model.

There are two main ways to code chromosomes: binary and real value encoding (see figure 5.7). Other coding techniques can be represented using trees, arrays, lists, strings of characters.

Binary coding is historically represented by an array of bits. It is mostly chosen as it is the original representation selected by Holland [Holland, 1975]. This coding is defined as strings of 0s and 1s. It aims to allow simple crossing and mutation operators. However it needs to be carefully parameterized as bits for one parameter have to cover its partition space within its search space range. The coding requires that a modification of a single bit does not generate a parameter to exit its specified range when the decoding process occurs to return to the variable space.

Real value coding is simple as it can be anything related to the problem. Chromosomes, for this type of coding, are a string of real values. The advantage of this coding technique is that the variable of the parameters can be directly used for the coding of individuals without requiring intermediary binary coding. This approach delivers greater precision than the binary coding according to Fleming *et al.* [Fleming and Purshouse, 2002].

5.3.3.2 Population generation

Genetic Algorithm begins with the generation of a population of P individuals. Each individual is described by N genes containing the parameter model (see figure 5.8).

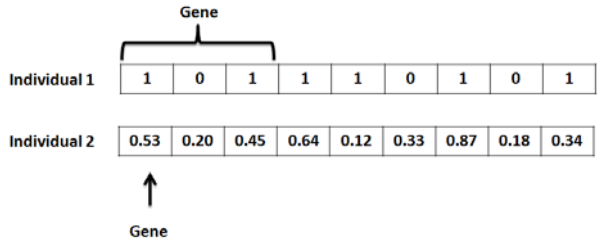

Figure 5.7: Coding representation: Binary coding for Individual 1 and Value coding for Individual 2.

There are two important aspects of the population: the initial population generation and the population size. Individuals are randomly generated to ensure that the pool of individuals is able to cover and explore the whole search space.

The population size depends on the problem and needs to be randomly chosen or defined empirically through test. The choice of the initial population sets the speed of convergence of the algorithm. A large population generally guaranties that the search space will have a high probability to be more explored than with a smaller population. However, it necessitates more time for the algorithm to converge.

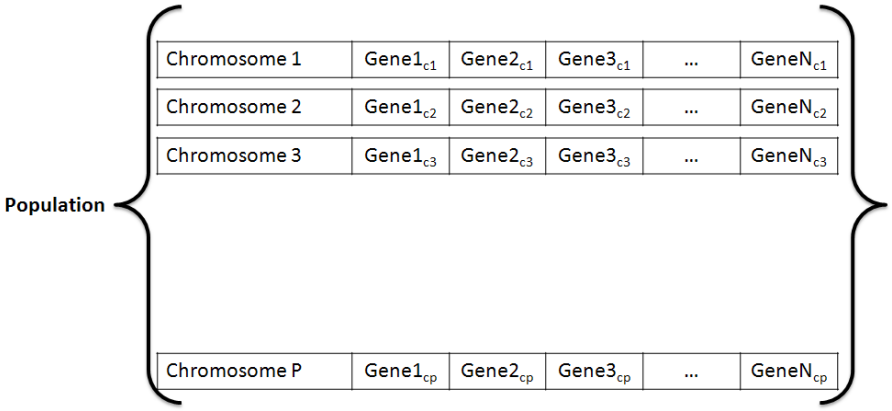

Figure 5.8: Population representation: a P population is composed of N genes.

The population evolves through selection and reproduction steps. The evolution leads to the creation of children from parents of the previous population (generation t). The population is iteratively evaluated by a fitness function which selects the best individual in regards to the model.

There are several strategies for the evolution of the population in the literature [Goldberg, 1989, Holland, 1992]. One strategy consists of selecting the nb_{best} best individuals

from an intermediate population composed of children and parents to form a new generation. Another strategy is based on a new population entirely composed of children. This approach might lose the best individual from the previous generation. An alternative method is a compromised from two previous approaches. Children regularly replace the weakest individuals from the current generation.

5.3.3.3 Fitness function

The fitness of an individual for genetic algorithm refers to an objective value that calculates the performance of the chromosome parameters in regards to the problem. This function is crucial to lead the population toward the global optimum. It implicitly performs a pressure on the selection toward this direction. The fitness function is applied to each chromosome and returns a single value of fitness which reflects the usefulness of the chromosome from the population.

Fitness function is problem dependent, meaning that one fitness function will be helpful to solve one problem but might not be generalized to other problems. Fitness function should remain not too computationally expensive as it will be evaluated numerous times in the GA process.

5.3.3.4 Selection

Selection is an operation based on the principal of adaptation of an individual from a population in its environment following the theory of natural selection. Following this concept, only fittest individuals to some criterion will survive and take part in the generation of a new population as parents. Selection is a technique that is usually based on the random picking of chromosomes according to their fitness values. Strong probability of selection is given to chromosomes with high fitness values, this refers to as the selection pressure.

The convergence speed of the population is affected by the type of selection pressure chosen. High selection pressure leads to fast convergence rates. Although, this might cause the convergence towards a local optimal. The selection process aims to both apply selection pressure and conserve population diversity.

There are several techniques for the parent's selection such as roulette wheel, ranking, tournament, random selection to mention some.

The roulette wheel selection (also refered to as fitness proportionate selection) is among the first selection techniques for GA. Considering a maximisation problem with only posi-

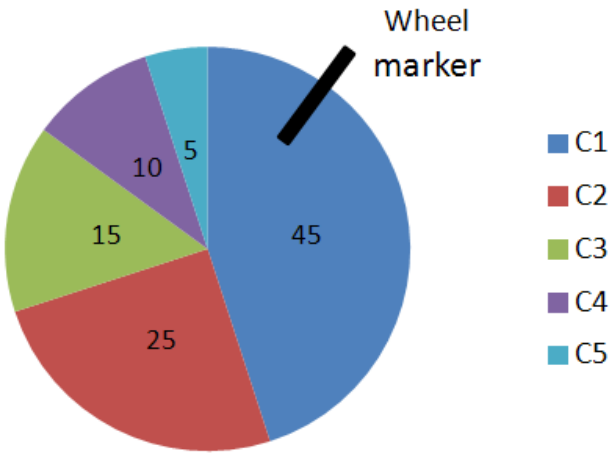

Figure 5.9: Roulette wheel selection: 5 individuals (C1 to C5) with probability of respectively 45, 25, 15, 10 and 5 based on their fitness.

tive fitness values, this technique gives to each individual a selection probability based on its performance. Figure 5.9 illustrates the wheel selection, where probability of selection is given to an individual based on their fitness in regards to the fitness of the population. The selection process is performed by spinning the wheel and individuals are selected to be a parent when the wheel marker stops on them. The wheel spins P times, with P the number of individuals in the population. The method tends to discard the least fit individual through after numerous spinning.

The ranking selection, as its named indicated, ranks the population. There is no randomness in this selection mode. This procedure will only conserve the nb_{best} best individuals based on their ranking position.

Tournament selection uses competition between pair of individuals to perform the selection pressure. The best individual of the pair corresponds to the one with the highest fitness value. This competition is repeated until the next generation is filled. The overall population of children has a higher average fitness.

The random selection chooses parents from the population randomly, uniformly and without effect of the fitness value. Each individual have a probability of $1/P$ to be selected with P, the population size.

The selection process is part of the overall GA procedure. To generate new other individuals for the next generation, another important procedure is the recombination operation which is applied to the initial population.

5.3.3.5 Genetic operators

After the selection process, the population undergoes reproduction to generate a new population. The crossing operation requires at least a pair of parents to generate two offspings/children. Mutation operation necessitates only one parent.

5.3.3.5.1 Crossing

The idea behind the crossing operation is the exchange of genetic information between parents. The exchange of genetic information expects that the children contain relevant information from the parents. The crossing combines two random parents to breed two children. The simplest procedure of crossing can be synthesized by three steps: The crossing operator randomly selects two individuals from the population; a random gene is selected from the chromosome; the gene information, at the specific location, is interchanged between the two parents and generate two children.

There are several types of crossing operators, mainly single crossing point (see figure 5.10) and multi-point crossing (see figure 5.11). Generally, the crossing procedure interchanges the gene of two parents in one or several points. This operation can be applied to different types of coding (real-value, binary) as it only involves gene swapping.

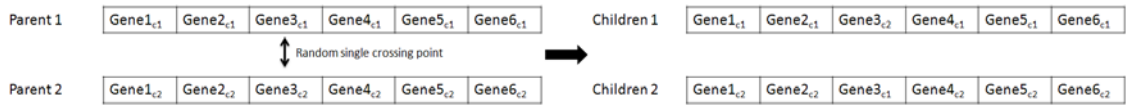

Figure 5.10: Single point crossing. The gene 3 is interchanged between parents 1 and 2.

The crossing is said to be lethal when crossing produces one or two individuals with weak fitness which is/are unlikely to reproduce themselves. To avoid the effect of numerous lethal crossings, the operation can be directed toward selection of individuals with good fitness to become parents. This process tends to limit the exploration of the search space and may lead to premature convergence.

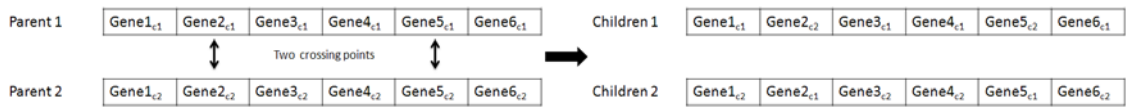

Figure 5.11: Two crossing points. The genes 2 and 5 are respectively interchanged between parents 1 and 2.

Eiben *et al.* [Eiben et al., 1994] suggest that crossing with multiple parents generate

better quality chromosome. Crossing of parents with close genes information rarely provides new information in the population, affecting the algorithm convergence speed. The crossing probability of an individual ranges from 0.6 to 0.95.

5.3.3.5.2 Mutation

The main idea of the mutation process is aimed at maintaining diversity in the population and avoiding to be trapped into a local minimum. After the crossing operation, some individuals of the intermediary population are selected for mutation operation. The mutation operation randomly introduces genetic information back into one parameter of individuals of the population.

The mutation process takes different forms regarding the coding of the population. For binary coded solution (see figure 5.12), the mutation randomly selects a bit and inverts it (named flipping). For real value mutation, the gene is randomly selected and a new gene is randomly generated within its variation range.

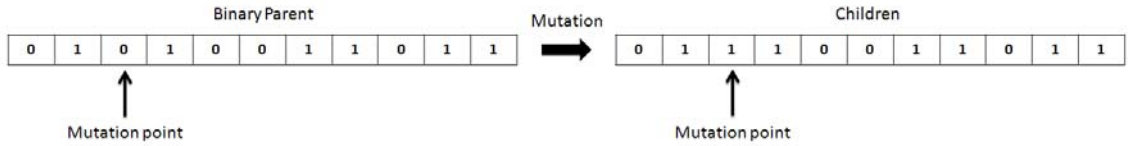

Figure 5.12: Mutation of a binary coded parent.

These two processes (crossing and mutation) result in the generation of a new population with different chromosomes from the initial one. Genetic operators are not systematically applied to every individual from a generation. The most common scheme is to perform sequentially the crossing follows then by the mutation operation on part of the population but there are an infinite number of possible combinations using multiple crossing and mutation operators in a single algorithm.

If the fitness function is appropriately selected, the average fitness of the new population is increased by this procedure. Although crossover and mutation are the main genetic operators, other operators have been developed and interested readers should refer to Eiben *et al.* [Eiben et al., 1994] for more information.

5.3.3.6 Termination

The GAs are techniques based on generation of population of solution through iterations. There are three ways for the GA to achieve the termination condition: a specific fitness

value is reached, the population converges to an optimal solution or a defined number of iteration is accomplished.

The random genetic diversity defines the variety of chromosomes in the population. The diversity becomes null when the entire population is identical. It is considered that the algorithm has converged. When the genetic diversity is low, it is unlikely that the diversity will increase again. In the case that the convergence happens early, it falls into local optima (premature convergence). It is important to preserve genetic diversity without preventing convergence. This leads to the dilemma of exploration - exploitation.

While designing the algorithm, it is necessary to find a trade-off between exploration of the search space (to avoid being trapped into a local optimum) and exploitation of the best individual. Too much exploitation leads to a convergence toward a local optimum whereas over exploration leads to the non-convergence of the algorithm. Exploitation step refers to the selection and crossing operation while exploration relates to the population initialisation and mutation. The effect of exploration and exploitation can be modified by the various algorithm parameters. However, the literature on GA does not provide an universal rule on how to tune the different parameters for successful outcome. It must be done empirically by testing and checking the effect of the various algorithm methods.

5.3.4 GA optimization for Kubelka-Munk inversion model

The aim of our overall system is to retrieve maps of skin parameters from our measured data (reflectance cube) (see figure 5.13). The maps are generated pixel by pixel as the analysis is performed one single reflectance spectra at a time. The parameters are obtained by inversing the KM model. The inversion refers to input defined parameters into the KM model to generate reflectance spectra. The comparison is calculated between a simulated spectra and a measured one. It provides a measurement of fitness to determine how "good" is the generated spectra. By optimizing the parameters of the inverse model, the simulated spectrum is modified and one can recover a simulated spectrum similar to the acquired one. As we previously presented, this optimization is carried out by Genetic Algorithm technique.

In this section, we detail the implementation of our technique to retrieve characteristic skin parameter maps from skin lesion. The idea of our technique is to integrate Genetic Algorithm to the inverse Kubelka-Munk model (see figure 5.14).

GA process is defined as a three stages operation. The first operation consists of the generation of a population composed of individuals. This is followed by the fitness calculation of the population. Finally, the evolution of the population is performed.

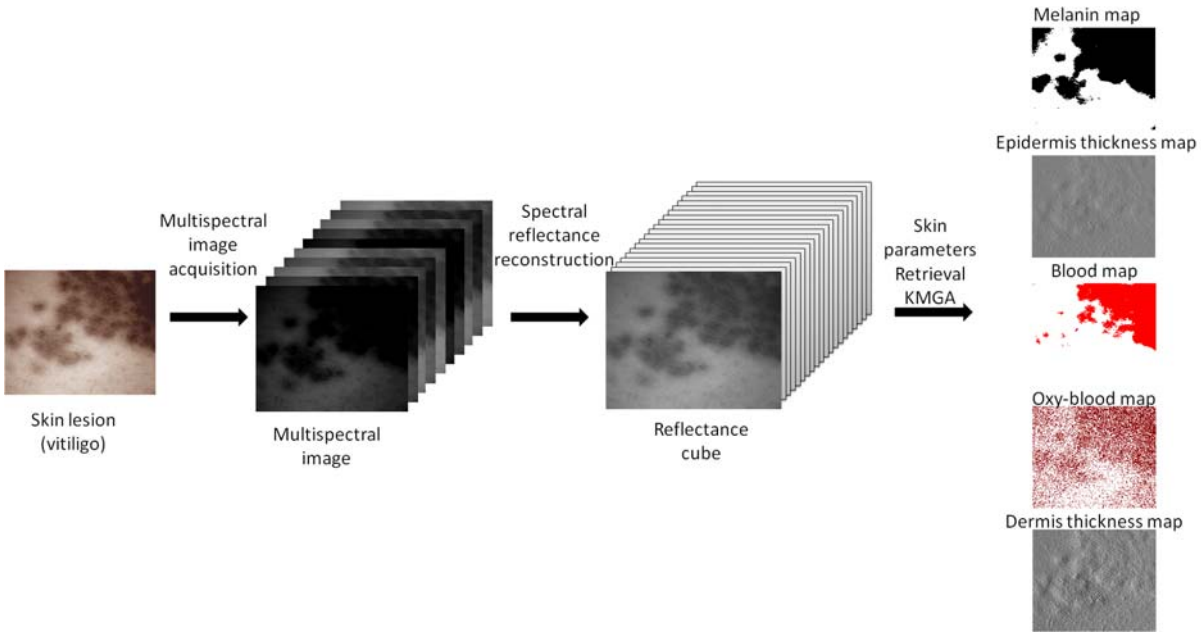

Figure 5.13: Asclepios full system: from the acquisition to skin parameter maps retrieval.

5.3.5 Initial population

GA initial procedure is the creation of a population of solution candidates (individuals, chromosomes). The population is composed of P individuals. Chromosomes of the population are encoded using real value function. This type of encoding was selected due to the large range values for each parameter (see table 5.3) which would imply a coding and decoding process in case of binary coding. As seen in section 5.1, five variable parameters are employed in the Kubelka-Munk model to simulate light propagation in skin.

$$C_p = \langle f_{mel}, D_{epidermis}, f_{blood}, C_{oxy}, D_{dermis} \rangle \tag{5.15}$$

These parameters are selected to encode the chromosomes of our GA. It is represented by equation 5.15. The initial population (see figure 5.15) is generated totally randomly to try to ensure large coverage of the search space.

To avoid problem (retrieval of unrealistic values) encountered by Zhang *et al.* [Zhang et al., 2005] and Choi [Choi, 2010], we limit the search space for each parameter to their minimum and maximum physiological values found in the literature.

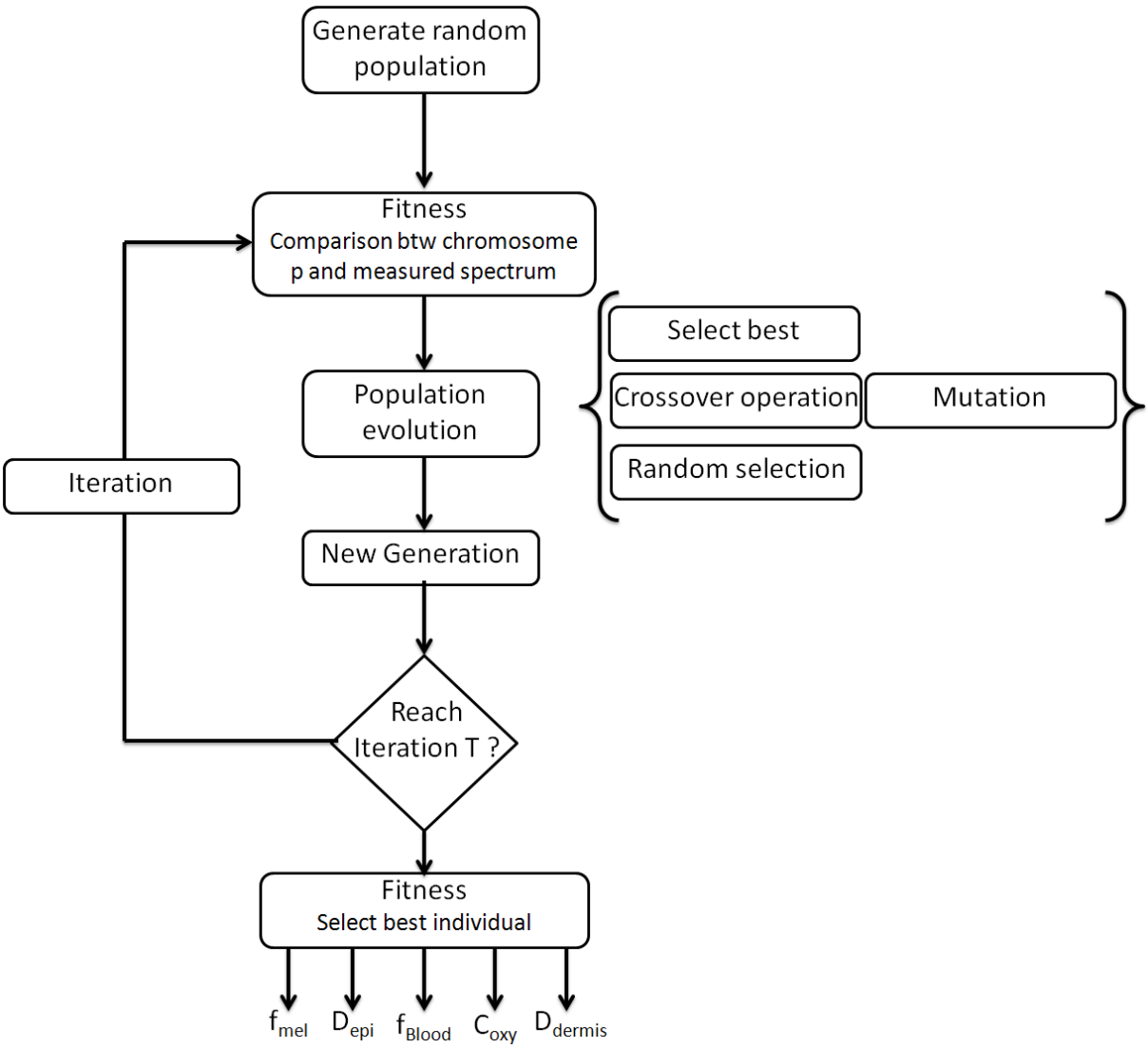

Figure 5.14: Overall GA implementation for the inverse Kubelka-Munk model.

5.3.6 Fitness function

Fitness function is probably the most important aspect of the genetic algorithm as it requires classifying the best individual which is the most similar to the measured spectrum.

Figure 5.16 represents the process of the fitness function. The fitness function is applied to every chromosome of the population. The genes of a chromosome are inputted into the forward KM model to generate a simulated spectrum. The fitness function calculates the similarity between a measured spectrum and a simulated one (using the forward KM

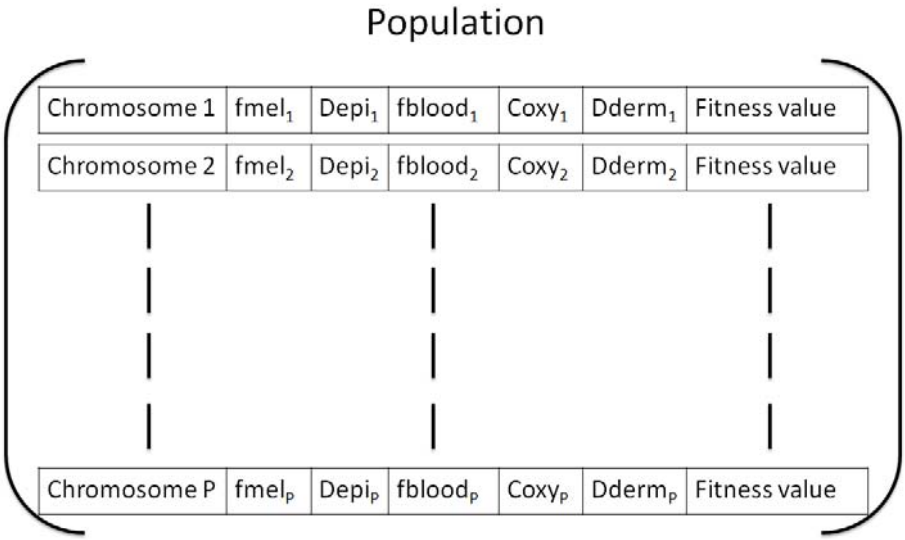

Figure 5.15: Coding representation of our GA.

Skin parameter	Range	Step	Search space size
Melanin concentration (f_{mel})	1.3 to 43%	0.1	417
Epidermis thickness (D_{epi})	0.025 - 0.15mm	0.001	125
Volume blood fraction (f_{blood})	0.2 - 7%	0.1	68
Oxygen Saturation (C_{oxy})	25 - 90%	1	65
Dermis thickness (D_{derm})	0.6-3mm	0.1	24

Table 5.3: Size of search spaces for each skin parameter.

model). We tested two additional metrics in addition to the three used in section 3.3.1. The calculated fitness value is used to classify the population from the best to worst one for the selection process.

In the search of an optimal fitness function for our GA application, the following five different metric scales are: the Root Mean Squared Error (RMSE), the Goodness of Fit Coefficient (GFC), the Reconstruction Percentage (RecP), the Modified Spectral Angle Similarity (MSAS) and the Spectral Similarity Value (SSV).

5.3.6.1 Root Mean Squared Error

The RMSE calculates the mean of Euclidean distance values between two spectra. Reconstruction is good when RMSE is close to zero. RMSE is calculated using the following formula:

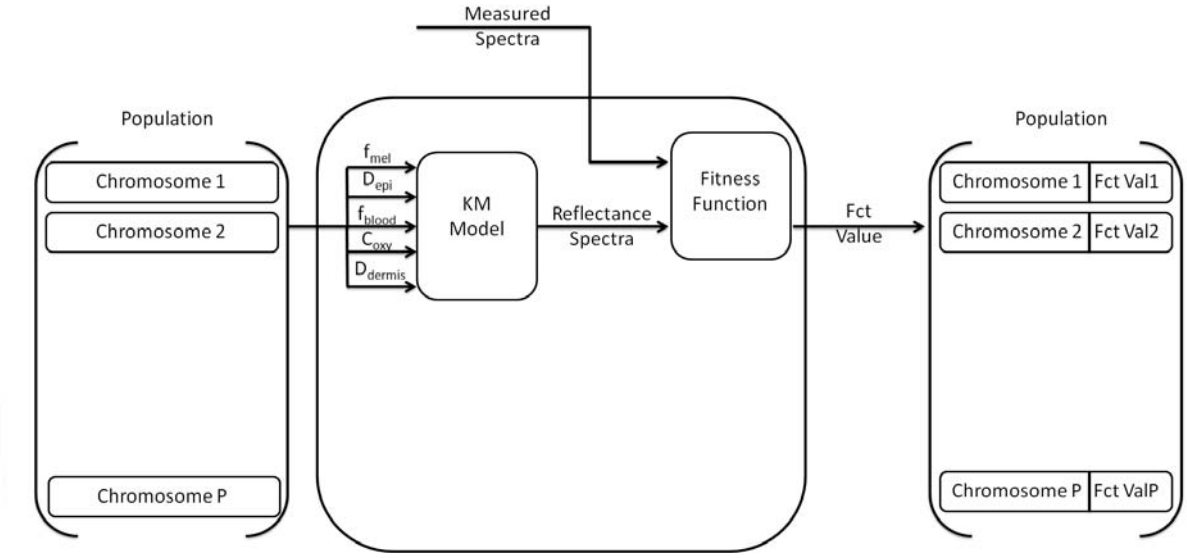

Figure 5.16: Fitness function of our GA.

$$RMSE = \frac{1}{N}\sum_{j=1}^{N} \|R_m(\lambda_j) - R_s(\lambda_j)\|^2 \tag{5.16}$$

where $R_m(\lambda_j)$ is the spectrum value measured with the spectrophotometer at wavelength λ_j and $R_s(\lambda_j)$ is the simulated spectra value at wavelength λ_j and N the number of samples.

5.3.6.2 Goodness of Fit Coefficient

The GFC is based on the Schwartz inequality and is calculated using the following formula:

$$GFC = \frac{\left|\sum_j R_m(\lambda_j) R_s(\lambda_j)\right|}{\left(\sum_j [R_m(\lambda_j)]^2\right)^{1/2}\left(\sum_j [R_s(\lambda_j)]^2\right)^{1/2}}. \tag{5.17}$$

This criterion has the advantage to be bounded between 0 and 1, providing an easy interpretation. According to Hernandez *et al.* [Hernández-Andrés et al., 2001], the reconstruction is good if the GFC is above 0.99 and perfect is higher than 0.9999.

5.3.6.3 Reconstruction Percentage

The RecP is a criterion which evaluates the distance between two spectra as a percentage of the measured spectrum. It requires a higher precision for the spectrum part having low amplitude. A good reconstruction will be close to 100%. It is defined by:

$$RecP = 1 - \frac{\sum_{j=1}^{N} \|R_m(\lambda_j) - R_s(\lambda_j)\|^2}{\sum_{j=1}^{N} \|R_s \lambda_j\|^2}. \tag{5.18}$$

5.3.6.4 Modified Spectral Angle Similarity

The Spectral Angle Similarity (SAS) value is expressed as a spectral angle between a reference and a simulated spectrum. The equation defining the angle is formulated by Yuhas *et al.* [Yuhas et al., 1992] as:

$$SAS = \arccos\left(\frac{\sum_{j=1}^{N} R_m(\lambda_j) R_s(\lambda_j)}{\sqrt{\sum_{j=1}^{N} R_m(\lambda_j)^2} \cdot \sqrt{\sum_{j=1}^{N} R_s(\lambda_j)^2}}\right) \tag{5.19}$$

Spectra have strong similarity for small angle value. Modification of this formula was proposed by Schwarz *et al.* [Schwarz and Staenz, 2001] to rescaled the SAS value between [0,1] instead of $[0, \frac{\pi}{2}]$ to facilitate the interpretation with other metric scales. The new SAS value called Modified Spectral Angle Similarity (MSAS) value is expressed by:

$$MSAS = \left(\frac{2SAS}{\pi}\right). \tag{5.20}$$

5.3.6.5 Spectral Similarity Value

The SSV is a combination of the Euclidean distance and correlation similarity. It is expressed by:

$$SSV = \sqrt{Ed^2 + (1-\rho)^2} \tag{5.21}$$

where Ed is the Euclidean distance (equation 5.22) between a measured spectra and a simulated one and ρ refers to the correlation similarity (equation 5.23). The Euclidean distance measures the average spectral reflectance whereas the correlation differentiates the shapes between two spectra. Overall, the SSV associates both average spectral reflectance and shape similarity. Best results are obtained for the SSV values that are the closest to zero [Granahan and Sweet, 2001].

Euclidean distance (Ed) measures the difference of magnitude between two vectors but is not able to differentiate their shapes. The Ed used in equation 5.21 is defined by:

$$Ed = \sqrt{\sum_{j=1}^{N}(R_m(\lambda_j) - R_s(\lambda_j))^2}. \tag{5.22}$$

The correlation coefficient measures the similarity between two spectra and is expressed by:

$$\rho = \frac{1}{N-1}\left(\frac{\sum_{j=1}^{N}(R_m(\lambda_j) - \mu_m)(R_s(\lambda_j) - \mu_s)}{\sigma_m \sigma_s}\right) \tag{5.23}$$

where μ is the mean and σ is the standard deviation of respectively the measured reflectance spectra and the simulated reflectance spectra.

5.3.7 Population evolution

The first stage of the evolution process is to apply genetic operation to the population t which will generate an intermediate population t' (called mating pool). For the evolution, the population undergoes selection, crossover and random operations. Then, few individuals from the intermediate population mutate to produce the next generation of the population.

The population initial t, the intermediate population t' and the next generation of the population $t+1$ all have the same size. The size of the intermediate population is expressed by

$$P' = Nb_{Best} + Nb_{Random} + \frac{Nb_{Crossing}}{2} \tag{5.24}$$

where Nb_{Best} is the number best individuals selected on their ranking, Nb_{Random} is the number of individuals randomly selected to reach the population t' and $Nb_{Crossing}$ is the number of pairs of parents that undergoes crossover operation.

After the fitness process is applied to the population, each chromosome has a fitness value. We chose a deterministic selection as we rank the population based on the fitness value. This is considered as an elitist selection.

Contrary to Whitley and al. [Whitley and Kauth, 1988, Whitley, 1989] with its genitor style algorithm, we do not directly transfert the best individuals to the new population $t+1$. The Nb_{Best} individuals are copied to the intermediate population t' but also kept in the population t meaning that they can still be selected by other genetic operators.

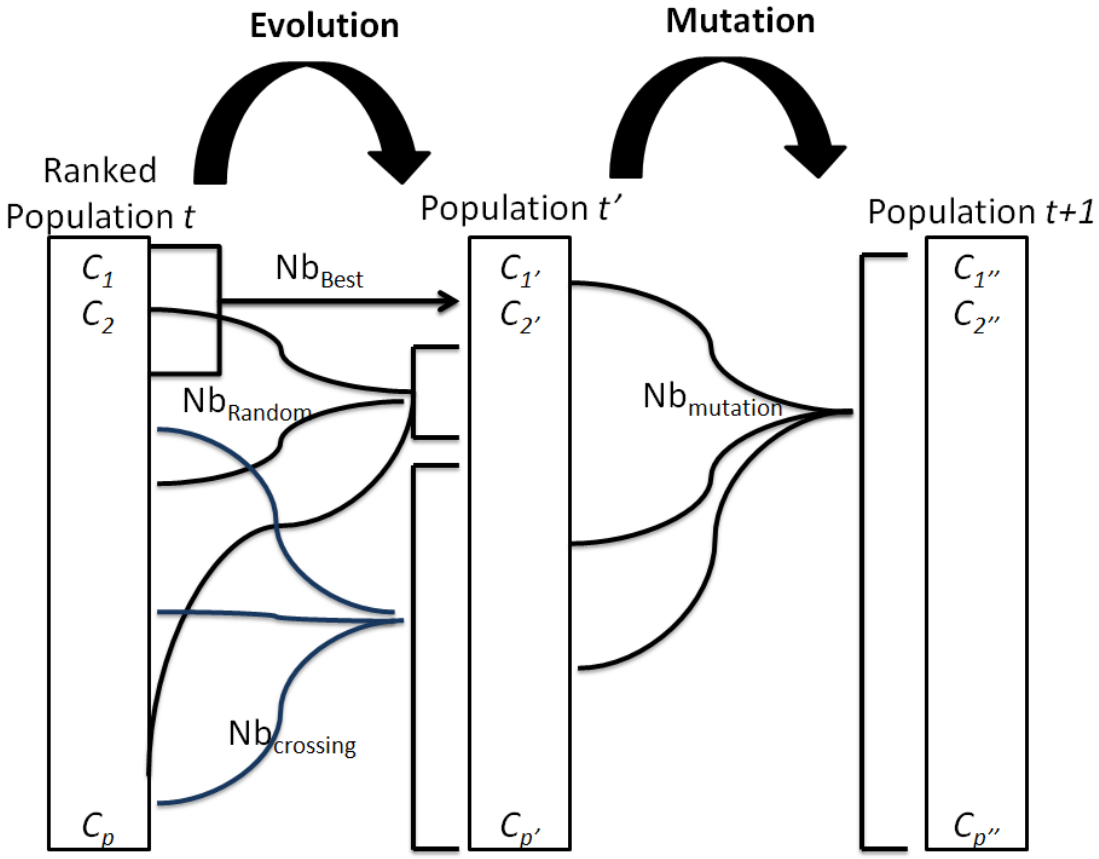

Figure 5.17: Population evolution representation. C, C' and C" refers respectively to a chromosome of the initial, intermediate and next population.

Among the different reproduction and evolution possibilities offered through the literature, Mühlenbein [Mühlenbein, 1992] states that only using mutation works quite well for evolution strategy when compared to Hill-climbers or hyperplane samplers. However to favour a wider exploration of the search space, we add also crossover operations.

During the next step of the evolution, the random operator selects individuals from the population and places them in the *t'* population. The aim of maintaining is to conserve diversity in the population.

Crossover operation consists of swapping one randomly selected parameters between two randomly chosen parents to generate two offsprings. In our method, chromosomes being composed of five parameters, the probability P_cg of a gene to be swapped is 0.2. The probability for a chromosome to be selected for crossover, between population t and

t', is defined as P_c and is expressed by:

$$P_c = \frac{Nb_{Crossing}}{Nb_{population}}. \tag{5.25}$$

The crossover operation is an important technique to increase the fitness of the population.

Following the crossover operation between population t and population t', a mutation operator is applied to the population t' in order to generate the next population. The mutation is applied to a low random number of children. The mutation alters randomly one parameter of the child chromosome by generating a new random value for the parameter. Again, the chromosome containing five parameters, the probability P_mc of a gene to mutate is 0.2. The probability for a chromosome to mutate from population t' to $t+1$ is defined as P_c and is expressed by:

$$P_c = \frac{Nb_{Mutation}}{Nb_{population}}. \tag{5.26}$$

The aim of mutation operator is to introduce some randomness to the search and increase the probability that no part of the search space is unexplored.

There are different criterions to stop the evolution of the algorithm. Due to the difficulty to reach a specific fitness function for different spectra, the termination criterion is chosen as a number of iterations. This technique has the advantage to set a finite computation time for the algorithm and if properly selected, one can reach optimum result. However, at the final iteration, the algorithm may not have yet converged.

5.3.8 Genetic Algorithm parameters selection

Each steps of the GA requires to be defined. As there is no golden rule for the selection of the different parameters, empirical methods were tested.

Over all the parameters required to be selected for the GA, there are two important steps of the algorithm that condition the evolution of the population. The population size and the choice of the fitness function. The latter is the basis of the GA as it serves for the evaluation of each chromosome of the population. Therefore, the first priority is the selection of a fitness function for our problem. We then set the population size. For these two processes, the crossing and mutation probabilities are randomly selected to be respectively 60% and 1%.

We chose to select the different GA parameters using their order of importance in

Fitness function	Error f_{mel}	Error D_{epi}	Error f_{Blood}	Error C_{oxy}	Error D_{derm}	Fitness value
RMSE	0.61923	1.58853	0.15156	0.34123	0.16036	0.25E-05
RecP	0.70624	4.50422	0.19175	0.05573	0.18067	7.51E-04
GFC	0.73465	7.84658	2.48428	0.01333	0.55049	1.61E-04
MSAS	0.73708	4.30711	0.76797	0.06918	0.33498	1.11E-02
SSV	0.73737	4.28300	0.14822	0.39916	0.13553	5.89E-02

Table 5.4: Average error in pourcentage for a defined simulated spectrum performed ten times.

the development of a GA technique. The most discriminative parameters is the fitness function (defining the quality of an individual), followed by the population size (referring to the exploration of the search space) and finally the number of iterations of the GA is defined (convergence of the population).

5.3.8.1 Fitness function

The variation of the different parameters affected the entire wave-range of the spectra (450 to 780 nm with a 10 nm step). Therefore, the fitness function is calculated over the entire working range as we do not favour a parameter to be selected.

The selection of one fitness function from the five presented in section 5.3.6 is obtained from forward calculation of reflectance spectra based on known parameters. Two characteristic sets of parameters were defined (corresponding to lightly and darkly pigmented skin) to estimate the quality of the fitness function for inverse problem. White Gaussian noise with amplitude of +/- 0.1 was added to the simulated spectra. The quality for each fitness function and simulated spectrum were performed ten times and averaged.

The population size is 500 and the number of iteration is set at 100 for the fitness function selection.

The quality of the fitness function is defined by the fitness values and by the average percentage of error between the input parameters and the retrieved ones which are dependent of the simulation. For fair discrimination between the function, GFC and RecP were inverted so that fitness values close to zero means good fitness.

Table 5.4 reveals that RMSE performs better than the four other fitness functions with lower noise percentage of the retrieve values and it has the lower fitness value.

Figure 5.19 and 5.18 respectively shows the comparison between the fair and darkly pigmented simulated spectrum and the five retrieved spectra. Best spectra are obtained with RMSE, RecP and SSV fitness function, with retrieved spectra clearly matching the

simulated spectra in comparison to spectra obtained using GFC and SAS fitness function which seem to either require more iteration or always fall in a local minimum.

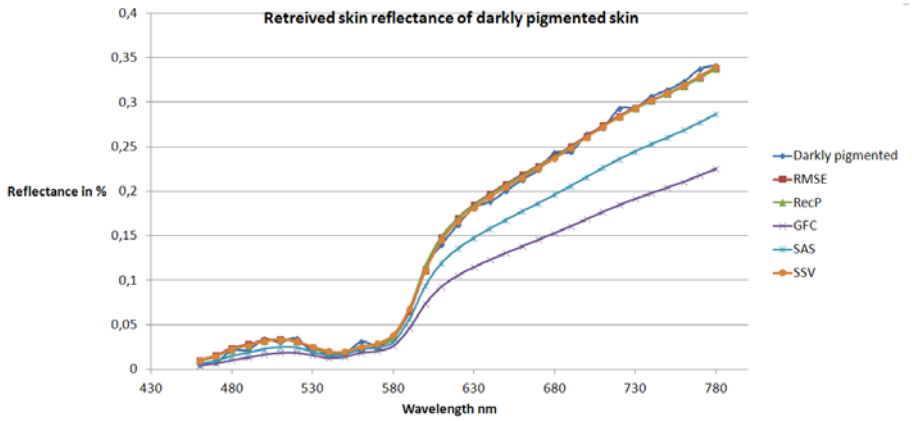

Figure 5.18: Retrieved reflectance spectra for a darkly pigmented skin using the five fitness functions.

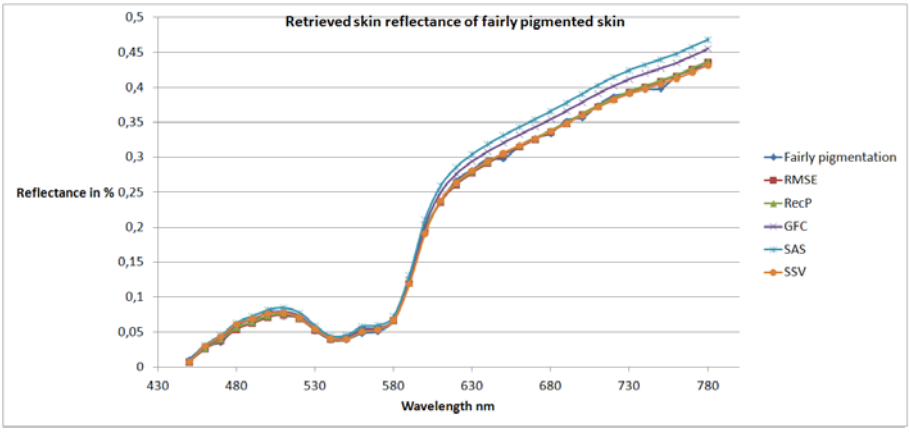

Figure 5.19: Retrieved reflectance spectra for a lightly pigmented skin using the five fitness functions.

According to the results obtained, we selected the RMSE as fitness function for our method for its lowest fitness value and its lower error rate for each parameters.

5.3.8.2 Population size

The convergence condition changes with the population size. A large population ensures the diversity over the search space and limit the risk of convergence towards local minima,

Population size	Fitness value
500	1.13E-05
300	7.19E-06
100	9,07E-06
50	4,77E-05
25	7,55E-05

Table 5.5: Average fitness value for different population sizes for three characteristic spectra performed ten times each.

but the execution time for each generation is increased. In opposition, a small population increases the local minimum trapping but offers fast execution speed.

The value of the RMSE fitness function is selected to quantify the effect of the population size. Five population sizes are tested: 500, 300, 100, 50, and 25 for 100 iterations. The tests are performed on three characteristic spectra, one represented by the lower limit of each parameter, one characterized by the average value for all parameter and a last one generated with the upper limit for all the parameters.

This process was performed ten times for each of the three spectra. It aims to generalize the fitness value for different spectra.

Table 5.5 shows that a population size of 300 individuals offers the best fitness value. It means that the obtained spectra after the final iteration matches best the simulated one. However, a population with 100 individuals obtained similar fitness value that a population of 300 individual. A large population requires higher computational time and with precision only slightly better (0.2E-05) for a population of 300 than for a population of 100, the precision gained was not judged sufficient in comparison to lost in computational time. Therefore we select a population size of 100 individuals.

5.3.8.3 Iteration

The algorithm is terminated after a number of iterations. Two reasons motivate the selection of this type of termination process: defining a fitness value to be reached by the population might lead to extensive computational time and moreover, selecting a fitness value too high might trap the algorithm into an infinite loop as it may never reach it. Therefore, the termination operator defines an iteration number T which corresponds to the convergence of the population.

Tests, using the previous set of parameters (RMSE and a population of 100 individuals), involve several iteration numbers (N = 100, 50, 25, 10) performed ten times each for

the three characteristic spectra to ensure objective selection. The analysis is performed on the convergence of the fitness value. The convergence of the population is the progression towards increasing uniformity. The average fitness will approach the fitness value fo the best individual.

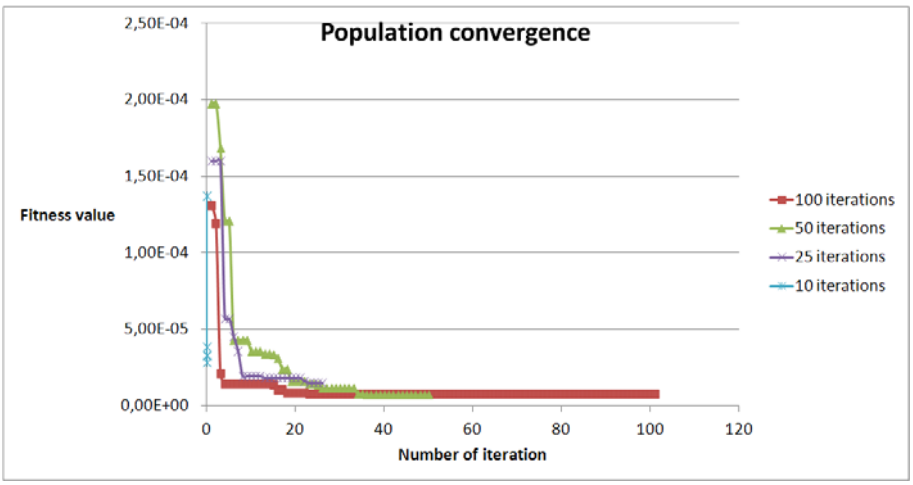

Figure 5.20: Convergence of a population composed of 100 individuals.

In figure 5.20, the results show the number of iteration as a function of the fitness value. With 10 iterations, the algorithm does not have time to converge. For 25, 50 and 100 iterations, we noticed that after around 20 to 25 iterations, the fitness value does not change and the population is considered to have converged. This values are the average convergences value obtained for the three spectra which reflects the limit of the search space, meaning that no drift have affected the test populations. As a result of the convergence rate, we select a total number of iteration of 25.

5.3.8.4 Crossing and mutation rate

Both crossing and mutation were selected from the literature [Syswerda, 1989] and respectively takes the probability value $P_c = 0.6$ and $P_m = 0.02$. We did not want to select a high mutation probability as we noticed that the convergence was not smooth and often temporarily increased.

The final parameters of our proposed genetic algorithm are detailed in table 5.6.

Fitness function	RMSE
Population size	100
Termination operator	25 iterations
Best selection nb	5
Random selection nb	25
Crossing nb	30
Mutation nb	2

Table 5.6: GA parameters for Kubelka-Munk inversion model.

5.4 Conclusion

We have presented an algorithm which aims to retrieve skin parameters based on a model of light propagation in skin coupled with Genetic Algorithm for optimization purpose. This algorithm outputs the concentration of melanin, the concentration of haemoglobin, the thickness of both epidermis and dermis and the relative blood oxygenation.

The proposed method of combining Kubelka-Munk model (with a layered skin structure) with GA optimization can retrieve accurately simulated skin parameters as suggested by the results.

The result shows that works can be performed on the skin model to incorporate more skin parameters to retrieve more information that could prove to be useful in the diagnosis of specific disease.

Our method could be improved on four aspects. The first aspect is the analysis of a more elaborate skin model of light propagation by including an increased number of parameters and layers; also this model may consider near infrared range by extending current model but this need to consider the physical effect of light propagation in NIR.

The second aspect would be to test and improve the population size, crossing and mutation probability and add other genetic operators that modify the evolution strategy reducing the number of iterations without affecting the search space ability.

The third perspective would be to select wavelength specific analysis for designated disease.

The fourth might be to study a way to process faster the reflectance cube. One way could be to parallelize the study to process several reflectance spectra at the same time. Also another approach could be to reduce the number of reflectance spectra either by dimension reduction analysis or by segmentation of the reflectance cube.

The proposed method could be helpful to evaluate and monitor over time the variation of the different skin parameters. The capacity of ASCLEPIOS system to perform repro-

ducible acquisition combined to the proposed method might help the temporal follow-up of skin lesions.

The following section will test the proposed method on real skin data from a healthy population and compare the result to literature values. Moreover, the analysis will be applied to two skin diseases: vitiligo and melasma.

Chapter 6

Analysis and Results

Quantitative and objective assessment of skin lesions is critical in the detection of variety of skin conditions. In order to use our method for clinically relevant skin analysis, we first validate our technique using a population of healthy participants and then apply our method to the measurement of parameters from patients with vitiligo or melasma skin lesions.

6.1 Model validation on healthy patients

We present the validation of our method based on participants from a healthy population and compare the results obtained with data from the literature.

The volume fraction of melanosome increases with the SPT type which is in accordance to the literature knowledge [Anderson and Parrish, 1982, Meglinski and Matcher, 2002, Shimada et al., 2001a]. Currently, the only method to classify and compare our system is the relation between STP and melanin concentration in skin.

When analysing the parameters, the skin chemical concentration (concentration of blood and melanin) is often more relevant than the physical conditions (epidermis and dermis thickness) because the chemical concentration is more likely to change over time than the physical parameters. One might consider the retrieval of the layer thicknesses however, as seen in the previous chapter; the variation of both thickness modifies the reflectance spectrum. The system is developed for explorative study, meaning that it does not concentrate on one skin area which could lead to set a constant thickness variable. We let the thickness parameters vary to match the difference of layers thickness at different location of the body and compare the relative body site thickness with study by Robertson

et Rees [Robertson and Rees, 2010] which measured the thickness of the epidermis using Reflectance Confocal Microscopy (RCM).

The data for the validation of our method of skin parameters retrieval is the same than the data used for the validation of the reflectance cube reconstruction. The volunteers were recruited between the months of October and November 2010. For information, the participant's data were classified into five groups based on their Fitzpatrick skin phototypes. It includes 18 type II, 21 type III, 56 types IV, 41 type V and 14 type VI (more information can be found about the population in section 3.3.2.1).

For each volunteer, three acquisitions were collected at different body locations (back of the hand, face and lower back). For each multispectral image acquisition, a reflectance cube was reconstructed between 450 to 780 nanometres with resolution of 10 nm.

For each reflectance cube, the distribution of the skin is fairly uniform as the data were taken from healthy patient and cared was taken to acquire with no visible lesions or naevus. The parameter estimation was performed on every reflectance cube. The average value of each parameter was calculated for each entire retrieved map because of low disparity within values of each map.

The aim of this validation is to corroborate the skin parameters values/concentration from the literature with the parameters retrieved using our method on skin sample from various SPT.

Our results, presented by SPT type, show the different retrieved parameters at different body location in table 6.1,6.2,6.3,6.3,6.5. The results are fairly consistent with the finding of Robertson et Rees [Robertson and Rees, 2010] which reveals a thicker epidermis layer for the back of the hand which agrees with our retrieved parameters. We considered their upper back values to compare to our lower back measurement. The decrease of thickness measured by RCM again matches the decrease of thickness calculated by our method. The major difference between the body locations is found for the melanin content of the back of the hand which is twice the one of face and lower back for SPT II, III but the trends, while slightly lower, is similar for the remaining SPT. Other parameters are not significantly different between the different body locations.

Figure 6.1 shows the estimated relative fraction of melanosome concentration from the five SPTs of the lower back. There is a gradual increase from 6% for SPT II to 43% for SPT VI, which is also noticed by [Shimada et al., 2001a, Igarashi et al., 2007, Van Gemert et al., 1989]. Similar trends are estimated for other body locations.

According to figure 6.2, we notice that the epidermis thickness is globally increasing with the skin phototypes (for SPT II to SPT IV) and this seems to not be correlated to

SPTII	Hand	Face	Back
Volume fraction of melanosome (%)	0,10085	0,05819	0,05346
Epidermis thickness (cm)	0,00133	0,00116	0,00115
Volume fraction of haemoglobin (%)	0,01120	0,01232	0,00542
Relative blood oxygen saturation (%)	0,30160	0,49089	0,46919
Dermis thickness (cm)	0,10563	0,09083	0,08886

Table 6.1: Parameters estimation for SPT II.

SPTIII	Hand	Face	Back
Volume fraction of melanosome (%)	0,18704	0,07496	0,05174
Epidermis thickness (cm)	0,00139	0,00121	0,00118
Volume fraction of haemoglobin (%)	0,01246	0,01338	0,00944
Relative blood oxygen saturation (%)	0,29703	0,40951	0,44803
Dermis thickness (cm)	0,11002	0,09477	0,09178

Table 6.2: Parameters estimation for SPT III.

SPTIV	Hand	Face	Back
Volume fraction of melanosome (%)	0,26451	0,15538	0,15535
Epidermis thickness (cm)	0,00158	0,00140	0,00138
Volume fraction of haemoglobin (%)	0,01080	0,01362	0,01192
Relative blood oxygen saturation (%)	0,28912	0,31052	0,32315
Dermis thickness (cm)	0,12636	0,10819	0,10262

Table 6.3: Parameters estimation for SPT IV.

SPTV	Hand	Face	Back
Volume fraction of melanosome (%)	0,35786	0,29091	0,33780
Epidermis thickness (cm)	0,00176	0,00159	0,00164
Volume fraction of haemoglobin (%)	0,01080	0,01362	0,01152
Relative blood oxygen saturation (%)	0,28912	0,29152	0,29584
Dermis thickness (cm)	0,12636	0,11511	0,11310

Table 6.4: Parameters estimation for SPT V.

SPTVI	Hand	Face	Back
Volume fraction of melanosome (%)	0,44695	0,41081	0,43413
Epidermis thickness (cm)	0,00202	0,00199	0,00209
Volume fraction of haemoglobin (%)	0,00573	0,00656	0,00666
Relative blood oxygen saturation (%)	0,31327	0,31007	0,30990
Dermis thickness (cm)	0,22173	0,19103	0,18721

Table 6.5: Parameters estimation for SPT VI.

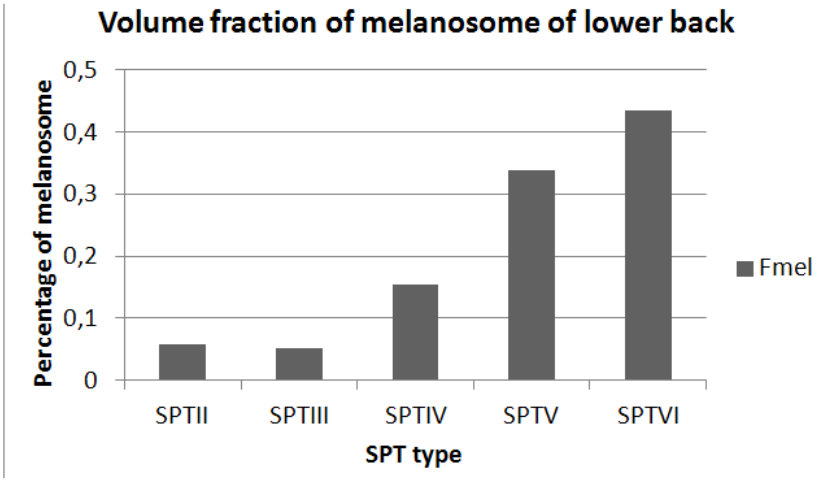

Figure 6.1: Volume fraction of melanosome of lower for each SPT.

the skin pigmentation. This finding is in accordance with the study of Lock-Andersen *et al.* [Lock-Andersen et al., 1997]. However, we notice strong increased of epidermis thickness for population of SPT V and VI. This might be an effect of the limitation of the model parameter rather than a difference of thickness from this single STP population according to the previous study which indicates a relatively constant epidermis thickness over the different STPs.

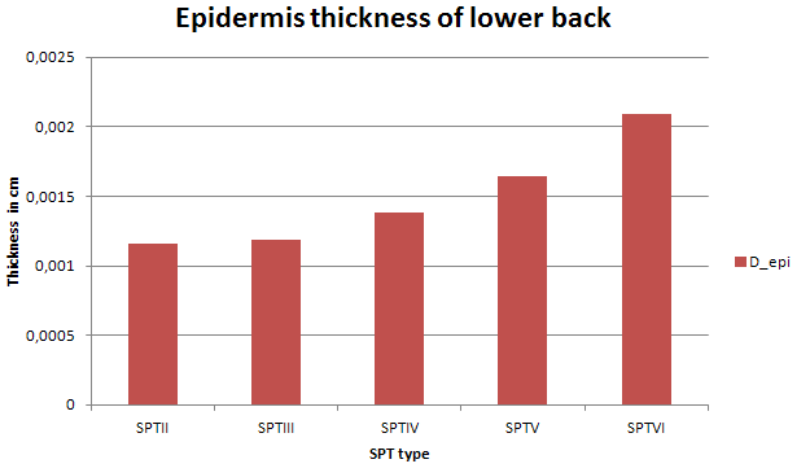

Figure 6.2: Epidermis thickness of lower for each SPT.

Another unexpected finding is the increase of the dermis thickness value for SPT VI population (see figure 6.3). This is inconsistent with the developped model and the effect of the dermis thickness (see figure 5.4) because SPT VI population has a low reflectance spectrum and retrieving a high dermis value means high reflectance value in the range from 600 to 780 nm. This might confirm the possible modelling errors with boundary limit of parameters affecting the overall search.

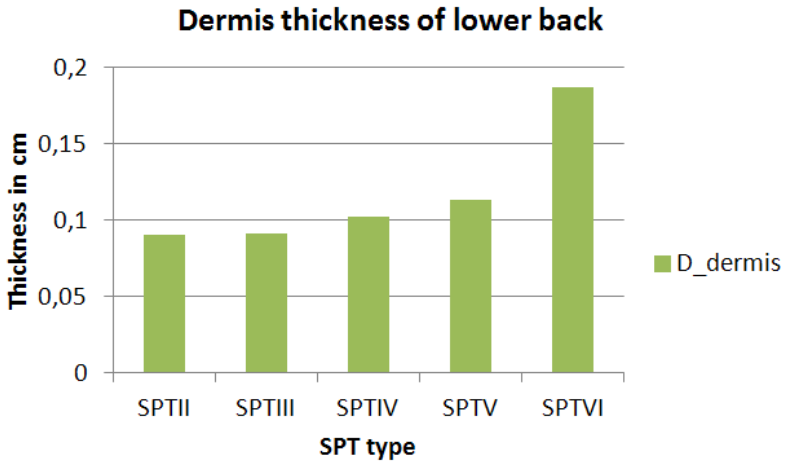

Figure 6.3: Dermis thickness of lower for each SPT.

From figure 6.4, we observed that the relative haemoglobin oxygen saturation is inversely proportional to the epidermis thickness and melanosome concentration. With less light being absorbed in the epidermis for low SPT type, more light might reach the dermis and retrieve more information about the relative oxygenation of the blood.

The volume fraction of haemoglobin retrieved from the different SPT is fairly uniform (see figure 6.5). Most of the haemoglobin retrieved ranges from 0.7% to 1.2% which is relatively close in regards to the potential variation of the volume fraction of haemoglobin (between 0.2 to 7%).

Figure 6.6 shows the volume fraction of melanosome of SPT III between different body locations. The difference between constitutive (lower back) and facultative skin colour (face and back of the hand) should reveal an increase quantity of melanosome for area exposed to the sun. However, there is a striking increase of melanosome concentration only in the back of the hand data and similar concentration is estimated for both the face and the lower back. This finding might be explained by the fact that the data were mainly acquired from Asian population (SPT III-IV-V). According to Choe *et al.* [Choe

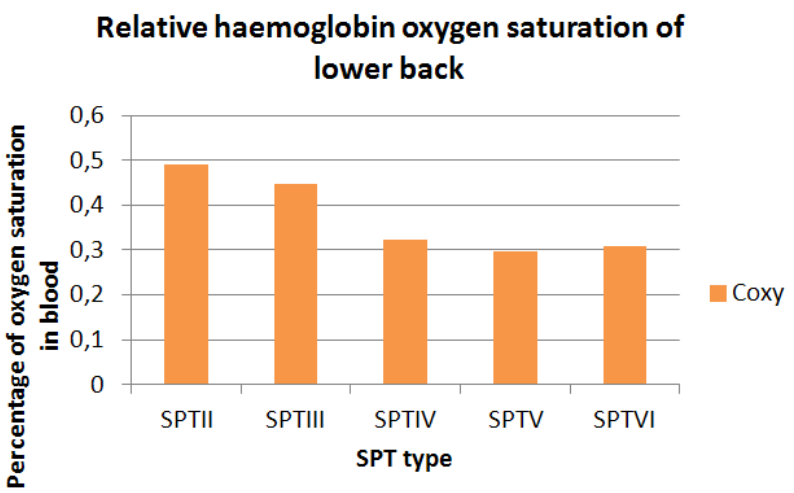

Figure 6.4: Relative haemoglobin oxygen saturation of lower for each SPT.

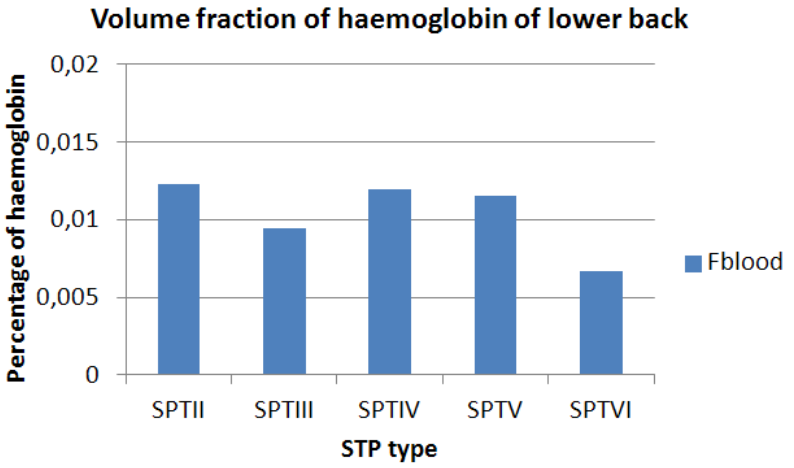

Figure 6.5: Volume fraction of haemoglobin of lower for each SPT.

et al., 2006], the skin phototype of Asian skin can be determined using constitutive skin. However no meaningful information can be extracted by the comparison of constitutive and facultative skin colours for individuals of this population. Knowing that most of the data has been acquired on Asian population, the fact that the concentration is similar between the face and the lower back might be justified.

Figures 6.7, 6.8, 6.9 features epidermis thickness, oxygen saturation and haemoglobin parameters with constant values between each site. The only other variation is denoted

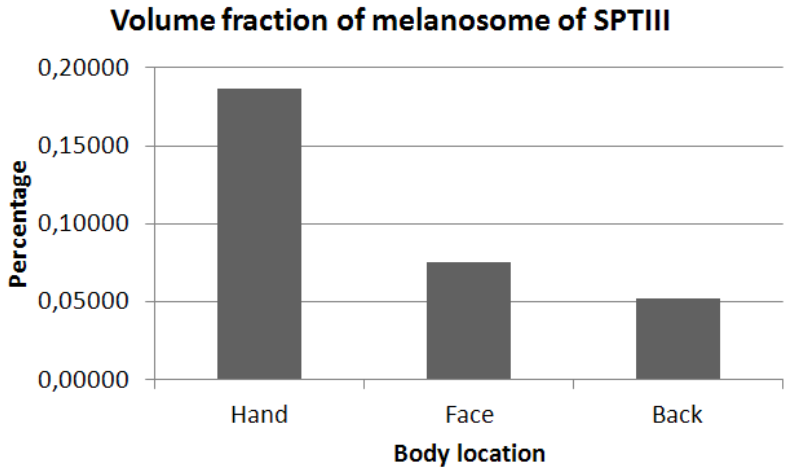

Figure 6.6: Volume fraction of melanosome at different body location for SPT III.

for the dermis layer of the back of the hand which is 0.02 cm thicker than the dermis of both face and lower back.

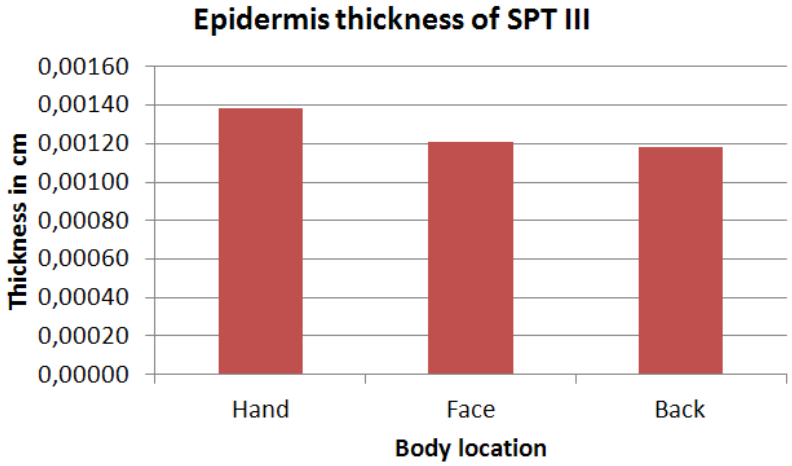

Figure 6.7: Epidermis thickness at different body location for SPT III.

Figure 6.10 reveals an increased of the dermis thickness from the back of the hand for SPT III. This trend is found with decreasing impact as the SPT type increases (see table 6.1,6.2,6.3,6.3,6.5).

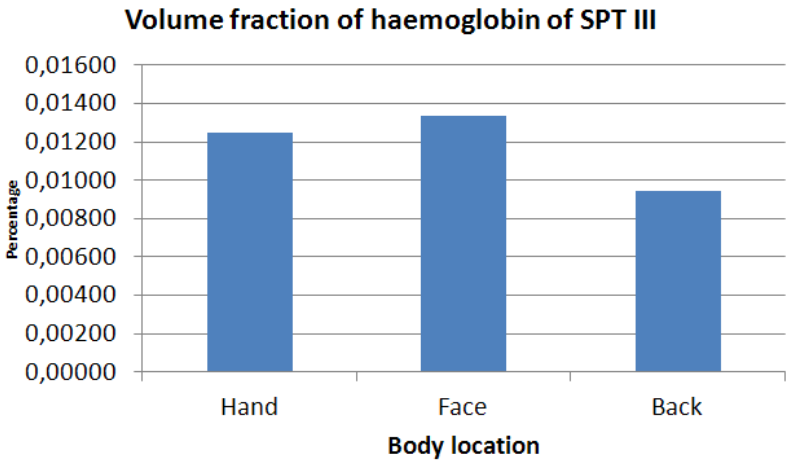

Figure 6.8: Volume fraction of haemoglobin at different body location for SPT III.

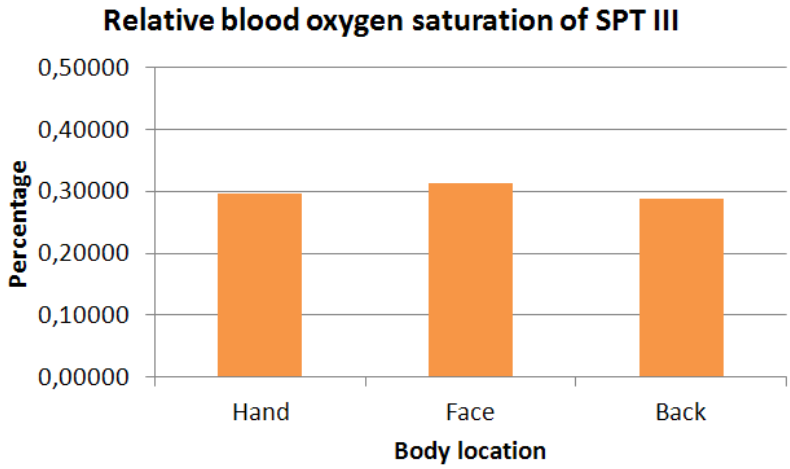

Figure 6.9: Relative haemoglobin oxygen saturation at different body location for SPT III.

6.2 Skin disorder

We applied our method to quantify and compare data acquired from two populations with skin diseases that have characteristic effect on the melanin composition.

The clinical data were acquired at the Department of Dermatology of Hospital Kuala Lumpur and Hospital Serdang (MALAYSIA) during the 'Skin Pigmentation Study' under

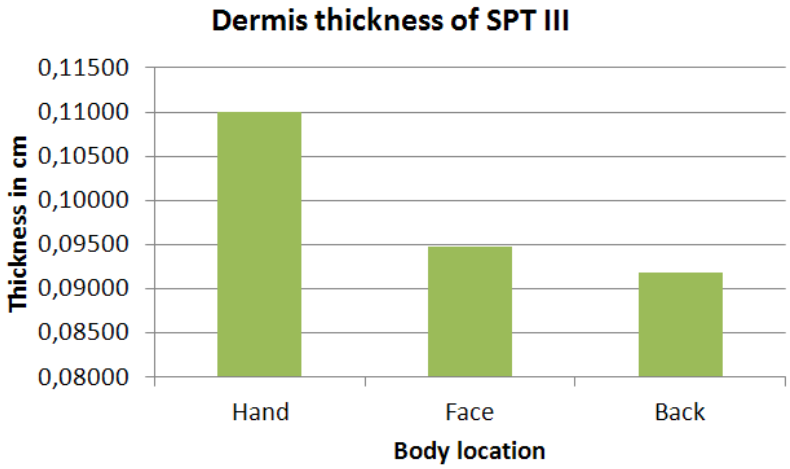

Figure 6.10: Dermis thickness at different body location for SPT III.

the supervision of Dr. Roshidah BABA (Head of Dermatology department) and with the collaboration of Dr. Noorlaily Md NOOR, Dr. Norashikin SHAMSUDIN, Hermawan NUGROHO and Prof. Ir. Dr. Ahmad FADZIL. This study is a collaborative work between these two hospitals and the Department of Electrical and Electronic Engineering of the University Teknologi Petronas (MALAYSIA). The research study was registered to the National Medical Research Register which supports the implementation of the National Institute of Health NIH guideline on the conduct of research in the Ministry of Health Malaysia (MOH). I participate to the study during my research exchange program at UTP. The acquisitions were performed using ASCLEPIOS system and spectrophotometer CM-2600d. The study was performed from December 2010 to February 2011. We acquired a total of 22 melasma data from 10 patients and a total of 110 vitiligo data from 32 patients.

Melasma (also called chloasma) is a hyperpigmentation skin disease that is characterised by an increase level of melanin released by melanocytes. The symptoms are characterised by dark, irregular and well demarcated skin lesion. It gradually develops on the face, forehead and lips. This disease is more common for women (with a female to male ratio of 9:1 [Montemarano and Lyford, 2011]). Risks factors include dark skin (most common in Asian and Hispanic population), hormonal (use of oral contraceptive), and sun exposure.

Vitiligo (also called leukoderma) is a common genetic auto-immune skin disease caused by the disappearance of melanocytes in the epidermis resulting in hypopigmentation. The symptom of vitiligo is the depigmentation of patches of skin with irregular shape. Lesions

Parameter	Relative difference	STD
Melanin	2.05581	0.09729
Epidermis thickness	1.12142	0.01619
Haemoglobin concentration	1.18293	0.03686
Blood oxygenation	0.91592	0.01232
Dermis thickness	1.08733	0.04054

Table 6.6: Average difference between melasma and healthy skin.

are often found at the body extremity (hands, feet) but mostly on the face, wrists and trunk.

All skin lesions were assessed by dermatologists. The acquisition process required the patient consent and all procedures were performed following the dermatology guideline.

All multispectral images acquired contain both healthy and hypo/hyperpigmented skin area. Every reflectance cube were analysed using our method, generating the fives skin parameter maps. The average parameter values are obtained from the two different areas (healthy and diseased) which are manually selected on each map. The relative difference between healthy and hypo/hyperpigmented skin area is calculated by the following formula:

$$R_{diff} = \frac{Val_{ref}}{Val_{measured}} \tag{6.1}$$

where Val_{ref} is the retrieved healthy skin parameter value and $Val_{measured}$ is the retrieved hypo/hyperpigmented skin parameter value. The R_{diff} represents the relative change between two values. This measure is unitless. A relative difference of 1 means that the two values are similar.

Table 6.6 and table 6.7 summarize the difference of parameters between healthy and disease affected reflectance spectra. Melasma lesions show that the melanin volume is 2.05 time higher than the healthy skin. Vitiligo lesions reveal a decrease by around four of the melanin concentration. To our knowledge, currently no study quantify the difference of melanin concentration between healthy and hypo/hyperpigmented skin lesion. The variation of the other parameters (epidermis and dermis thickness, haemoglibin concentration and relative blood oxygenation) is not significant.

The standard deviations of the average melanin difference for both melasma and vitiligo are high. This is a result of the inclusion of all types of vitiligo (mild to severe) and all SPT types. For SPT II and III, the difference between melasma and healthy skin will be very high, sometime with a relative difference of 4, whereas for SPT V and VI, the relative

Parameter	Relative difference	STD
Melanin	0.27121	0.02577
Epidermis thickness	0.95333	0.04285
Haemoglobin concentration	1.05469	0.10874
Blood oxygenation	1.07154	0.03022
Dermis thickness	1.05924	0.06173

Table 6.7: Average difference between vitiligo and healthy skin.

difference is around 1.3 to 1.5 as the original melanin concentration is already high.

Figure 6.11 present the results of the five parameters retrieved using our method on a vitiligo lesion. The melanin map is clearly affected in the area of vitiligo lesions (white patch on the subfigure 6.11(a)). The variation of epidermis/dermis thickness, haemoglobin concentration and relative oxygenation parameters are only of around 10% which we do not consider to be characteristic for melasma and vitiligo diseases. This finding is conformed to the medical expectation which states that vitiligo only modifies the melanin content of the skin.

6.3 Conclusion

We presented the validation of the retrieval of parameters using our method applied to reflectance cubes of different SPT groups which agrees with the literature.

Similar to the possible error noticed in the validation of the model for SPT VI where we questioned the dermis thickness value of SPT VI, we retrieve a comparable high value for melasma lesions. This acknowledges the possible model error for strongly pigmented skin. This result needs to take into account that the skin model used in our method is a simplified representation of the skin, only considering limited parameters in addition to the limitation of the Kubelka-Munk model.

It seems that the information retrieved about the layers (epidermis and dermis) thickness (for SPT II to SPT V) is in relative good agreement with studies made with other imaging techniques. However we do not state, neither takes for granted that the retrieved thickness values are exact and reliable. Further studies need to be performed to validate the estimation of layer thickness by measurement of reflectance spectrum. This finding requires to be analysed either non-invasively using ultrasound imaging or optical coherence tomography technology measurement or invasively using the golden standard of histology.

The results show that our research methods can retrieve skin parameters in accordance

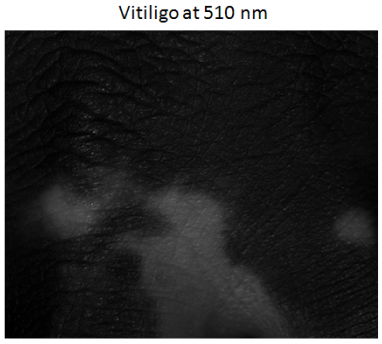

(a) Reflectance image of Vitiligo at 510 nm.

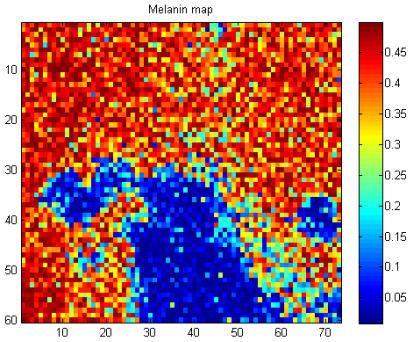

(b) Volume fraction of melanosome map.

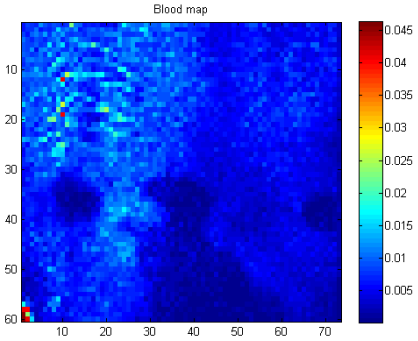

(c) Volume fraction of haemoglobin map.

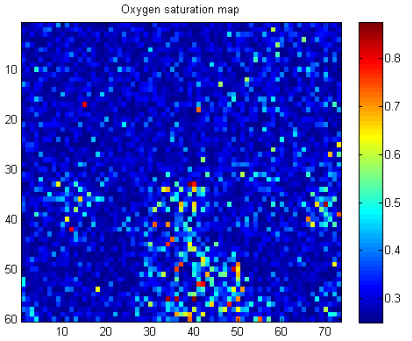

(d) Relative blood oxygenation map.

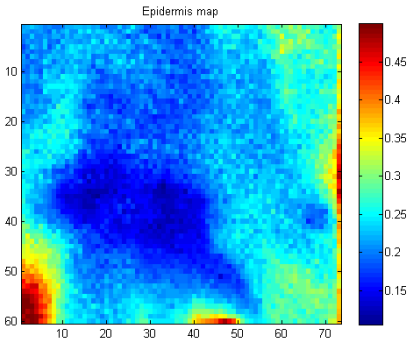

(e) Epidermis thickness map.

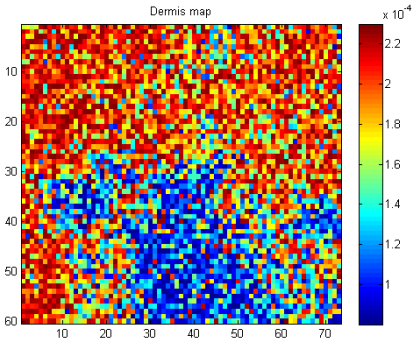

(f) Dermis thickness map.

Figure 6.11: A set of six subfigures composed of one monoband image of healthy lesion ((a)) and five skin parameter maps((b),(c),(d),(e),(f))

.

with the accepted skin knowledge. This method may be useful for other studies of skin diseases with pigmentation.

Chapter 7

Conclusion

During this thesis, we based our work on the phenomenon of light interaction with skin as it provides important information about the skin chemical composition and structure. The objectives of the thesis were to develop an imaging system that acquires reproducible and objective image of skin lesions and to retrieve useful skin parameters.

After presenting different optical acquisition systems currently used to measure the skin for which we pointed out their limitations, it became evident that the spectral and spatial information of skin lesions are important to compare skin disorders and normal skin within a single acquisition.

Our approach to answer this problem is first the development of a Multispectral Imaging system. It was designed to provide additional spectral information to the dermatologist. This acquisition is reproducible as the system is protected from external light and calibrated. The multispectral images are reconstructed into reflectance cubes by means of a neural network based algorithm. Such cube contains only the spectral reflectance information of the skin, excluding the other information of the element optical path. The accuracy of the reconstruction was validated during an experimental study involving 150 participants from five of the six skin phototypes (SPT II to VI).

Then some skin parameters were retrieved using the inverse Kubelka-Munk theory based on a two layer skin model and optimized by Genetic Algorithm. The validation of the developed algorithm was tested on a set of skin data acquired for the validation of the previously described system. The results retrieved by the algorithm are in good accordance with the data from the literature. The usefulness of the developed technique was proved during a clinical study based on vitiligo and melasma skin lesions. The technique was able to obtain five skin parameters maps (melanin concentration, epidermis/dermis

thickness, haemoglobin concentration and the relative blood oxygenation) for each lesion in correlation with the expected skin composition of the lesions.

7.1 Work perspectives

The future work of this project aims to modify the illuminating device to facilitate the acquisition of specific spectral bands. Based on the current generic system, it targets to acquire images over the same spectral band (therapeutic window) but with a new illumination based on programmable light source. This will permit to acquire either full spectral frame images or target spectral images.

In accordance to dermatologist, one or two pathologies will be chosen for the future system to tackle the screening of a disease for society needs. This enhanced tool might prove to provide better targeted diagnosis information for specific characterisation of skin disease. A possible utility of the system would be to use it for screening purpose, as screening may find disease at an early stage. The research on one or two specific pathology should use ASCLEPIOS capacity to analyse the characteristic wavelengths of the disease. This will help in the development of a specific system target for one pathology.

The second perspective will be to study how to calibrate the reconstruction process in the near infrared. This will enhance the spectral potential of the system. Currently the calibration is limited to the visible range (Gretag MacBeth) due to a lack of material with spectral characteristics in the near infrared.

Another work direction includes the validation of the current model versus ground truth information obtained from skin biopsy. The study of an extended model with increased numbers of layers and parameters should boost the skin parameters information that one can retrieve from the reflectance cube. Other parameters such as bilirubin may be added to the skin model to study disease like jaundice. Additional features such as lesion tracking might be study on a reflectance cube to analysis the temporal evolution of a lesion after treatments. It might help the dermatologist to objectively quantify the progression of the disease by detecting lesion changes with our multispectral imaging system before visual change, similarly to the works of Nugroho *et al.* [Nugroho et al., 2007] on RGB camera.

The research on one or two specific pathologies should use ASCLEPIOS capacity to analyse the characteristic wavelengths of the disease. This will help in the development of a specific system targetted for one pathology.

Furthermore, we think that such a system and methods can be applied to other medical domains which use similar light matter interaction. This can be addressed by the

modification of the hand-held device for larger or smaller area of interest (chapter 3). The analysis of the measured data would require modification of the parameters presented in chapter 5 to match the structure and composition of the organ studied.

The acquisition system might be helpful for domains other than medical one such as food processing [Okamoto and Lee, 2009] or cultural heritage analysis [Simon et al., 2010].

Publications

Journal

Jolivot, R., P. Vabres, and F. Marzani. Reconstruction of hyperspectral cutaneous data from an artificial neural network-based multispectral imaging system. *Computerized Medical Imaging and Graphics*. August 2010.

Books

Mitra, J., R. Jolivot, P. Vabres and F. Marzani. Blind source separation of skin chromophores on a hyperspectral cube. *Skin Research and Technology*, 16 (4), November 2010.

Jolivot, R., P. Vabres and F. Marzani. An open system to generate hyperspectral cubes for skin optical reflectance analysis. *Skin Research and Technology*, 16 (4), November 2010.

International conferences

Galeano Zea, J.A., R. Jolivot and F. Marzani. Analysis of Human Skin Hyper-Spectral Images by Non-negative Matrix Factorization. 10^{th} *Mexican International Conference on Artificial Intelligence*, Springer, Heidelberg, Lecture Notes in Computer Science, Part II, LNAI 7095, pp. 431-442, Puebla, Mexico, November 2011.

Fadzil, M. H. A., H. Nugroho, R. Jolivot, F. Marzani, N. Shamsuddin and R. Baba. Modelling of Reflectance Spectra of Skin Phototypes III. *International Visual Informatics Conference 2011*, Springer, Heidelberg, Lecture Notes in Computer Science, Volume 7066/2011, pp. 352-360, Selangor, Malaysia, November 2011.

Jolivot, R., H. Nugroho, P. Vabres, M. H. A. Fadzil and F. Marzani. Validation of a 2D multispectral camera: application to dermatology/cosmetology on a population cover-

ing five skin phototypes. *SPIE European Conferences for Biomedical Optics*, Munich, Germany, May 2011. Proc. SPIE 8087, 808729;

Mitra, J., R. Jolivot, P. Vabres, and F. Marzani. Source separation on hyperspectral cube applied to dermatology. *SPIE Medical Imaging, Computer-Aided Diagnosis*, 7624 , pp. 762431-1-762431-11, San Diego, CA, USA, February 2010.

Jolivot, R., P. Vabres, and F. Marzani. Calibration of MultisSpectral Imaging System applied to dermatology. *E-MEDISYS*, Fez, Morocco, January 2010.

Research seminar

Jolivot, R., P. Vabres, and F. Marzani. ASCLEPIOS: un système d'acquisition et de quantification d'images multispectrales de réflectance en dermatologie. *GDRMeeting Journée thématique: Analyse d'images couleur et multispectrales en biologie et médecine*, Paris, France, October 2011.

Bibliography

[Agero et al., 2006] Agero, A. L. C., Taliercio, S., Dusza, S. W., Salaro, C., Chu, P., and Marghoob., A. A. (2006). Conventional and polarized dermoscopy features of dermatofibroma. *Archives of dermatology*, 124:1431–1437.

[Anderson et al., 1981] Anderson, R., Hu, J., and Parrish, J. (1981). *Optical radiation transfer in the human skin and applications in in vivo remittance spectroscopy*. Number 28 in Bioengineering and the Skin. MTP Press Limited.

[Anderson and Parrish, 1981] Anderson, R. and Parrish, J. (1981). The optics of human skin. *Journal of Investigative Dermatology*, 77(1):13–19.

[Anderson and Parrish, 1982] Anderson, R. and Parrish, J. (1982). *The science of photomedicine*. Chapter 6; Optical properties of human skin. Plenum Press.

[Argenziano et al., 2002] Argenziano, G., Soyer, H. P., Chimenti, S., Argenziano, G., and Ruocco, V. (2002). Impact of dermoscopy on the clinical management of pigmented skin lesions. *Clinics in Dermatology*, 20(3):200 – 202.

[Arrazola Peter, 2005] Arrazola Peter, Mullani Nizar A., A. W. (2005). Derm lite ii: An innovative portable instrument for dermoscopy without the need of immersion fluids. *SKINmed: Dermatology for the Clinician*, 4(2):78–83.

[Balas et al., 2001] Balas, C., Themelis, G., Papadakis, A., Vasgiouraki, E., Argyros, A., Koumantakis, E., Tosca, A., and Helidonis, E. (2001). A novel hyper-spectral imaging system: Application on in-vivo detection and grading of cervical precancers and of pigmented skin lesions. In *CVBVS'01 workshop*, pages 109–117, Hawaii, USA.

[Baruah et al., 2000] Baruah, M., Pushkarna, N., Pushkarna, R., Mohanty, S., and Bhargava, S. (2000). Evaluation of skin lesions with color doppler and spectral analysis. *Indian Journal of Radiology and Imaging*, 10(4):233–236.

[Bashkatov et al., 2005] Bashkatov, A. N., Genina, E. A., Kochubey, V. I., and Tuchin, V. V. (2005). Optical properties of human skin, subcutaneous and mucous tissues in the wavelength range from 400 to 2000nm. *Journal of Physics D Applied Physics*, 38(15):2543–2555.

[Bearnam and Levenson, 2003] Bearnam, G. and Levenson, R. (2003). *Biological Imaging Spectroscopy*, chapter Chapter 8, pages 1–26. CRC Press.

[Benvenuto-Andrade et al., 2007] Benvenuto-Andrade, C., Dusza, S. W., Agero, A. L. C., Scope, A., Rajadhyaksha, M., Halpern, A. C., and Marghoob, A. A. (2007). Differences Between Polarized Light

Dermoscopy and Immersion Contact Dermoscopy for the Evaluation of Skin Lesions. *Arch Dermatol*, 143(3):329–338.

[Bigio and Mourant, 1997] Bigio, I. J. and Mourant, J. R. (1997). Ultraviolet and visible spectroscopies for tissue diagnostics: fluorescence spectroscopy and elastic-scattering spectroscopy. *Physics in Medicine and Biology*, 42(5):803.

[Biocompatibles.com, 2011] Biocompatibles.com (2011). Siascopy.

[Bowmaker and Dartnall, 1980] Bowmaker, J. K. and Dartnall, H. J. (1980). Visual pigments of rods and cones in a human retina. *The Journal of Physiology*, 298(1):501–511.

[Burton et al., 2009] Burton, K., Jeon, J., Wachsmann-Hogiu, S., and Farkas, D. (2009). *Biomedical Optical Imaging*, chapter Chapter 2, pages 1–44. Oxford University Press.

[Chang et al., 2002] Chang, S. K., Dawood, M. Y., Staerkel, G., Utzinger, U., Atkinson, E. N., Richards-Kortum, R. R., and Follen, M. (2002). Fluorescence spectroscopy for cervical precancer detection: Is there variance across the menstrual cycle? *Journal of Biomedical Optics*, 7(4):595–602.

[Choe et al., 2006] Choe, Y. B., Jang, S. J., Jo, S. J., Ahn, K. J., and Youn, J. I. (2006). The difference between the constitutive and facultative skin color does not reflect skin phototype in asian skin. *Skin Research and Technology*, 12(1):68–72.

[Choi, 2010] Choi, S. H. (2010). Fast and robust extraction of optical and morphological properties of human skin using a hybrid stochastic-deterministic algorithm: Monte-carlo simulation study. *Lasers in Medical Science*, 25(5):733–741.

[Choo-Smith et al., 2002] Choo-Smith, L.-P., Edwards, H. G. M., Endtz, H. P., Kros, J. M., Heule, F., Barr, H., Robinson, J. S., Bruining, H. A., and Puppels, G. J. (2002). Medical applications of raman spectroscopy: From proof of principle to clinical implementation. *Biopolymers*, 67(1):1–9.

[CK electronic, 2011] CK electronic (2011). Mexameter©mx18.

[Claridge et al., 2006] Claridge, E., Hidovic-Rowe, D., Espina, F. O., Styles, I., Ersbol, B., and Jorgensen, T. (2006). Quantifying composition of human tissues from multispectral images using a model of image formation. *MICCAI06 Workshop on Biophotonics Imaging for Diagnostics and Treatment*, pages 7–14.

[Corporation, 1998] Corporation, K. M. C. (1998). Precise color communication: color control from perception to instrumentation. Technical report, Osaka, Japan.

[Cortex, 2011] Cortex (2011). Dermaspect. http://www.cortex.dk/dermaspectrometer.htm.

[Cotton, 1997] Cotton, S. (1997). A noninvasive skin imaging system. Technical report, Proceedings of the Conference on Intelligent Information Processing (IIP 2000) of the International Federation for Information Processing Sixteenth World Computer Congress (WCC 2000.

[Cotton et al., 2001] Cotton, S., Moncrieff, M., Claridge, E., and Hall, P. (2001). The theory of siascope. *Melanoma Research*, 11:98.

[Darwin, 1859] Darwin, C. (1859). *On the origin of species*. New York :D. Appleton and Co.,. http://www.biodiversitylibrary.org/bibliography/28875.

[Dawson et al., 1980a] Dawson, J. B., Barker, D. J., Ellis, D. J., Cotterill, J. A., Grassam, E., Fisher, G. W., and Feather, J. W. (1980a). A theoretical and experimental study of light absorption and scattering by in vivo skin. *Physics in Medicine and Biology*, 25(4):695.

[Dawson et al., 1980b] Dawson, J. B., Barker, D. J., Ellis, D. J., Grassam, E., Cotterill, J. A., Fisher, G. W., and Feather, J. W. (1980b). A theoretical and experimental study of light absorption and scattering by in vivo skin. *Physics in Medicine and Biology*, 25(4):695–709.

[Diffey et al., 1984] Diffey, B., Oliver, R., and Farr, P. (1984). A portable instrument for quantifying erythema induced by ultraviolet radiation. *British Journal of Dermatology*, 111(6):663–672.

[Doi and Tominaga, 2003] Doi, M. and Tominaga, S. (2003). Spectral estimation of human skin color using the kubelka-munk theory. volume 5008, pages 221–228. SPIE.

[Dominic and Moncrieff, 2001] Dominic, M. and Moncrieff, S. (2001). The Clinical Application of Spectrophotometric Intracutaneous Analysis for the Diagnosis of Cutaneous Malignant Melanoma by. *Health Policy*, (September).

[Douven and Lucassen, 2000a] Douven, L. F. A. and Lucassen, G. W. (2000a). Retrieval of optical properties of skin from measurement and modeling the diffuse reflectance. volume 3914, pages 312–323. SPIE.

[Douven and Lucassen, 2000b] Douven, L. F. A. and Lucassen, G. W. (2000b). Retrieval of optical properties of skin from measurement and modeling the diffuse reflectance. 3914(1):312–323.

[Dowling, 1996] Dowling, J. (1996). Retinal processing of vision. *Greger R, Windhorst U (eds) Comprehensive human physiology. Springer-Verlag, Berlin Heidelberg New York*, pages 773–788.

[Edwards et al., 1995] Edwards, H. G. M., Williams, A. C., and Barry, B. W. (1995). Potential applications of ft-raman spectroscopy for dermatological diagnostics. *Journal of Molecular Structure*, 347:379 – 387. Molecular Spectroscopy and Molecular Structure 1994.

[Eiben et al., 1994] Eiben, A. E., Raué, P.-E., and Ruttkay, Z. (1994). Genetic algorithms with multi-parent recombination. In *PPSN*, pages 78–87.

[Elbaum et al., 2001a] Elbaum, M., Kopf, A. W., Rabinovitz, H. S., Langley, R. G., Kamino, H., Mihm, M. C., Sober, A. J., Peck, G. L., Bogdan, A., Gutkowicz-Krusin, D., and et al. (2001a). Automatic differentiation of melanoma from melanocytic nevi with multispectral digital dermoscopy: a feasibility study. *Journal of the American Academy of Dermatology*, 44(2):207–218.

[Elbaum et al., 2001b] Elbaum, M., Kopf, A. W., Rabinovitz, H. S., Langley, R. G. B., Kamino, H., Mihm, M. C., Sober, A. J., Peck, G. L., Bogdan, A., Gutkowicz-Krusin, D., Greenebaum, M., Keem, S., Oliviero, M., and Wang, S. (2001b). Automatic differentiation of melanoma from melanocytic nevi with multispectral digital dermoscopy: A feasibility study. *Journal of the American Academy of Dermatology*, 44(2):207 – 218.

[Eosciences, 2011] Eosciences (2011). Melafind.

[Fitzpatrick, 1975] Fitzpatrick, T. (1975). Soleil et peau. *Journal de Medecine Esthetique*, 2:33–34.

[Fleming and Purshouse, 2002] Fleming, P. and Purshouse, R. (2002). Evolutionary algorithms in control systems engineering: a survey. *Control Engineering Practice*, 10(11):1223 – 1241.

[Folm-Hansen, 1999] Folm-Hansen, J. (1999). *On chromatic and geometrical calibration*. PhD thesis, Technical University of Denmark.

[Garcia-Uribe et al., 2011] Garcia-Uribe, A., Smith, E., Zou, J., Duvic, M., Prieto, V., and Wang, L. (2011). In-vivo characterization of optical properties of pigmented skin lesions including melanoma using oblique incidence diffuse reflectance spectrometry. *Journal of Biomedical Optics*, 16(2).

[Georgakoudi et al., 2003] Georgakoudi, I., Motz, J., Backman, V., Angheloiu, G., Haka, A., Mller, M., Dasari, R., and Feld, M. (2003). *Quantitative characterization of biological tissue using optical spectroscopy*, chapter Chapter 31, pages 1–33. CRC Press.

[Georgakoudi et al., 2002] Georgakoudi, I., Sheets, E. E., Müller, M. G., Backman, V., Crum, C. P., Badizadegan, K., Dasari, R. R., and Feld, M. S. (2002). Trimodal spectroscopy for the detection and characterization of cervical precancers in vivo. *Am J Obstet Gynecol*, 186(3):374–82.

[Gill et al., 1981] Gill, P., Murray, W., and Wright, M. (1981). The levenber-marquardt method. *Practical Optimization*, pages 136–137.

[Gillies et al., 2000] Gillies, R., Zonios, G., Anderson, R., and Kollias, N. (2000). Fluorescence excitation spectroscopy provides information about human skin in vivo. *Journal of Investigative Dermatology*, 115:704–707.

[G.N. Stamatas, 2008] G.N. Stamatas, B.Z. Zmudzka, N. K. J. B. (2008). In vivo measurement of skin erythema and pigmentation: new means of implementation of diffuse reflectance spectroscopy with a commercial instrument. *British Journal of Dermatology*, 159(3):683–690.

[Gniadecka et al., 1996] Gniadecka, M., Wulf, H. C., Mortensen, N. N., and Poulsen, T. (1996). Photoprotection in vitiligo and normal skin. a quantitative assessment of the role of stratum corneum, viable epidermis and pigmentation. *Acta Derm Venereol*, 76(6):429–32.

[Goldberg, 1989] Goldberg, D. E. (1989). *Genetic Algorithms in Search, Optimization, and Machine Learning*. Addison-Wesley.

[Gomez et al., 2004] Gomez, D., Carstensen, J., and Ersbell, B. (2004). Precise multi-spectral dermatological imaging. In *Nuclear Science Symposium Conference Record, 2004 IEEE*, volume 5, pages 3262 – 3266 Vol. 5.

[Granahan and Sweet, 2001] Granahan, J. and Sweet, J. (2001). An evaluation of atmospheric correction techniques using the spectral similarity scale. In *Geoscience and Remote Sensing Symposium, 2001. IGARSS '01. IEEE 2001 International*, volume 5, pages 2022 –2024 vol.5.

[Hajizadeh-Saffar et al., 1990] Hajizadeh-Saffar, M., Feather, J. W., and Dawson, J. B. (1990). An investigation of factors affecting the accuracy of in vivo measurements of skin pigments by reflectance spectrophotometry. *Physics in Medicine and Biology*, 35(9):1301.

[Hanlon et al., 2000] Hanlon, E. B., Manoharan, R., Koo, T. W., Shafer, K. E., Motz, J. T., Fitzmaurice, M., Kramer, J. R., Itzkan, I., Dasari, R. R., and Feld, M. S. (2000). Prospects for in vivo raman spectroscopy. *Physics in Medicine and Biology*, 45(2):R1–59.

[Hardeberg, 1999a] Hardeberg, J. (1999a). *Acquisition and reproduction of colour images: colorimetric and multispectral approaches*. PhD thesis, Ecole Nationale Sup érieure des T él écommunications, Paris.

[Hardeberg, 1999b] Hardeberg, J. Y. (1999b). Color management: Principles and solutions. *NORSIGnalets, the quaterly magazine of the Norwegian Signal Processing Society*, 3:6–12. Available from http://www.norsig.no/NORSIGnalet/vol1999-nr3.pdf.

[Hernández-Andrés et al., 2001] Hernández-Andrés, J., Romero, J., and Raymond L. Lee, J. (2001). Colorimetric and spectroradiometric characteristics of narrow-field-of-view clear skylight in granada, spain. *J. Opt. Soc. Am. A*, 18(2):412–420.

[Hill and Mancill, 1994] Hill, B. and Mancill, C. (1994). Multispectral image pick-up system.

[Holland, 1992] Holland, J. (1992). Genetic algorithms. *Scientific American*, pages 66–72.

[Holland, 1975] Holland, J. H. (1975). *Adaptation in Natural and Artificial Systems*. University of Michigan Press, Ann Arbor.

[Igarashi et al., 2007] Igarashi, T., Nishino, K., and Nayar, S. K. (2007). The appearance of human skin: A survey. *Found. Trends. Comput. Graph. Vis.*, 3(1):1–95.

[Ikeda et al., 2003] Ikeda, I., Urushihara, K., and Ono, T. (2003). A pitfall in clinical photography: the appearance of skin lesions depends upon the illumination device. *Archives of Dermatological Research*, 294:438–443. 10.1007/s00403-002-0360-9.

[Imai et al., 2000] Imai, F. H., Rosen, M. R., and Berns, R. S. (2000). Comparison of spectrally narrow-band capture versus wide-band with a priori sample analysis for spectral reflectance estimation. In *in Proc. of Eighth Color Imaging Conference: Color Science and Engineering, Systems, Technologies and Applications, IS&T*, pages 234–241.

[Jacques, 1996] Jacques, S. (1996). Origins of tissues optical properties in the uva, visible and nir regions. *Trends in Optics and Photonics: Advances in Optical Imaging and Photon Migration*, 2:364–371.

[Jacques, 1998a] Jacques, S. (1998a). Optical absorption of melanin. *Oregon Medical Laser Center Monthly news and articles on Biomedical Optics and Medical Lasers*.

[Jacques and McAuliffe, 1991] Jacques, S. and McAuliffe, D. (1991). The melanosome: threshold temperature for explosive vaporization and internal absorption coefficient during pulsed laser irradiation. *Photochemistry and Photobiology*, 53(6):769–75.

[Jacques, 1998b] Jacques, S. L. (1998b). Skin optics. Oregon Medical Laser Center News.

[Kim and Moscoso, 2005] Kim, A. D. and Moscoso, M. (2005). Light transport in two-layer tissues. 10(3):034015.

[Kingman, 2005] Kingman, S. (2005). Growing awareness of skin disease starts flurry of initiatives. *Bulletin of the World Health Organization*, 83:891 – 892.

[Klinker et al., 1990] Klinker, G., Shafer, S. A., and Kanade, T. (1990). A physical approach to color image understanding. *International Journal of Computer Vision*, 4(1):7–38.

[Kollias et al., 1997] Kollias, N., Gillies, R., Cohn-Goihman, C., Phillips, S. B., Muccini, J. A., Stiller, M. J., and Drake, L. A. (1997). Fluorescence photography in the evaluation of hyperpigmentation in photodamaged skin. *Journal of the American Academy of Dermatology*, 36(2 Pt 1):226–230.

[Kollias et al., 2002] Kollias, N., Zonios, G., and Stamatas, G. N. (2002). Fluorescence spectroscopy of skin. *Vibrational Spectroscopy*, 28(1):17 – 23.

[Krishnaswamy and Baranoski, 2004] Krishnaswamy, A. and Baranoski, G. V. G. (2004). A biophysically-based spectral model of light interaction with human skin. *Computer Graphics Forum*, 23(3):331–340.

[Kröse and van der Smagt, 1996] Kröse, B. and van der Smagt, P. (1996). *An Introduction to Neural Networks*. The University of Amsterdam, 8 edition.

[Kuberla and Munk, 1931] Kuberla, P. and Munk, F. (1931). Ein beitrag zur optik der farbanstriche. *Zurich Tech. Physik*, 12:543.

[Lawson et al., 1997] Lawson, E. E., Edwards, H. G. M., Williams, A. C., and Barry, B. W. (1997). Applications of raman spectroscopy to skin research. *Skin Research and Technology*, 3(3):147–153.

[Levenson et al., 2003] Levenson, R., Cronin, P., and Pankratov, K. (2003). Spectral imaging for brightfiel microscopy. *Proc. SPIE 4959*, pages 27–33.

[Levine et al., 1991] Levine, N., Sheftel, S., Eytan, T., Dorr, R., Hadley, M., Weinrach, J., Ertl, G., Toth, K., McGee, D., and Hruby, V. (1991). Induction of skin tanning by subcutaneous administration of a potent synthetic melanotropin. *Journal of the American Medical Association.*, 266(19):2730–6.

[Loane et al., 1997] Loane, M. A., Gore, H. E., Corbett, R., Steele, K., Mathews, C., Bloomer, S. E., Eedy, D. J., Telford, R. W., and Wootton, R. (1997). Effect of camera performance on diagnostic accuracy: preliminary results from the northern ireland arms of the uk multicentre teledermatology trial. *J Telemed Telecare*, 3(2):83–8.

[Lock-Andersen et al., 1997] Lock-Andersen, J., Therkildsen, P., de Olivarius, F. F., Gniadecka, M., Dahlstrem, K., Poulsen, T., and Wulf, H.-C. (1997). Epidermal thickness, skin pigmentation and constitutive photosensitivity. *Photodermatology, Photoimmunology & Photomedicine*, 13(4):153–158.

[Lorentzen et al., 1999] Lorentzen, H., Weismann, K., Petersen, C., Larsen, F. G., Secher, L., and Skodt, V. (24 June 1999). Clinical and dermatoscopic diagnosis of malignant melanoma: Assessed by expert and non-expert groups. *Acta Dermato-Venereologica*, 79:301–304(4).

[Lucas et al., 2006] Lucas, R., McMichael, T., Smith, W., and Armstrong, B. (2006). Solar ultraviolet radiation global burden of disease from solar ultraviolet radiation. *Environmental Burden of Disease Series - World Health*, No. 13.

[Magnain et al., 2008] Magnain, C., Elias, M., and Frigerio, J.-M. (2008). Skin color modeling using the radiative transfer equation solved by the auxiliary function method: inverse problem. *J. Opt. Soc. Am. A*, 25(7):1737–1743.

[Mansouri, 2005] Mansouri, A. (2005). *Etude, conception et réalistion d'un système multispectral de vision pour des applications de proximité et développement d'algorithmes de reconstrusction de la réflectance.* PhD thesis, Université de Bourgogne.

[Mansouri et al., 2005a] Mansouri, A., Gee, C., Guillemin, J. P., Marzani, F. S., and Gouton, P. (2005a). Multispectral image acquisition and spectral reflectance reconstruction: application to plant detection. *7th International Conference on Quality Control by Artificial Vision (QCAV)*, pages 367–371.

[Mansouri et al., 2005b] Mansouri, A., Marzani, F., and Gouton, P. (2005b). Development of a protocol for ccd calibration application to a multispectral imaging system. *International Journal of Robotics and Automation, Special Issue on Color Image Processing and Analysis for Machine Vision, Acta Press*, 20 (2):94–100.

[Mansouri et al., 2005c] Mansouri, A., Marzani, F., and Gouton, P. (2005c). Neural networks in two cascade algorithms for spectral reflectance reconstruction. In *ICIP (2)*, pages 718–721.

[Mansouri et al., 2005d] Mansouri, A., Sanchez, M., Marzani, F. S., and Gouton, P. (2005d). Spectral reflectance estimation from multispectral images using neural networks. *Physics in Signal and Image Processing PSIP.*

[Marchesini et al., 1994] Marchesini, R., Ballerini, M., Bartoli, C., Pignoli, E., Sichirollo, A., Tomatis, S., Zurrida, S., and Cascinelli, N. (1994). Telespectrophotometry of human skin diseases by means of a ccd camera. *Proc. SPIE 2081*, pages 168–173.

[Marghoob et al., 2003] Marghoob, A., Swindle, L., Moricz, C., Sanchez Negron, F., Slue, B., Halpern, A., and Kopf, A. (2003). Instruments and new technologies for the in vivo diagnosis of melanoma. *Journal of the American Academy of Dermatology*, 49(5):777–797.

[Martinez et al., 2002] Martinez, K., Cupitt, J., Saunders, D., and Pillay, R. (2002). Ten years of art imaging research. *Proceedings of the IEEE*, 90(1):28 –41.

[Mathews, 2008] Mathews, S. A. (2008). Design and fabrication of a low-cost, multispectral imaging system. *Appl. Opt.*, 47(28):F71–F76.

[McIntosh et al., 2001] McIntosh, L. M., Summers, R., Jackson, M., Mantsch, H. H., Mansfield, J. R., Howlett, M., Crowson, A. N., and Toole, J. W. P. (2001). Towards Non-Invasive Screening of Skin Lesions by Near-Infrared Spectroscopy. *Journal of Investigative Dermatology*, 116(1):175–181.

[Meglinski and Matcher, 2003] Meglinski, I. and Matcher, S. (February 2003). Computer simulation of the skin reflectance spectra. *Computer Methods and Programs in Biomedicine*, 70:179–186(8).

[Meglinski and Matcher, 2002] Meglinski, I. V. and Matcher, S. J. (2002). Quantitative assessment of skin layers absorption and skin reflectance spectra simulation in the visible and near-infrared spectral regions. *Physiological Measurement*, 23(4):741.

[Meglinsky and Matcher, 2001] Meglinsky, I. and Matcher, S. (2001). Modelling the sampling volume for skin blood oxygenation measurements. *Medical and Biological Engineering and Computing*, 39:44–50. 10.1007/BF02345265.

[Mehrubeoglu et al., 2000] Mehrubeoglu, M., Kehtarnavaz, N., Marquez, G., and Wang, L. V. (2000). Characterization of skin lesion texture in diffuse reflectance spectroscopic images. In *Proceedings of the 4th IEEE Southwest Symposium on Image Analysis and Interpretation*, pages 146–, Washington, DC, USA. IEEE Computer Society.

[MellesGriot,] MellesGriot, C. Interference filters technical note. Online.

[Metropolis and Ulam, 1949] Metropolis, N. and Ulam, S. (1949). The monte carlo method. *Journal of the American Statistical Association*, 44(247):335–341.

[MHT Optics, 2011] MHT Optics (2011). Spectroshade system. http://www.mht.ch/index.php?uri=derma.html.

[Moncrieff et al., 2002] Moncrieff, M., Cotton, S., Claridge, E., and Hall, P. (2002). Spectrophotometric intracutaneous analysis: a new technique for imaging pigmented skin lesions. *The British journal of dermatology*, 146(3):448–457.

[Montemarano and Lyford, 2011] Montemarano, A. and Lyford, H. (2011). Melasma. Online. http://emedicine.medscape.com/article/1068640-overview.

[Mühlenbein, 1992] Mühlenbein, H. (1992). How genetic algorithms really work: Mutation and hillclimbing. In *PPSN*, pages 15–26.

[Myrick and Angel, 1990] Myrick, M. L. and Angel, S. M. (1990). Elimination of background in fiber-optic raman measurements. *Appl. Spectrosc.*, 44(4):565–570.

[Nakao et al., 1995] Nakao, D., Tsumura, N., and Miyake, Y. (1995). Realtime multispectral image processing for mapping pigmentation in human skin. In *in Proc. Ninth IS&T/SID Color Imaging Conference, IS&T*, pages 80–84.

[Nehal et al., 2002] Nehal, K., Oliviera, S., Marghoob, A., Christos, P., Dusza, S., Tromberg, J., and Halpern, A. (2002). Use of and beliefs about baseline photography in the management of patients with pigmented lesions: a survey of dermatology residency programmes in the united states. *Melanoma Research*, 12(2):161–7.

[Neumaier, 1998] Neumaier, A. (1998). Solving ill-conditioned and singular linear systems: A tutorial on regularization. *SIAM Review*, 40:636–666.

[Nischal and Khopkar, 2005] Nischal, K. and Khopkar, U. (2005). Dermoscope. *Indian journal of dermatology, venereology and leprology*, 71:300–303.

[Nishidate et al., 2004] Nishidate, I., Aizu, Y., and Mishina, H. (2004). Estimation of melanin and hemoglobin in skin tissue using multiple regression analysis aided by monte carlo simulation. *Journal of Biomedical Optics*, 9(4):700–10.

[Nugroho et al., 2007] Nugroho, H., Fadzil, M., Yap, V., Norashikin, S., and Suraiya, H. (2007). Determination of skin repigmentation progression. pages 3442 –3445.

[Numahara, 2001] Numahara, T. (2001). From the standpoint of dermatology. *The Journal of Digital Color Imaging in Biomedicine*, pages 67–72.

[Okamoto and Lee, 2009] Okamoto, H. and Lee, W. S. (2009). Green citrus detection using hyperspectral imaging. *Comput. Electron. Agric.*, 66:201–208.

[Ornberg et al., 1999] Ornberg, R. L., Woerner, B. M., and Edwards, D. A. (1999). Analysis of stained objects in histological sections by spectral imaging and differential absorption. *The Journal of histochemistry and cytochemistry*, 47:1307–1313.

[Pearl et al., 2009] Pearl, R., Townley, W., Stott, D., and Grobbelaar, A. (2009). Diagnosis of skin lesions by trainee surgeons: experience improves accuracy. *Annals of The Royal College of Surgeons of England*, 91:494–499(6).

[Perednia, 1991] Perednia, D. A. (1991). What dermatologists should know about digital imaging. *Journal of the American Academy of Dermatology*, 25(1, Part 1):89 – 108.

[Photonfocus, 2010] Photonfocus (2010). Cmos camera mv1-d1312l series technical note. Online.

[Pilotto et al., 2001] Pilotto, S., Pacheco, M., Silveira Jr, L., Balbin Villaverde, A., and Zngaro, R. (2001). Analysis of near-infrared raman spectroscopy as a new technique for a transcutaneous non-invasive diagnosis of blood components. *Lasers in Medical Science*, 16:2–9. 10.1007/PL00011332.

[Prahl, 1988] Prahl, S. (December 1988). *Light Transport in Tissue*. PhD thesis, The University of Texas at Austin, TX, USA.

[Prahl, 1999] Prahl, S. A. (1999). Optical absorption of hemoglobin. online.

[Preece and Claridge, 2004] Preece, S. J. and Claridge, E. (2004). Spectral filter optimization for the recovery of parameters which describe human skin. *IEEE Trans. Pattern Anal. Mach. Intell.*, 26:913–922.

[Press et al., 1992] Press, W., Teukolsky, S., Vetterling, W., and Flannery, B. (1992). *Numerical Recipes in C*. Cambridge University Press, Cambridge, UK, 2nd edition.

[Prigent et al., 2010a] Prigent, S., Descombes, X., Zugaj, D., Martel, P., and Zerubia, J. (2010a). Multispectral image analysis for skin pigmentation classification. In *Image Processing (ICIP), 2010 17th IEEE International Conference on*, pages 3641 –3644.

[Prigent et al., 2010b] Prigent, S., Descombes, X., Zugaj, D., and Zerubia, J. (2010b). Spectral analysis and unsupervised svm classification for skin hyper-pigmentation classification. In *Proc. IEEE Workshop on Hyperspectral Image and Signal Processing : Evolution in Remote Sensing (WHISPERS)*, Reykjavik, Iceland.

[Raman and Krishnan, 1928] Raman, C. and Krishnan, K. (1928). A new type of secondary radiation. *Nature*, 121:501–502.

[Ramanujam, 2000] Ramanujam, N. (2000). Fluorescence spectroscopy of neoplastic and non-neoplastic tissues. *Neoplasia*, 2:89–117.

[Ramanujam et al., 1996] Ramanujam, N., Mitchell, M. F., Mahadevan, A., Thomsen, S., Malpica, A., Wright, T., Atkinson, N., and Richards-Kortum, R. (1996). Spectroscopic diagnosis of cervical intraepithelial neoplasia (cin) in vivo using laser-induced fluorescence spectra at multiple excitation wavelengths. *Lasers in Surgery and Medicine*, 19(1):63–74.

[Rib és, 2003] Rib és, A. (2003). *Analyse multispectrale et reconstruction de la r éflectance spectrale de tableaux de maître*. PhD thesis, Ecole Nationale Sup érieure des T él écommunications, Paris.

[Rigel, 1997] Rigel, D. S. (1997). Epiluminescence microscopy in clinical diagnosis of pigmented skin lesions. *The Lancet*, 349(9065):1566 – 1567.

[Robertson and Rees, 2010] Robertson, K. and Rees, J. (2010). Variation in epidermal morphology in human skin at different body sites as measured by reflectance confocal microscopy. *Acta Derm. Venereol*, 90:368–373.

[Rothmann et al., 1998] Rothmann, C., Bar-Am, I., and Malik, Z. (1998). Spectral imaging for quantitative histology and cytogenetics. *Histology and Histopathology*, 13(3):921–926.

[Rowe, 2002] Rowe, M. H. (2002). Trichromatic color vision in primates. *News in Physiological Sciences*, 17:93–98.

[Ruifrok and Johnston, 2001] Ruifrok, A. C. and Johnston, D. A. (2001). Quantification of histochemical staining by color deconvolution. *Analytical and quantitative cytology and histology the International Academy of Cytology and American Society of Cytology*, 23(4):291–299.

[Schwarz and Staenz, 2001] Schwarz, J. and Staenz, K. (2001). Adaptative threshold for spectral matching of hyperspectral data. *Canadian Journal of Remote Sensing*, vol. 27:216–224.

[Shi and DiMarzio, 2007] Shi, T. and DiMarzio, C. A. (2007). Multispectral method for skin imaging: development and validation. *Appl. Opt.*, 46(36):8619–8626.

[Shimada et al., 2001a] Shimada, M., Yamada, Y., Itoh, M., and Yatagai, T. (2001a). Melanin and blood concentration in a human skin model studied by multiple regression analysis: assessment by monte carlo simulation. *Journal of Physics in Medicine and Biology*, 46:2397–2406.

[Shimada et al., 2001b] Shimada, M., Yamada, Y., Itoh, M., and Yatagai, T. (2001b). Melanin and blood concentration in human skin studied by multiple regression analysis: experiments. *Physics in Medicine and Biology*, 46(9):2385.

[Simon et al., 2010] Simon, C., Huxhagen, U., Mansouri, A., Heritage, A., Boochs, F., and Marzani, F. S. (2010). Integration of high-resolution spatial and spectral data acquisition systems to provide complementary datasets for cultural heritage applications. pages 75310L 1–9.

[Sinichkin et al., 1996] Sinichkin, Y. P., Uts, S. P., and Pilipenko, E. A. (1996). Spectroscopy of human skin in vivo: 1. reflection spectra. *Optics and Spectroscopy*, 80:228–234.

[Soon et al., 2003] Soon, S. L., McCall, C. O., and Chen, S. C. (2003). Computerized digital dermoscopy: Sensitivity and specificity aren't enough. *Journal of Investigative Dermatology*, 121:214–215.

[Soyer et al., 1987] Soyer, H.-P., Smolle, J., Kerl, H., and Stettner, H. (1987). Early diagnosis of malignant melanoma by surface microscopy. *The Lancet*, 330(8562):803 – 803.

[Stamatas et al., 2004] Stamatas, G. N., Zmudzka, B. Z., Kollias, N., and Beer, J. Z. (2004). Non-invasive measurements of skin pigmentation in situ. *Pigment Cell Research*, 17(6):618–626.

[Störring et al., 2000] Störring, M., Andersen, H. J., and Granum, E. (2000). Estimation of the illuminant color from human skin color. In *FG '00: Proceedings of the Fourth IEEE International Conference on Automatic Face and Gesture Recognition 2000*, page 64, Washington, DC, USA. IEEE Computer Society.

[Svaasand et al., 1995] Svaasand, L., Norvang, L., Fiskerstrand, E., Stopps, E., Berns, M., and Nelson, J. (1995). Tissue parameters determining the visual appearance of normal skin and port-wine stains. *Lasers in Medical Science*, 10:55–65. 10.1007/BF02133165.

[Syswerda, 1989] Syswerda, G. (1989). Uniform crossover in genetic algorithms. In *Proceedings of the 3rd International Conference on Genetic Algorithms*, pages 2–9, San Francisco, CA, USA. Morgan Kaufmann Publishers Inc.

[Takiwaki, 1998] Takiwaki, H. (1998). Measurement of skin color: practical application and theoretical considerations. *The journal of medical investigation JMI*, 44(3-4):121–126.

[Tomatis et al., 2005a] Tomatis, S., Carrara, M., Bono, A., Bartoli, C., Lualdi, M., Tragni, G., Colombo, A., and Marchesini, R. (2005a). Automated melanoma detection with a novel multispectral imaging system : Results of a prospective study. *Physics in medicine & biology*, 50(8):1675–1687.

[Tomatis et al., 2005b] Tomatis, S., Carrara, M., Bono, A., Bartoli, C., Lualdi, M., Tragni, G., Colombo, A., and Marchesini, R. (2005b). Automated melanoma detection with a novel multispectral imaging system: results of a prospective study. *Physics in medicine and biology*, 50(8):1675–87.

[Tominaga, 1996] Tominaga, S. (1996). Multichannel vision system for estimating surface and illumination functions. *J. Opt. Soc. Am. A*, 13(11):2163–2173.

[Tsumura et al., 2003] Tsumura, N., Ojima, N., Sato, K., Shiraishi, M., Shimizu, H., Nabeshima, H., Akazaki, S., Hori, K., and Miyake, Y. (2003). Image-based skin color and texture analysis/synthesis by extracting hemoglobin and melanin information in the skin. *ACM Trans. Graph.*, 22(3):770–779.

[Tuchin, 2000] Tuchin, V. V. (2000). Tissue optics: Light scattering methods and instruments for medical diagnosis. *Press Monograph (SPIE)*, 166.

[Twersky, 1962] Twersky, V. (1962). Multiple scattering of waves and optical phenomena. *J. Opt. Soc. Am.*, 52(2):145–169.

[Twersky, 1970] Twersky, V. (1970). Absorption and multiple scattering by biological suspensions. *J. Opt. Soc. Am.*, 60(8):1084–1093.

[Van Gemert et al., 1989] Van Gemert, M., Jacques, S., Sterenborg, H., and Star, W. (1989). Skin optics. *Biomedical Engineering, IEEE Transactions on*, 36(12):1146 –1154.

[Vazquez-Lopez et al., 2003] Vazquez-Lopez, F., Manjón-Haces, J., Lopez-Escobar, M., Perez-Oliva, N., and Marghoob, A. A. (November 2003). Sequential image analysis and measurement of pigmented lesions: false variations due to patient positioning. *Clinical and Experimental Dermatology*, 28:657–660(4).

[Verhoeven and Schmitt, 2010] Verhoeven, G. J. and Schmitt, K. D. (2010). An attempt to push back frontiers digital near-ultraviolet aerial archaeology. *Journal of Archaeological Science*, 37(4):833 – 845.

[Verkruysse et al., 2005a] Verkruysse, W., Zhang, R., Choi, B., Lucassen, G., Svaasand, L. O., and Nelson, J. S. (2005a). A library based fitting method for visual reflectance spectroscopy of human skin. *Physics in Medicine and Biology*, 50(1):57–70.

[Verkruysse et al., 2005b] Verkruysse, W., Zhang, R., Choi, B., Lucassen, G., Svaasand, L. O., and Nelson, J. S. (2005b). A library based fitting method for visual reflectance spectroscopy of human skin. *Physics in Medicine and Biology*, 50(1):57.

[Vo-Dinh and Cullum, 2003] Vo-Dinh, T. and Cullum, B. (2003). *Fluorescence Spectroscopy for Biomedical Diagnostics*, chapter Chapter 28, pages 1–49. CRC Press.

[Vo-Dinh et al., 2004] Vo-Dinh, T., Stokes, D. L., Wabuyele, M. B., Martin, M. E., Song, J. M., Jagannathan, R., Michaud, E., Lee, R. J., and Pan, X. (2004). A hyperspectral imaging system for in vivo optical diagnostics. *Engineering in Medicine and Biology Magazine, IEEE*, 23:40–49.

[Vogel et al., 2007] Vogel, A., Chernomordik, V. V., Riley, J. D., Hassan, M., Amyot, F., Dasgeb, B., Demos, S. G., Pursley, R., Little, R. F., Yarchoan, R., Tao, Y., and andjbakhche A. H. (2007). Using noninvasive multispectral imaging to quantitatively assess tissue vasculature. *Journal of Biomedical Optics*, 12(5):051604–+.

[Waggoner et al., 2001] Waggoner, A. S., Wachman, E. S., and Farkas, D. L. (2001). *Optical Filtering Systems for Wavelength Selection in Light Microscopy.* John Wiley & Sons, Inc.

[Wagnieres et al., 1998] Wagnieres, G. A., Star, W. M., and Wilson, B. C. (1998). In vivo fluorescence spectroscopy and imaging for oncological applications. *Photochemistry and Photobiology*, 68(5):603–632.

[Wang et al., 1995] Wang, L., Jacques, S. L., and Zheng, L. (1995). Mcml–monte carlo modeling of light transport in multi-layered tissues. *Computer Methods and Programs in Biomedicine*, 47(2):131 – 146.

[Wang et al., 2008] Wang, S. Q., Dusza, S. W., Scope, A., Braun, R. P., Kopf, A. W., and Marghoob, A. A. (2008). Differences in dermoscopic images from nonpolarized dermoscope and polarized dermoscope influence the diagnostic accuracy and confidence level: A pilot study. *American Society of Dermatologic Surgery*, 34:1389–1395.

[WheelsBridge, 2008] WheelsBridge (2008). The technology of tissue viability imaging. Online.

[Whitley, 1989] Whitley, D. (1989). The genitor algorithm and selective pressure. In Kaufmann, M., editor, *Proceedings of the 3rd International Conference on Genetic Algorithms*, pages 116–121.

[Whitley and Kauth, 1988] Whitley, D. and Kauth, J. (1988). Genitor: a different genetic algorithm. In *Proceedings of the Rocky Mountain Conference on Artificial Intelligence*, pages 118–130., Denver, CO.

[World Health Organization, 2011] World Health Organization (2011). Skin cancers. online.

[Wyszecki and Stiles, 2000] Wyszecki, G. and Stiles, W. S. (2000). *Color Science: Concepts and Methods, Quantitative Data and Formulae (Wiley Series in Pure and Applied Optics).* Wiley-Interscience, 2 edition.

[Yamaguchi et al., 2008] Yamaguchi, M., Haneishi, H., and Ohyama, N. (2008). Beyond red–green–blue (rgb): Spectrum-based color imaging technology. *Journal of Imaging Science and Technology*, 52(1):010201.

[Yamaguchi et al., 1997] Yamaguchi, M., Iwama, R., Ohya, Y., Obi, T., Ohyama, N., Komiya, Y., and Wada, T. (1997). Natural color reproduction in the television system for telemedicine. *Proc. SPIE 3031*, pages 482–489.

[Yamaguchi et al., 2005] Yamaguchi, M., Mitsui, M., Murakami, Y., Fukuda, H., Ohyama, N., and Kubota, Y. (2005). Multispectral color imaging for dermatology: application in inflammatory and immunologic diseases. *IS&T/SID 13th color Imaging Conference*, pages 52–58.

[Yamamoto et al., 2008] Yamamoto, T., Takiwaki, H., Arase, S., and Ohshima, H. (2008). Derivation and clinical application of special imaging by means of digital cameras and image j freeware for quantification of erythema and pigmentation. *Skin Research and Technology*, 14(1):26–34.

[Yi et al., 2011] Yi, D., Wang, C., Qi, H., Kong, L., Wang, F., and Adibi, A. (2011). Real-time multispectral imager for home-based health care. *Biomedical Engineering, IEEE Transactions on*, 58(3):736 –740.

[Young, 1997] Young, A. R. (1997). Chromophores in human skin. *Phys Med Biol*, 42:789–802.

[Yudovsky and Pilon, 2010] Yudovsky, D. and Pilon, L. (2010). Rapid and accurate estimation of blood saturation, melanin content, and epidermis thickness from spectral diffuse reflectance. *Applied Optics*, 49(10):1707–1719.

[Yuhas et al., 1992] Yuhas, R., Goetz, A., and Boardman, J. (1992). Discrimination among semi-arid landscape endmembers using the spectral angle mapper (sam) algorithm. *In Summuries of the Third Annual JPL Airborne Geoscience Workshop*, I(JPL Publication 92-14):147–149.

[Zhang et al., 2005] Zhang, R., Verkruysse, W., Choi, B., Viator, J. A., Jung, B., Svaasand, L. O., Aguilar, G., and Nelson, J. S. (2005). Determination of human skin optical properties from spectrophotometric measurements based on optimization by genetic algorithms. *Journal of Biomedical Optics*, 10(2):024030.

[Zonios et al., 2001] Zonios, G., Bykowski, J., and Kollias, N. (2001). Skin melanin, hemoglobin, and light scattering properties can be quantitatively assessed in vivo using diffuse reflectance spectroscopy. *Journal of Investigative Dermatology*, 117:1452–1457.